Fast neutrino flavour conversions

Stability analysis in the linear regime

Tobias Stirner

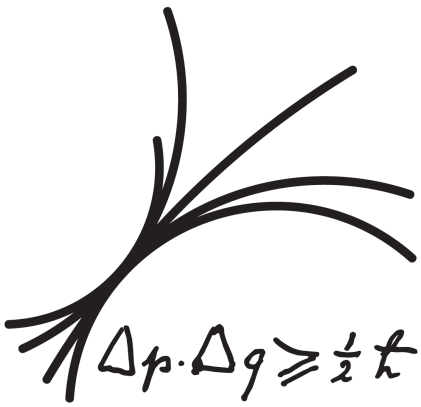

München 2020

Fast neutrino flavour conversions

Stability analysis in the linear regime

Dissertation
an der Fakultät für Physik
der Ludwig–Maximilians–Universität
München

vorgelegt von
Tobias Stirner
aus Troisdorf

München, den 05. Juni 2020

Dissertation

an der Fakultät für Physik
der Ludwig-Maximilians-Universität München
vorgelegt von Tobias Stirner
am 05. Juni 2020.

Erstgutachter: PD Dr. Georg Raffelt
Zweitgutachter: Prof. Dr. Günter Sigl

Tag der mündlichen Prüfung: 17. Juli 2020

Zusammenfassung

Aufgrund ihrer besonderen Eigenschaften sind Neutrinos wertvolle Boten physikalischer Informationen. Insbesondere durch ihre oftmals geringe Wechselwirkungsrate mit anderen Materiekomponenten ermöglichen sie Einblicke in unzugängliche Regionen, wie das Innere von Sternen. Für die richtige Interpretation von Neutrinosignalen ist ein umfassendes Verständnis der damit verbundenen Prozesse unumgänglich. Zu diesen Prozessen gehört die Umwandlung von Neutrinoflavours, die durch die Mischung von Neutrinos verursacht wird. Während der Propagation in einem Medium kann die Wechselwirkung mit der Umgebung die Korrelation zwischen verschiedenen Flavours beeinflussen, d.h. Flavourkonversionen werden verstärkt oder unterdrückt. Bei hohen Neutrinodichten, wie sie z.B. in Kernkollaps-Supernovae oder bei der Verschmelzung zweier Neutronensterne auftreten, bilden die Neutrinos selbst das Medium, sodass Neutrino-Neutrino-Wechselwirkungen die Flavourentwicklung dominieren und kollektiver Flavourmoden auftreten können. Eine Klasse kollektiver Phänomene wird als schnelle Flavourkonversion bezeichnet, da die Längenskala, bei der die Oszillation auftritt, deutlich kürzer ist als die Skala anderer Oszillationseffekte. Die Umwandlung findet statt, wenn eine anfänglich kleine Flavourkohärenz instabil wird und exponentiell wächst. Dabei hängt die Existenz von instabilen schnellen Flavourmoden entscheidend von der Leptonenzahlverteilung ab.

Diese Arbeit widmet sich der Untersuchung des theoretischen Ursprungs der schnellen Flavourkonversionen. Zu deren Beschreibung wird auf die Matrix der Flavourdichten zurückgegriffen und die entsprechende Bewegungsgleichung hergeleitet. Dabei werden auch die Refraktionsterme berücksichtigt, welche durch die Wechselwirkung mit einem Medium entstehen. Auf Basis dieses Ergebnisses und durch Linearisierung der Bewegungsgleichung wird die Dispersionsrelation der Flavourkorrelationsfunktion berechnet. Der Zusammenhang zwischen Instabilitäten in der Korrelationsfunktion und Vorzeichenwechseln in der Winkelverteilung der Leptonenzahl wird für axialsymmetrische Sys-

teme nachgewiesen. Für diesen Beweis wird der vollständige Satz von Eigenfunktionen bestimmt und die jeweiligen Funktionen von kollektiven und nicht-kollektiven Moden an kritischen Punkten gleichgesetzt. In diesem Zusammenhang wird der Unterschied zwischen der Stabilität von Moden, die die Axialsymmetrie erhalten oder brechen, demonstriert. Schließlich wird die Annahme der Axialsymmetrie verworfen und es werden Beispiele für allgemeine Konfigurationen untersucht, d.h. mit beliebigen Wellenvektoren und nichtsymmetrischen Leptonenzahlverteilungen.

Abstract

Due to their special properties neutrinos are valuable messengers of physical information. In particular the low interaction rate in matter allows us to receive neutrino signals from otherwise inaccessible regions, like the interior of stars. For the correct interpretation of these signals a profound comprehension of associated processes is necessary. One of them is the conversion of neutrino flavours caused by neutrino mixing. When neutrinos propagate in a medium, the interaction with the environment can influence the mixing, i.e. enhance or suppress flavour conversions. At high neutrino densities, as they occur for example in core-collapse supernovae or neutron-star mergers, neutrinos themselves are the medium and neutrino-neutrino interactions can dominate the flavour evolution, which leads to the appearance of collective flavour modes. One class of collective phenomena is called fast flavour conversion because the length scale at which the oscillation takes place is much shorter than the scale of other oscillation effects. The conversion occurs when the initially small flavour coherence becomes unstable and grows exponentially. The existence of unstable fast-flavour modes depends crucially on the angular lepton-number distribution.

This thesis is dedicated to investigate the theoretical origin of fast flavour conversions. For this purpose the formalism based on the matrix of flavour densities is applied and the corresponding equation of motion is derived including refraction terms from the interaction with a medium. The result is used to calculate the dispersion relation for the flavour correlation function as long as its equation of motion can be linearised. The connection between instabilities in the correlation function and crossings in the angular lepton number distribution is proven for axially symmetric systems by deriving the full set of eigenfunctions and matching them for collective and non-collective modes. In this context the difference between the stability of symmetry preserving and breaking modes is demonstrated. Finally the assumption of axial symmetry is dropped and examples are studied for general settings, i.e. with arbitrary wave vectors and non-symmetric lepton-number distributions.

Publications

This thesis comprises the results of my research at the Max Planck Institute for Physics from January 2017 till June 2020. They have been published in the following papers:

1. T. Stirner, G. Sigl, G. Raffelt: "Liouville term for neutrinos: Flavor structure and wave interpretation", *JCAP* **1805** (2018) 016, [1803.04693];

2. S. Airen, F. Capozzi, S. Chakraborty, B. Dasgupta, G. Raffelt, T. Stirner: "Normal-mode analysis for collective neutrino oscillations", *JCAP* **1812** (2018) 019, [1809.09137];

3. F. Capozzi, G. Raffelt, T. Stirner: "Fast neutrino flavor conversion: Collective motion vs. decoherence", *JCAP* **1909** (2019) 002, [1906.08794].

Several chapters of this thesis are based on these papers.

Contents

CHAPTER 1

Introduction

Neutrinos are light and very weakly interacting elementary particles with spin $\frac{1}{2}$. For each charged lepton, i.e. electron, muon and tau, there exists one corresponding neutrino ν_e, ν_μ, ν_τ. Experiments have shown that this flavour is not conserved. This means that for example a neutrino which was produced with electron flavour can also be detected as ν_μ or ν_τ. This phenomenon is denoted as neutrino oscillation or more general flavour conversion and has important consequences for astrophysical processes.

Flavour transformation has a direct influence on neutrino signals. For their correct interpretation a profound understanding of the occurring effects is mandatory. In vacuum the calculation is straightforward, but becomes more complicated in a medium because of neutrino refraction. The medium influences mixing and under specific circumstances can cause significant flavour conversion. In environments with high neutrino fluxes, like core-collapse supernovae, the neutrinos themselves can be the medium, which makes the evolution equation nonlinear and gives rise to collective flavour conversion. Collective transformations modify the neutrino signal in a detector and in addition can play an important role in processes in astrophysical environments. Examples are the synthesis of heavy elements and the revival of the supernova shock wave, which are both not understood completely. This thesis is intended to clarify the theoretical foundation of a particular collective phenomenon, namely fast flavour conversion.

The structure of this thesis is as follows: In the remainder of this chapter an overview of neutrino physics is given. Their role in the Standard Model and the flavour mixing therein are reviewed. Afterwards a brief overview of neutrino oscillations in vacuum and matter is given. The chosen observable to describe neutrino oscillations is the matrix of flavour densities, which consists of the occupation numbers for the mass or flavour states and their respective correla-

tions. This matrix is introduced in ch. 2 and its evolution equation is derived. Interaction terms are implemented. The rest of the thesis focuses on unstable modes of the flavour correlation function. In ch. 3 the dispersion relation of this function is computed, which depends on the angular spectrum. Different input parameters are applied to classify the instabilities. Subsequently the eigenfunctions of non-collective modes are derived and the connection to collective instabilities demonstrated. In the final chapter previous symmetry assumptions are discarded and the directional dependence of unstable modes pointed out.

1.1 Historical overview

At the beginning of the last century the energy spectrum and spin structure of β-decay was an unresolved issue. While one part of the community questioned the strict conservation of energy, Pauli proposed the existence of a light and very weakly interacting particle with spin 1/2. Nowadays it is known as electron neutrino. As the story goes he was not very convinced by his idea and said to Walter Baade [1]:

> "I've done a terrible thing today, something which no theoretical physicist should ever do. I have suggested something that can never be verified experimentally."

His theoretical claim was correct, but the prediction on its detectability wrong. In 1956 Cowan and Reines detected electron antineutrinos from a nuclear reactor via inverse beta decay [2]

$$\bar{\nu}_\mathrm{e} + \mathrm{p}^+ \rightarrow \mathrm{e}^+ + \mathrm{n}. \tag{1.1}$$

The observation of neutrinos corresponding to the other leptons, μ and τ, followed later [3, 4]. Furthermore the decay width of the Z-boson indicated that there are no further (light) generations [5].

The experimental evidence for flavour conversion of solar and atmospheric neutrinos was found in the measurements of Super-Kamiokande and SNO respectively [6, 7]. In both experiments the data on the neutrino flux did not match the theoretical prediction without flavour transformations originating in a mixing in the neutrino mass term. However, implementing flavour conversion fitted the measurement with high significance and proved the existence of neutrino masses.

Nowadays the number of neutrino detectors has increased considerably. Their measurements are essential to constrain some of the oscillation parameters and some of them allow research on more "exotic" questions, like the density profile of the earth. In astronomy high-energy neutrinos are an important observation channel. Their weak interaction enables them to carry information from dense and hot regions, where other particles, like photons

or protons, are trapped. Because neutrinos are also not deflected by magnetic fields, their signal is reliable for the identification of astronomical sources. This feature was used in multi-messenger astronomy to find the origin of highly energetic cosmic rays [8].

1.2 Neutrinos in the Standard Model

The Standard Model of particle physics conjoins the established matter content and forces in the universe in the framework of quantum field theory and gauge theory. It is invariant under local transformations belonging to the $SU(3)_{\mathrm{C}} \otimes SU(2)_{\mathrm{L}} \otimes U(1)_{\mathrm{Y}}$ group after electroweak symmetry breaking. The subscripts denote the charges to which the gauge bosons of the group couple. $SU(3)_{\mathrm{C}}$ is the symmetry group for colour [9,10], a charge that is exclusive to quarks, and hence not relevant in this thesis. The charges of $SU(2)_{\mathrm{L}}$ and $U(1)_{\mathrm{Y}}$ are left-handed chirality and weak hypercharge respectively and their gauge bosons form the $W^{\pm}$, Z-bosons and the photon [11–13]. The spontaneous symmetry breaking in the electroweak sector is important because it gives masses to fermions via the Higgs mechanism [14, 15] and moreover to the W and Z-boson. These masses are the reason for the low interaction rates when the energy transfer between scattering particles, like neutrinos and electrons, is small compared to the electroweak scale.

In the Standard Model neutrinos only interact via the massive gauge bosons of the weak interaction, i.e. W and Z-bosons. A coupling to the photon is possible in loop processes, which induces an effective dipole moment for the neutrino [16]. These interaction channels have very small cross sections, so that neutrinos can be generally considered to be freely streaming. For example we have $\sigma \sim 10^{-41}\,\mathrm{cm}^2$ for inverse beta decay with a single proton and a neutrino energy of $E_\nu = 10\,\mathrm{MeV}$ [17]. Theses numbers imply a mean free path of almost a light year in water. For high-energy neutrinos of ($\infty''\,\mathrm{GeV}$) the situation is different as they cannot pass astronomical objects like the earth due to their high cross section with common matter.

Although the predictions of the Standard Model are successful for a plethora of processes, it does not include neutrino masses. In principle, it is not problematic to construct a mass term (with or without the Higgs mechanism) and add it to the theory. But it is not clear yet if neutrinos have a Dirac mass like the other fermions, a Majorana mass, or both. The last two options would make neutrinos Majorana particles, which means that particles and antiparticles are identical. Because of this ambivalence the implementation of neutrino masses in the model is not possible.

If neutrinos are Dirac particles like all other fermions, the mass term is a combination of a left- and a right-handed field $\psi_{\mathrm{L,\,R}}$ [18]

$$\mathcal{L}^{\mathrm{D}}_{\mathrm{mass}} = -m^{\mathrm{D}}_{\nu} \left(\bar{\psi}_{\mathrm{L}} \psi_{\mathrm{R}} + \bar{\psi}_{\mathrm{R}} \psi_{\mathrm{L}} \right) . \tag{1.2}$$

Here and afterwards natural units are applied, i.e. $\hbar = c = 1$. Left and

right-handed fields are eigenstates of the chirality operator corresponding to the eigenvalues ∓ 1. Therefore a Dirac mass term mixes chiral eigenstates. If eq. (1.2) should complete the Standard Model in the neutrino sector, these right-handed components must exist, but until now experimental evidence for them is missing.

The mass term of a Majorana particle is formed by a left-handed neutrino field and its charge-conjugated counterpart [19], which is denoted by the superscript C

$$\mathcal{L}^{\mathrm{M}}_{\mathrm{mass}} = -m^{\mathrm{M}}_{\nu} \left(\bar{\psi}^{C}_{\mathrm{L}} \psi_{\mathrm{L}} + \bar{\psi}_{\mathrm{L}} \psi^{C}_{\mathrm{L}} \right) . \tag{1.3}$$

This combination is only possible because the neutrino has no electromagnetic charge. However, the Majorana mass violates lepton number, which for instance allows for the occurrence of neutrinoless double beta decay. For an unstable isotope with atomic number A and mass number Z the reaction $(A,\, Z) \to (A, Z+2) + 2\mathrm{e}^{-}$ would be possible. Several experiments are looking for it with different nuclei, but until today only bounds on $m_{\beta\beta}$ are known, which is a weighted sum of the neutrino masses. The KamLAND-Zen experiment found the most stringent bound $m_{\beta\beta} < 0.165\,\mathrm{eV}$ at 90% confidence level (CL) from Xenon decay [20].

The difficulty to determine the mass term is connected with the value of the neutrino mass, which is much lower than those of other fermions, and so only upper limits are currently available. Direct measurements use the beta decay spectrum of tritium and found $m_{\nu} < 1.1\,\mathrm{eV}$ (90% CL) [21], whereas a more stringent bound from cosmology claims $\sum m_{\nu} < 0.11\,\mathrm{eV}$ (95% CL) [22]. Experiments sensitive to the absolute mass scale have not achieved the necessary resolution to observe the searched effects, e.g. a lowered endpoint in beta decay spectrum or neutrinoless double beta decay. On the other hand the mass squared differences are measured with a precision on the percent level in oscillation experiments [23]. With pure vacuum oscillation data it is not possible to specify the sign of Δm^2, which leaves open the question about the mass ordering. Until now only $m_1 < m_2$ was inferred from solar neutrinos, which carry additional information due to the matter effect in the sun. This leaves two possible scenarios, which are shown in fig. 1.1 and are called normal ordering for $m_1 < m_2 < m_3$ and inverted ordering for $m_3 < m_1 < m_2$. The definition of the mass states is inspired by the contribution of the electron neutrino, which decreases with the index.

Meanwhile theorists have been looking for an explanation of the smallness of m_{ν}, which is at least six orders of magnitude below the electron mass. A popular theory is the seesaw mechanism, where Dirac and Majorana mass terms enter. The lighter mass eigenstate with $m_1 \sim \left(m^{\mathrm{D}}_{\nu}\right)^2 / m^{\mathrm{M}}_{\mathrm{R}}$ is suppressed by the very heavy right-handed Majorana mass, which is assumed to have the scale of grand unified theories $m^{\mathrm{M}}_{\mathrm{R}} \sim 10^{12}\,\mathrm{GeV}$. The Dirac mass term could then be of the order of the electroweak scale. Such a scenario explains the mass gap and in addition might provide a candidate for dark matter as the second mass eigenstate with $m_2 \sim m^{\mathrm{M}}_{\mathrm{R}}$ would be inert to interactions apart

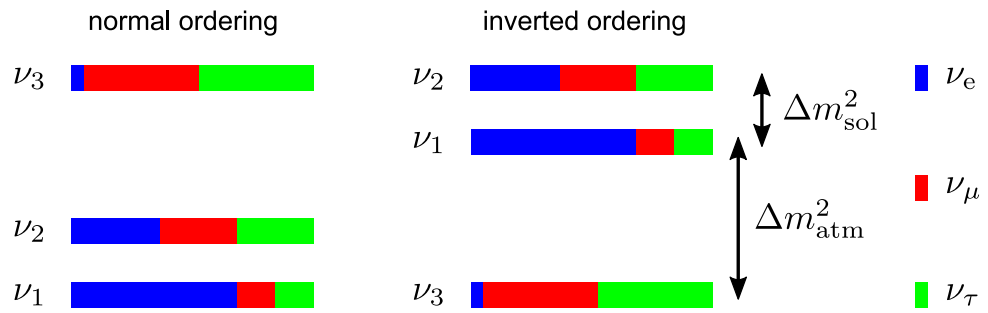

Figure 1.1: Neutrino oscillation data allow two possible mass orderings, the normal and the inverted order, which are displayed for the mass eigenstates ν_1, ν_2 and ν_3. The length of the coloured bars indicates the probability fraction to measure a particular flavour eigenstate from a mass eigenstate. One can see that the muon (red) and tau neutrino (green) have nearly identical contributions to $\nu_{1,2,3}$, which represents the fact that they are almost maximally mixed. The naming of the squared mass differences accounts for the fact that the oscillation between the different states was first observed for atmospheric and solar neutrinos.

from gravity. Moreover the seesaw mechanism is also promising to explain the matter-antimatter asymmetry in the universe. Heavy Majorana neutrino can decay and generate an asymmetry in the lepton sector, which is converted to a baryon asymmetry by sphalerons.

1.3 Flavour mixing

In the Standard Model there exists no one-to-one correspondence between the mass and the flavour of a fermion. This is due to the different bases in which the corresponding operators are diagonal. The bases are related via

$$|\psi_\alpha\rangle = U^*_{\alpha i}\,|\psi_i\rangle\,. \tag{1.4}$$

Summation over repeated indices is implied. Here and in the following Greek indices represent flavour states, i.e. $\alpha \in \{\mathrm{e},\,\mu,\,\tau\}$, while Roman indices denote mass states, $i \in \{1,\,2,\,3\}$. $U_{i\alpha}$ is the neutrino mixing matrix, which can be parameterised by the mixing angles ϑ_{12}, ϑ_{23}, ϑ_{13} and a complex phase δ_{CP}.

The violation of flavour charge was first observed in the weak interaction of quarks. It was Cabibbo's idea that this effect is due to a mixing of flavours [24]. Later his work was advanced by Kobayashi and Maskawa, who were able to explain CP-violation with a 3×3 matrix with a non-zero complex phase [25]. In the quark sector the mixing matrix is dominated by diagonal elements, i.e. the mixing is small.

Flavour mixing in the lepton sector was predicted by Pontecorvo [26] and the structure of the associated mixing matrix worked out by Maki, Nakagawa and Sakata [27]. Accordingly the matrix is called PMNS-matrix and

in contrast to the CKM-matrix for quarks it is not dominated by diagonal elements. Figure 1.1 visualises the composition of mass states out of flavour states and as one can see the fractions are mostly of the same order. If neutrinos are Dirac particles, the number of mixing angles and complex phases in the PMNS and CKM-matrix are identical. For Majorana particles more complex phases appear because the mass term violates $U(1)$-symmetry for lepton number conservation. These phases have no effect for neutrino oscillations, so that calculations can be performed without the necessity to specify whether neutrinos are Dirac or Majorana fermions.

A full treatment of oscillations with three generations is cumbersome. Since we are interested in theoretical possibilities that follow from neutrino mixing the number of generations is limited to two. This simplifies calculations and the mixing matrix

$$U = \begin{pmatrix} \cos\vartheta_\mathrm{v} & \sin\vartheta_\mathrm{v} \\ -\sin\vartheta_\mathrm{v} & \cos\vartheta_\mathrm{v} \end{pmatrix}, \tag{1.5}$$

where ϑ_v is the vacuum mixing angle.

Since there is a mixing in the lepton sector, which causes the flavour oscillation of neutrinos, one might ask if the charged leptons e, μ and τ do the same. The question was discussed in the literature [28–30] and its answer is negative, but not for fundamental physical reasons. In order to understand them it is important to consider the historical context of the experimental evidence for charged leptons and neutrinos. Electrons, muons and taus were detected as particles with identical spin and charge, but distinguishable by their respective mass. Accordingly charged leptons are defined via their mass eigenstates. On the other hand the neutrino masses could not be measured, but the different species ν_e, ν_μ and ν_τ were always encountered in conjunction with an electron, muon or tau. Therefore neutrinos were defined by means of their respective interaction "partner" particle. Of course, these definitions can be changed and the relative mixing between neutrinos the other leptons attributed to the latter, but this is not practicable. Nevertheless oscillation of the interaction eigenstates of charged leptons exists in principle. However, to observe it a highly energetic beam with a pure neutrino mass eigenstate is required, which is not realistic in the end.

1.4 Neutrino oscillations

For the calculation of neutrino oscillations an appropriate observable and its evolution equation are required. In this thesis the matrix of densities ϱ is used, which subsumes all flavours and their correlations [31]. Its diagonal entries specify the occupation number of each flavour and the off-diagonal components the correlation between two flavours. The equation of motion is a Liouville equation, which is often written as [31–37]

$$(\partial_t + \mathbf{v}\cdot\partial_\mathbf{x})\,\varrho = -\mathrm{i}\,[\mathsf{H},\,\varrho]\,. \tag{1.6}$$

In the formula $\mathbf{v}$ is a velocity vector with unit length in the ultra-relativistic approximation. The Hamiltonian H is a flavour (or mass) matrix depending on the basis of ϱ. The derivation of eq. (1.6) is the topic of ch. 2.

1.4.1 Vacuum oscillations

Neutrino oscillation phenomena are based on the interference of different propagation eigenstates. These states are produced with small differences in energy or momentum, which leads to a growing phase difference between them. To illustrate this, a one-dimensional, stationary system with two flavours in vacuum is considered. In vacuum the mass and propagation basis are identical, so that eq. (1.6) becomes in the ultra-relativistic approximation

$$\partial_x \begin{pmatrix} \varrho_{11} & \varrho_{12} \\ \varrho_{21} & \varrho_{22} \end{pmatrix} = \mathrm{i}\,\frac{\Delta m^2}{2E} \begin{pmatrix} 0 & -\varrho_{12} \\ \varrho_{21} & 0 \end{pmatrix}. \tag{1.7}$$

In this formula the vacuum mixing angle ϑ_v is hidden in ϱ_{12}, which vanishes for $\vartheta_\mathrm{v} = 0$. Obviously the occupation number of mass eigenstates remains constant, whereas the mass correlation oscillates in the spatial coordinate x with the oscillation length

$$l_\mathrm{osc} \equiv \frac{4\pi E}{\Delta m^2}. \tag{1.8}$$

For solar neutrinos the mass squared difference $\Delta m^2 = 7.6 \times 10^{-5}\,\mathrm{eV}^2$ results in an oscillation length of $l_\mathrm{osc} = 5\,\mathrm{km/GeV}$.

The phase difference between the mass states translates to a periodically changing number of neutrinos in the flavour basis. The two bases are related via the vacuum mixing matrix from eq. (1.5). Assuming that a source emits mono-energetic neutrinos of flavour α the probability to measure the other flavour β is

$$P_{\nu_\alpha \to \nu_\beta} = \sin^2(2\vartheta_\mathrm{v}) \sin^2\left(\frac{x}{l_\mathrm{osc}}\right). \tag{1.9}$$

The formula is blind to the sign of Δm^2, which is the reason for the undetermined mass ordering. Note that in eq. (1.7) the trace of ϱ is conserved and so only the flavour content changes, but not the total number of neutrinos.

1.4.2 Matter effect

As soon as neutrinos propagate through matter the electroweak potential sourced by other particles leads to refraction, so that the previous identification of neutrino mass and propagation eigenstates does not hold anymore. Relying on Fermi's effective theory of weak interaction the Hamiltonian obtains the additional term

$$\mathsf{H}^\mathrm{mat} = \sqrt{2} G_\mathrm{F} \begin{pmatrix} n_\mathrm{e} - \frac{1}{2} n_\mathrm{n} & 0 \\ 0 & -\frac{1}{2} n_\mathrm{n} \end{pmatrix}, \tag{1.10}$$

where n_e is the electron density and n_n the neutron density. This equation is only valid for ordinary matter, as for example it does not include muons, which would be present in a supernova. Note that the Hamiltonian is written in the interaction basis and the neutral-current contributions of electrons and protons cancel each other as long as the medium is not charged. The interaction with neutrons does not influence neutrino oscillations since it contributes equally to every flavour and is projected out by the commutator on the right hand side of eq. (1.6).

The interaction with electrons nullifies the identification of the mass and propagation basis. Therefore a new mixing angle ϑ_m is introduced to connect the flavour and propagation basis [38]

$$\tan\left(2\vartheta_\mathrm{m}\right) = \tan\left(2\vartheta_\mathrm{v}\right)\left[1 \mp \frac{2\sqrt{2}G_\mathrm{F}En_\mathrm{e}}{\Delta m^2\cos\left(2\vartheta_\mathrm{v}\right)}\right]^{-1}. \tag{1.11}$$

For neutrinos the formula holds with a minus sign in the brackets and for antineutrinos with a plus sign. The reason for the sign change originates in the potential sourced by electrons, which affects them differently.

For a specific combination of neutrino energy and electron density the inverse factor becomes infinite and so the mixing maximal, i.e. $\vartheta_\mathrm{m} = \frac{\pi}{4}$. This resonant mixing is the basis of the so-called MSW-effect [39,40]. When neutrinos propagate through a medium with slowly changing density, which passes through the critical density, a significant amount of neutrinos can be converted to the other flavour.

The inclusion of matter effects was particularly successful to explain the solar neutrino signal. The electron number density of the sun slowly decreases from its centre and is high enough to be critical for neutrinos from nuclear fusion. Therefore a significant fraction of electron neutrinos is converted to muon neutrinos, which led to a mismatch between the measured and predicted solar electron neutrino flux. The MSW-effect resolved this so-called solar neutrino problem. In a less dense environment like the earth the matter effect is much smaller, but still measurable for solar neutrinos. It leads to a flux asymmetry between up- and down-going solar neutrinos, also called day-night asymmetry [41].

For atmospheric neutrinos the situation is slightly different due to their higher energy. For example the density in the inner core of the earth can already be critical if their energy is of the order 10 GeV. Then also for these neutrinos the resonance condition is satisfied.

If the electron density n_e is large in eq. (1.11), which is possible in very dense environments, the inverse factor suppresses the mixing. Then the interaction eigenstates are almost propagation eigenstates.

1.4.3 Neutrino-neutrino interaction

Apart from the coupling of neutrinos to the surrounding medium also the interaction of neutrinos with each other can change the flavour content. It was noticed by Pantaleone that a neutrino-neutrino scattering process has an impact on the correlation of different flavours [42]. This effect becomes only relevant at very high ν-densities, as they occur for example in core-collapse supernovae. In an isotropic setting the neutrino interaction potential, which enters the Hamiltonian in eq. (1.6), is

$$\mathsf{H}^{\nu\nu} = \sqrt{2}\, G_{\mathrm{F}} \left(\varrho - \bar{\varrho}\right) , \tag{1.12}$$

where $\bar{\varrho}$ is the matrix of densities for antineutrinos.

This discovery started the investigation of collective phenomena in the neutrino flavour sector. Collectivity occurs when the neutrino-neutrino interaction dominates the equation of motion, which becomes nonlinear and typically cannot be solved analytically then. For this reason simplifying assumptions were necessary to investigate possible phenomena. Among these the synchronised and the bipolar oscillation are probably the most well-known. Synchronised oscillation can occur in a homogeneous and isotropic neutrino medium, whose potential is strong enough to overcome the frequency spread of different modes [43,44]. Usually each mode oscillates with its own frequency, but the interaction can accelerate slow modes and slow down fast ones, so that effectively the system can be described by a single mode. However, it is questionable if the necessary conditions on the environment are realistic on neutrino oscillation scales [45, 46].

Bipolar oscillations are important in isotropic environments with a comparable number of neutrinos and antineutrinos [44, 47–49]. The phenomenon is driven by the pairwise conversion of a neutrino and an antineutrino from one flavour to another. This process does not change the overall flavour content of the ensemble, but when looking at the matrix of densities for neutrinos and antineutrinos respectively large variations in the diagonal elements are observable. Immediately after production the difference between ϱ and $\bar{\varrho}$ in eq. (1.12) becomes large and dominates the evolution. Mathematically it corresponds to a pendulum that starts in the upright, unstable position and then falls over leading to an oscillation with large amplitude. Phenomenologically bimodal oscillations are observable as a so-called spectral swap [50–52]. Because they only arise above an energy threshold, a sharp transition appears, where ν_{e} and ν_{μ} switch their respective spectrum. Also this phenomenon is probably not relevant in realistic settings because it was shown later that already small anisotropies make the system decohere quickly [53, 54].

A part of this thesis deals with the rather new topic of fast flavour conversion. In the past few years this collective phenomenon has been studied theoretically [55–74], and in the context of supernovae [75–86] and neutron star mergers [87, 88]. The reason for the attribute “fast” is the difference in

scales compared to other oscillation phenomena. In vacuum the only scale is the oscillation frequency l_{osc} from eq. (1.8). Matter adds another scale with H^{mat}, which can be larger and smaller than l_{osc}, so that either can dominate the oscillation length. With the interaction between neutrinos a third length scale comes into play, which can be much smaller than the other two. For neutrino densities as they occur in supernovae it can go down to $\mathcal{O}(10\,\text{cm})$ [79].

The different energy scales only provide information on the oscillation length. The important parameter to investigate flavour *conversion* is the amplitude of the oscillation, i.e. the mixing angle between propagation and flavour basis. In matter the mixing becomes large, when the density is critical. In a neutrino medium the conversion is driven by instabilities, which lead to a fast growth of the mixing angle and are comparable to that of bipolar oscillations. We will look for unstable collective modes in the flavour correlation functions, the off-diagonal elements in the matrix of densities. They describe the overlap between different flavours and therefore are directly connected to their mixing. A very powerful tool for the search of instabilities there is the dispersion relation because unstable are clearly identifiable due to their complex energies. When the energy ω of a plane wave $\sim \mathrm{e}^{\mathrm{i}\omega t}$ acquires an imaginary value, the previously complex exponential becomes real and so either decays or blows up in time. As ω scales with $\mathsf{H}^{\nu\nu}$ from eq. (1.12) in a dense neutrino gas, the conversion takes place on the length scale corresponding to the neutrino potential and is therefore much faster than others. The important parameter, which determines the stability of modes, is almost solely the angular lepton distribution. In this context the surrounding matter has minor influence on the mixing. Because the fast flavour conversion is only initiated by the mixing angle, but driven by the instability, a high matter density cannot suppress it. In order to identify systems with fast flavour conversion easily, criteria on the parameters, which induce instabilities, need to be derived.

The motivation to understand collective effects is not only theoretically driven, but might be important to model and predict accurately the processes in particular environments. A sufficient neutrino abundance is only reached in the early universe, neutron star mergers and core-collapse supernovae. In all of them neutrinos affect the synthesis of nuclei and in the case of supernovae neutrinos might play an additional role. When the star collapses, matter agglomerates in its centre until almost nuclear density is reached and a proto-neutron star formed. The continuously infalling material bounces off this surface and the shock wave appears, which is supposed to eject the outer layers of the star. Via different processes a shock wave loses energy during the propagation and stalls [89]. One of the proposed mechanism to revive it and make the star explode is called neutrino reheating [90], where neutrinos serve as energy transmitters from the inner core to the shock wave. Since for this process the interaction with other fermions is of major importance, possible flavour conversions need to be comprehended and implemented in the simulations.

1.4.4 Ongoing discussions

One frequently discussed topic is the interpretation of the Liouville equation which can be either a wave or a particle transport equation. If it is regarded as an equation for particle transport, neutrinos are often modelled as wave packets. This perception has the drawback that the equation of motion must be solved for each mode individually, but on the other hand the system remains linear even with neutrino-neutrino interactions [91]. The physical reason for the linearity is that a neutrino cannot change its own flavour. Considering eq. (1.6) to be a wave equation does not have the advantage of linearity. However, by refraining from the wave packet approach a closed set of equations is obtained. Additionally in this way the interference character of neutrino oscillations is conveyed.

The other topic is the validity of the mean field approximation and the role of neutrino entanglement. The mean field approximation is relevant as soon as neutrino-neutrino interactions might play a role. It claims that quantum effects like entanglement are smoothed out due to the high number of particles. Mathematically this means that the expectation value of a product of operators is approximately identical to the product of each expectation value, i.e. $\langle \hat{\varrho}\hat{\bar{\varrho}} \rangle \approx \langle \hat{\varrho} \rangle \langle \hat{\bar{\varrho}} \rangle$. The mean field approximation has been recently challenged by numerical calculations which indicate a significant influence of entanglement in systems with up to nine neutrinos [92]. Because the results are not conclusive for a high number of quantum states we stick with the mean field approximation in the following.

CHAPTER 2

Evolution equation for mixed flavour states

The fact that neutrino propagation and their interaction with matter are not describable in the same basis has not only led to confusions in calculations, but also to various ways of deriving and interpreting the evolution equation of neutrino flavours. The differences are based on different approaches, so that results in the literature are not contradictory. Here the formalism based on the matrix of flavour densities is used. In this chapter the equation of motion for the matrix of densities is derived. The main assumptions are motivated, namely mean-field approximation and the ultra-relativistic limit. The result is used for calculations in the subsequent chapters.

2.1 Matrix of densities

Before deriving the equation of motion, neutrino states are combined in a flavour or mass vector $\psi_\alpha = (\psi_\mathrm{e}, \psi_\mu, \psi_\tau, \ldots)_\alpha$. The exact number of fields is arbitrary, since it does not affect the following calculation and opens the possibility to include hypothetical sterile neutrinos. For the derivation of a formula for neutrino flavour evolution during propagation an intuitive first starting point is Schrödinger's equation

$$\mathrm{i}\partial_t|\psi_\alpha\rangle = \mathsf{H}_{\alpha\beta}|\psi_\beta\rangle = \frac{m^2_{\alpha\beta}}{2E}|\psi_\beta\rangle. \tag{2.1}$$

Here $\mathcal{H}_{\alpha\beta}$ has diagonal and off-diagonal terms, where the latter couple the flavour components in $|\psi_\alpha\rangle$. With the substitution $\partial_t = c\partial_x$, which is applicable for relativistic neutrinos, predictions on the conversion and survival probability can be made between the source and a detector. When performing the calculation it becomes clear that eq. (2.1) – despite its deficiencies – gives

correct results for the propagation in vacuum or a medium, e.g. generated by electrons or nucleons.

However, the use of a vector of wavefunctions is not satisfactory for every physical system. When neutrinos undergo scattering with matter, information about flavour correlations can be lost to the environment and the states decohere [93–95]. In such a scenario the wavefunction alone does not provide sufficient information to model interaction effects, which directly influence the correlation between different flavours. In order to include these correlations explicitly we change to a density matrix formulation with $\rho_{\alpha\beta} \equiv |\psi_\alpha\rangle\langle\psi_\beta|$, which is governed by the von Neumann equation

$$\partial_t \rho = -\mathrm{i}\,[\mathsf{H},\, \rho]\,. \tag{2.2}$$

Since anyway the interest is focused on transition probabilities between flavours, it is reasonable to deal with them from the start.

In this thesis the entanglement of neutrinos with their environment is not taken into account as we restrict the system to forward scattering, cf. sec. 2.4. Nevertheless, the density matrix is a useful tool, escpecially for the implementation of neutrino-neutrino interactions.

A quantum mechanical approach to neutrino oscillations is reasonable as a starting point, but not sufficient for more complicated systems. First of all neutrinos are relativistic particles with spin $\frac{1}{2}$ and furthermore they can be produced and annihilated, which leads to source and sink terms in the differential equation. To take these properties into account a QFT equivalent to eq. (2.2) needs to be found, which must be consistent with Dirac's equation for fermionic fields in the mass basis

$$(\mathrm{i}\gamma^\mu \partial_\mu - m_i)\,\hat{\Psi}_i = 0. \tag{2.3}$$

The hat sign denotes an operator in Fock space. Changing this equation to its equivalent for a flavour field $\hat{\Psi}_\alpha = U^*_{\alpha i}\hat{\Psi}_i$ with mixing matrix $U_{i\alpha}$ is straightforward. The main difference is the mass term, which becomes $M_{\alpha\beta} = U_{\alpha i} M_{ij} U^\dagger_{j\beta}$ with $M_{ij} = \mathrm{diag}\,\{m_1,\, m_2,\, m_3,\, \dots\}$. As it is easy to see the differential equations are now coupled via the off-diagonal terms in $M_{\alpha\beta}$, so that the flavour fields do not evolve independently in contrast to their massive counterparts.

Various ways of proceeding from eq. (2.3) to the equation of motion can be found depending on the level of generality and method. In almost all of them the ultra-relativistic limit is taken, so that all effects which are related to the neutrino mass are small. Nevertheless it must be specified which effects are taken into account as the mass does not only lead to flavour oscillation. For example also helicity flips are generated by the mass and considering them adds a new dimension to the evolution of a neutrino gas. However, for this thesis the only relevant consequence of the neutrino mass is the flavour mixing and other phenomena like helicity flips are not regarded.

Furthermore for non-isotropical systems it must be decided how to deal with the spin structure of the fermion field Ψ in the Hamiltonian. In an

unpolarised medium it is allowed to average over all spin configurations, which will be done in the upcoming calculation. In the presence of magnetic fields this simplification is not applicable and the influence of spin must be treated more carefully.

In the literature different derivations of the equation of motion can be found. In refs. [32, 33, 96] the assumptions are similar, i.e. all of them include the spin structure and the mass term for helicity flips. However, the respective methods vary from Dirac's equation with a Wigner transformation [32] via the Keldysh formalism [33] to a two-particle irreducible action [96]. A heuristic approach, which just employs basic physical principles, is also possible [34]. In this paper the transition from a quantum mechanical system with possible superposition of states and Fermi statistics to a classical distribution function for flavour states is investigated.

In order to form the matrix of densities a plane wave expansion for an ultra-relativistic, left-handed fermion field is used

$$\hat{\Psi}_i\left(t,\,\mathbf{x}\right) = \int \frac{\mathrm{d}^3 p}{\left(2\pi\right)^3 \sqrt{2E_{\mathbf{p}}}} \left[\hat{a}_i\left(t,\,\mathbf{p}\right) u_{\mathbf{p}} + \hat{b}_i^\dagger\left(t,\,-\mathbf{p}\right) v_{-\mathbf{p}}\right] \mathrm{e}^{-\mathrm{i}\mathbf{p}\cdot\mathbf{x}}. \tag{2.4}$$

The time-dependent operator $\hat{a}_i$ annihilates a left-handed neutrino and its counterpart $\hat{b}_i^\dagger$ creates a right-handed anti-neutrino, so that the neutrino field is permanently left-handed. According to the previous assumption helicity flips are ruled out. The Fock-space operators obey the anti-commutation relations at equal time

$$\left\{\hat{a}_i\left(t,\,\mathbf{p}\right),\,\hat{a}_j^\dagger\left(t,\,\mathbf{p}'\right)\right\} = \left(2\pi\right)^3 \delta^{(3)}\left(\mathbf{p}-\mathbf{p}'\right)\delta_{ij}. \tag{2.5}$$

With the operators $\hat{a}_i\left(t,\,\mathbf{p}\right)$ and $\hat{b}_i\left(t,\,\mathbf{p}\right)$ it is possible to define two-point correlators for neutrinos and anti-neutrinos by introducing the matrix of densities for each of them

$$\hat{\varrho}_{ij}\left(t,\,\mathbf{p},\,\mathbf{p}'\right) \equiv \hat{a}_j^\dagger\left(t,\,\mathbf{p}\right)\hat{a}_i\left(t,\,\mathbf{p}'\right) \tag{2.6a}$$

$$\hat{\bar{\varrho}}_{ij}\left(t,\,\mathbf{p},\,\mathbf{p}'\right) \equiv \hat{b}_i^\dagger\left(t,\,\mathbf{p}\right)\hat{b}_j\left(t,\,\mathbf{p}'\right). \tag{2.6b}$$

It contains all relevant information to describe neutrino oscillations. Specifically neutrino-neutrino coupling can be included with an appropriate interaction term as well as collisions with the surrounding medium. In the following only $\hat{\varrho}$ and $\hat{\bar{\varrho}}$ are considered, whereas combinations of $\hat{a}$ and $\hat{b}$ that violate the lepton number or correlate particles and antiparticles are not taken into account. The reversed order of indices in eqs. (2.6) was used in ref. [31] to ensure that the rotation between the mass and flavour basis is identical for $\hat{\varrho}$ and its antineutrino counterpart.

The expectation value of eq. (2.6a) is the matrix of densities $\varrho \equiv \langle\hat{\varrho}\rangle$ (note the different notation compared to the density matrix ρ). The difference between ϱ and ρ becomes clear when looking at their diagonal entries.[1] For

[1] The matrices are only comparable when the momenta $\mathbf{p}$ and $\mathbf{p}'$ are integrated out in ϱ.

the matrix of densities the values on the diagonal are occupation numbers of flavour or mass eigenstates and their sum, i.e. the trace of ϱ, is the total neutrino number of the ensemble. Furthermore additional particles can be created or annihilated via the appropriate operators $\hat{a}$ and $\hat{a}^\dagger$, so that Tr ϱ is not necessarily conserved. On the other hand the density matrix ρ belongs to an inherent one-particle system, so that its trace is always unity and its diagonal components correspond to probabilities to encounter a specific eigenstate.

2.2 Wigner transformation

Until now the interpretation of $\varrho(t, \mathbf{p}, \mathbf{p}')$ as the transition function between momentum modes is rather abstract. With the Wigner transformation it is possible to assign an almost classical interpretation to it.

Every function can be Wigner transformed as long as it depends on two variables of the same unit. Mathematically it corresponds to performing a Fourier transformation with respect to the difference of these variables [97]. The formula for the transformation and its inverse are

$$F(\mathbf{x}, \mathbf{p}) = \int \frac{\mathrm{d}^3\Delta}{(2\pi)^3}\, \mathrm{e}^{\mathrm{i}\boldsymbol{\Delta}\cdot\mathbf{x}} F\left(\mathbf{p} - \tfrac{\boldsymbol{\Delta}}{2}, \mathbf{p} + \tfrac{\boldsymbol{\Delta}}{2}\right) \tag{2.7}$$

$$F(\mathbf{k}, \mathbf{k}') = \int \mathrm{d}^3x\, \mathrm{e}^{-\mathrm{i}(\mathbf{k}-\mathbf{k}')\cdot\mathbf{x}} F\left(\mathbf{x}, \tfrac{\mathbf{k}+\mathbf{k}'}{2}\right). \tag{2.8}$$

Note that the second equation is equivalent to

$$F\left(\mathbf{p} - \tfrac{\boldsymbol{\Delta}}{2}, \mathbf{p} + \tfrac{\boldsymbol{\Delta}}{2}\right) = \int \mathrm{d}^3x\, \mathrm{e}^{-\mathrm{i}\boldsymbol{\Delta}\cdot\mathbf{x}} F(\mathbf{x}, \mathbf{p}) \tag{2.9}$$

with the substitutions $\boldsymbol{\Delta} = \mathbf{k}' - \mathbf{k}$ and $\mathbf{p} = \frac{1}{2}(\mathbf{k}' + \mathbf{k})$, which will be used later.

The power of the Wigner transformation becomes apparent in a system with two different scales. In the case of oscillating neutrinos one of them is the neutrino momentum scale at which sharp peaks of F appear when $\mathbf{k} \approx \mathbf{k}'$ in particular without or only weak interactions. The other one is the wavelength of flavour oscillations, which is much larger and more interesting for our deliberations. Averaging over momentum smooths out those former variations, so that we end up with a slowly changing function of $\mathbf{x}$.

The Wigner transformation only makes sense in inhomogeneous systems. In a homogeneous system, e.g. the early universe, the different momentum modes in eq. (2.6a) decouple, i.e. $\langle \hat{\tilde{\varrho}}(t, \mathbf{p}, \mathbf{p}') \rangle \propto \delta^{(3)}(\mathbf{p} - \mathbf{p}')$. In this case the matrix of densities is a four-dimensional function of time and momentum. The motivation for the upcoming calculations is a supernova scenario, which is far from being homogeneous with consequences for the evolution equation.

A special case is the Wigner function, which is obtained by performing Wigner transformation for a product of quantum mechnical wavefunctions or

Fock-space operators. The matrix of flavour densities is a Wigner function following from the two-point correlators in eqs. (2.6)

$$\hat{\varrho}_{ij}\left(t,\,\mathbf{x},\,\mathbf{p}\right)=\int\frac{\mathrm{d}^3\Delta}{\left(2\pi\right)^3}\,\mathrm{e}^{\mathrm{i}\boldsymbol{\Delta}\cdot\mathbf{x}}\,\hat{a}_j^\dagger\left(t,\,\mathbf{p}-\tfrac{\boldsymbol{\Delta}}{2}\right)\,\hat{a}_i\left(t,\,\mathbf{p}+\tfrac{\boldsymbol{\Delta}}{2}\right). \tag{2.10}$$

The result is an almost classical particle distribution function, i.e. a diagonal entry of ϱ specifies the occupation number of a neutrino mode with momentum $\mathbf{p}$ at a particular point in spacetime.

The interpretation of $\langle\hat{\varrho}\left(t,\,\mathbf{x},\,\mathbf{p}\right)\rangle$ as a distribution function must be treated with care. The matrix of densities is still a quantum and not a classical object and so all values it attains for fixed position and momentum are physically meaningless as Heisenberg's uncertainty principle is violated. In order to restore the interpretation of ϱ as position dependent occupation numbers the uncertainty principle must be implemented by hand via averaging over an appropriate volume of configuration space. This process also makes the Wigner function positive definite [98], which was an issue because negative occupation numbers do not make sense. For neutrino oscillations this behaviour of the Wigner function is not relevant as the oscillation scale is much larger than the quantum scale of a neutrino.

A modification of eq. (2.7) is the Husimi transformation [99]. It is obtained by smoothing the original function F, e.g. the Wigner function, with the help of Gaussians for position and momentum [37]

$$F_{\mathrm{H}}\left(\mathbf{x},\,\mathbf{p}\right)=\int\frac{\mathrm{d}^3x'\mathrm{d}^3p'}{\left(2\pi\eta\sigma\right)^3}\,F\left(\mathbf{x},\,\mathbf{p}\right)\exp\left\{-\frac{\left(\mathbf{x}-\mathbf{x}'\right)^2}{2\eta^2}-\frac{\left(\mathbf{p}-\mathbf{p}'\right)^2}{2\sigma^2}\right\}. \tag{2.11}$$

The quantities η and σ are the length and momentum scales, respectively, over which the Wigner function $F\left(\mathbf{x},\,\mathbf{p}\right)$ is smeared and as long as $\eta\sigma\geq\hbar$ holds, F_{H} is positive definite [98]

A question that might arise, when looking at eq. (2.10), is why the matrix of densities was not Wigner transformed in the time sector as well. This was done in ref. [32, 33, 35, 96] and leads to manifestly Lorentz invariant structure of the differential equation for $\varrho\left(t,\,\mathbf{x},\,E,\,\mathbf{p}\right)$. In our setting we make the approximation that all neutrinos are on-shell, i.e. their energy uniquely fixed by position, momentum and conceivably time. This assumption only applies to free particles, which are not realised in nature strictly speaking. Therefore scattering processes must be rare enough that neutrinos can be modelled as free in the meantime. Especially the effect of neutrinos that appear in loop processes cannot be taken into account.

2.3 Moyal equation

For deriving the equation of motion of ϱ it is necessary to deduce one for the creation and annihilation operators $\hat{a}_i^\dagger$ and $\hat{a}_i$ as they appear in eq. (2.4). The obvious choice is the Heisenberg equation $\mathrm{i}\partial_t \hat{A} = \left[\hat{A},\, \hat{H}\right]$ for an operator $\hat{A}$ and the Hamiltonian $\hat{H}$, which can be written in the form

$$\hat{H} = \int \frac{\mathrm{d}^3 p}{(2\pi)^3} \frac{\mathrm{d}^3 p'}{(2\pi)^3}\, \hat{a}_i^\dagger\left(\mathbf{p}'\right) \mathsf{H}_{ij}\left(\mathbf{p},\, \mathbf{p}'\right) \hat{a}_j\left(\mathbf{p}\right). \tag{2.12}$$

Here H_{ij} is the transition matrix between two mass states in different momentum modes. For brevity the time dependence of all quantities is not stated explicitly from now on.

In general H is an operator in the Fock space of those particles, which contribute to the refraction of neutrinos. Thus eq. (2.12) is only valid as long as the expectation value of that operator can be taken. This is relevant, when neutrino-neutrino interaction has an effect because then the expectation value of $\hat{\mathsf{H}}$ is only calculable in the mean-field approximation. Without additional terms would appear in the equation of motion. The basis of this approximation is the assumption that the expectation value of every product of operators is (approximately) equivalent to the product of their individual expectation values, i.e. $\langle \hat{\varrho}\hat{\varrho} \rangle = \langle \hat{\varrho} \rangle \langle \hat{\varrho} \rangle$. Physically this means that entanglement between neutrinos is either negligible or non-existent. The validity of the mean-field approximation has been questioned recently. In ref. [92] it is argued that at high density entanglement between different neutrinos cannot be neglected and leads to additional effects. If this turns out to be true, the mean-field approach is not applicable and concepts from many-body physics have to used. As explained in subsection 1.4.4 we stay in the mean-field setting, since this issue has not been finally resolved and the contradicting results from older papers not been refuted [100, 101].

A short comment about the connection of eqs. (2.3) and (2.4) with Heisenberg's equation and the way of writing the Hamiltonian is appropriate. Plugging the plane wave expansion into Dirac's equation it is straightforward to derive a first order wave equation for $\hat{a}_i$ by multiplying with $u_{\mathbf{p}}\gamma^0$ from the right. The equivalence then becomes obvious, when eq. (2.12) is used in the Heisenberg equation for $\hat{a}_i$ and the anticommutators applied to derive

$$\mathrm{i}\partial_t \hat{a}_i\left(\mathbf{p}\right) = \int \frac{\mathrm{d}^3 p'}{(2\pi)^3} \mathsf{H}_{ik}\left(\mathbf{p}',\, \mathbf{p}\right) \hat{a}_k\left(\mathbf{p}'\right). \tag{2.13}$$

The corresponding equation for the antiparticle operator $\hat{b}_i$ is computed analogously.

With eq. (2.13) it is straightforward to compute the time evolution of the matrix of densities $\varrho\left(\mathbf{p},\, \mathbf{p}'\right)$. Taking the expectation value and performing a

Wigner transformation we get

$$\begin{aligned} \mathrm{i}\partial_t \hat{\varrho}_{ij}(\mathbf{x},\mathbf{p}) = \int \frac{\mathrm{d}^3\Delta}{(2\pi)^3}\,\frac{\mathrm{d}^3p'}{(2\pi)^3}\,\mathrm{e}^{\mathrm{i}\boldsymbol{\Delta}\cdot\mathbf{x}} \\ \times\Big[\mathsf{H}_{ik}\left(\mathbf{p}+\tfrac{\boldsymbol{\Delta}}{2},\mathbf{p}'\right)\,\hat{a}_j^\dagger\left(\mathbf{p}-\tfrac{\boldsymbol{\Delta}}{2}\right)\,\hat{a}_k\left(\mathbf{p}'\right) \\ -\hat{a}_k^\dagger\left(\mathbf{p}'\right)\,\hat{a}_i\left(\mathbf{p}+\tfrac{\boldsymbol{\Delta}}{2}\right)\,\mathsf{H}_{kj}\left(\mathbf{p}-\tfrac{\boldsymbol{\Delta}}{2},\mathbf{p}'\right)\Big]. \end{aligned} \tag{2.14}$$

The definition of $\boldsymbol{\Delta}_1$ and $\boldsymbol{\Delta}_2$ via $\mathbf{p}' = \mathbf{p} + \frac{1}{2}(\boldsymbol{\Delta}_1 - \boldsymbol{\Delta}_2)$ and $\boldsymbol{\Delta} = \boldsymbol{\Delta}_1 + \boldsymbol{\Delta}_2$ leads to the more symmetric expression

$$\begin{aligned} \mathrm{i}\partial_t \hat{\varrho}_{ij}\left(\mathbf{x},\,\mathbf{p}\right) = \int\frac{\mathrm{d}^3\Delta_1}{(2\pi)^3}\,\frac{\mathrm{d}^3\Delta_2}{(2\pi)^3}\,\mathrm{e}^{\mathrm{i}(\boldsymbol{\Delta}_1+\boldsymbol{\Delta}_2)\cdot\mathbf{x}} \\ \times\Big[\mathsf{H}_{ik}\left(\mathbf{p}_1+\tfrac{\boldsymbol{\Delta}_2}{2},\mathbf{p}_1-\tfrac{\boldsymbol{\Delta}_2}{2}\right)\,\hat{a}_j^\dagger\left(\mathbf{p}_2-\tfrac{\boldsymbol{\Delta}_1}{2}\right)\,\hat{a}_k\left(\mathbf{p}_2+\tfrac{\boldsymbol{\Delta}_1}{2}\right) \\ -\hat{a}_k^\dagger\left(\mathbf{p}_1-\tfrac{\boldsymbol{\Delta}_2}{2}\right)\,\hat{a}_i\left(\mathbf{p}_1+\tfrac{\boldsymbol{\Delta}_2}{2}\right)\,\mathsf{H}_{kj}\left(\mathbf{p}_2-\tfrac{\boldsymbol{\Delta}_1}{2},\mathbf{p}_2+\tfrac{\boldsymbol{\Delta}_1}{2}\right)\Big], \end{aligned} \tag{2.15}$$

where the notation $\mathbf{p}_1 = \mathbf{p} + \frac{1}{2}\boldsymbol{\Delta}_1$ and $\mathbf{p}_2 = \mathbf{p} - \frac{1}{2}\boldsymbol{\Delta}_2$ was used for brevity. Notice that evaluating the integrals over $\mathrm{d}^3\Delta_{1,2}$ does not produce Wigner transforms because $\boldsymbol{\Delta}_{1,2}$ is also hidden in $\mathbf{p}_{1,2}$. However, under the integral we can substitute for each factor the inverse Wigner transformation in the form of equation (2.9) and find

$$\begin{aligned} \mathrm{i}\partial_t \hat{\varrho}_{\mathbf{x},\mathbf{p}} = \int \frac{\mathrm{d}^3\Delta_1}{(2\pi)^3}\,\frac{\mathrm{d}^3\Delta_2}{(2\pi)^3}\,\mathrm{d}^3x_1\,\mathrm{d}^3x_2\,\mathrm{e}^{-\mathrm{i}\boldsymbol{\Delta}_1\cdot(\mathbf{x}_1-\mathbf{x})-\mathrm{i}\boldsymbol{\Delta}_2\cdot(\mathbf{x}_2-\mathbf{x})} \\ \times\Big[\mathsf{H}_{\mathbf{x}_2,\mathbf{p}_1}\,\hat{\varrho}_{\mathbf{x}_1,\mathbf{p}_2} - \hat{\varrho}_{\mathbf{x}_2,\mathbf{p}_1}\,\mathsf{H}_{\mathbf{x}_1,\mathbf{p}_2}\Big], \end{aligned} \tag{2.16}$$

where $\mathbf{x}_{1,2}$ are the conjugate variables to $\boldsymbol{\Delta}_{1,2}$.

To obtain the argument $\mathbf{p}$ instead of $\mathbf{p}_{1,2}$ we use the shift operator in the form $F(\mathbf{k}+\mathbf{q}) = \mathrm{e}^{\mathbf{q}\cdot\partial_\mathbf{k}}F(\mathbf{k})$. This construction implies e.g. for the Hamiltonian $\mathsf{H}(\mathbf{x}_2,\mathbf{p}_1) = \mathrm{e}^{\frac{1}{2}\boldsymbol{\Delta}_1\cdot\partial_\mathbf{p}}\mathsf{H}(\mathbf{x}_2,\mathbf{p})$ and overall we find

$$\begin{aligned} \mathrm{i}\partial_t \hat{\varrho}_{\mathbf{x},\mathbf{p}} = \int \frac{\mathrm{d}^3\Delta_1}{(2\pi)^3}\,\frac{\mathrm{d}^3\Delta_2}{(2\pi)^3}\,\mathrm{d}^3x_1\,\mathrm{d}^3x_2 \\ \times\Big[\mathsf{H}_{\mathbf{x}_2,\mathbf{p}}\,\mathrm{e}^{-\mathrm{i}\boldsymbol{\Delta}_1\cdot\left(\mathbf{x}_1-\mathbf{x}+\frac{\mathrm{i}}{2}\overleftarrow{\partial}_\mathbf{p}\right)-\mathrm{i}\boldsymbol{\Delta}_2\cdot\left(\mathbf{x}_2-\mathbf{x}-\frac{\mathrm{i}}{2}\overrightarrow{\partial}_\mathbf{p}\right)}\,\hat{\varrho}_{\mathbf{x}_1,\mathbf{p}} \\ -\hat{\varrho}_{\mathbf{x}_2,\mathbf{p}}\,\mathrm{e}^{-\mathrm{i}\boldsymbol{\Delta}_1\cdot\left(\mathbf{x}_1-\mathbf{x}+\frac{\mathrm{i}}{2}\overleftarrow{\partial}_\mathbf{p}\right)-\mathrm{i}\boldsymbol{\Delta}_2\cdot\left(\mathbf{x}_2-\mathbf{x}-\frac{\mathrm{i}}{2}\overrightarrow{\partial}_\mathbf{p}\right)}\,\mathsf{H}_{\mathbf{x}_1,\mathbf{p}}\Big], \end{aligned} \tag{2.17}$$

where $\overleftarrow{\partial}_\mathbf{p}$ means that the differential operator is to be applied to the expression left of it. Representing the delta function as $\delta^{(3)}(\mathbf{x}) = \int \mathrm{d}^3\Delta\,\mathrm{e}^{\mathrm{i}\boldsymbol{\Delta}\cdot\mathbf{x}}/(2\pi)^3$ it is now straightforward to evaluate the integrals[2] and, for example, the first term in square brackets becomes $\mathsf{H}\big(\mathbf{x}+\frac{\mathrm{i}}{2}\overrightarrow{\partial}_\mathbf{p},\mathbf{p}\big)\,\hat{\varrho}\big(\mathbf{x}-\frac{\mathrm{i}}{2}\overleftarrow{\partial}_\mathbf{p},\mathbf{p}\big)$. The differential

[2]The δ-function of a momentum derivative arising in eq. (2.17) can be avoided. This is

operator in the argument of one matrix is to be applied to the other matrix. A more elegant way to express this structure is found by using once more the shift operator to lift the deviation from $\mathbf{x}$ in the arguments to an exponential,

$$\mathrm{i}\partial_t \hat{\varrho}_{\mathbf{x},\mathbf{p}} = \mathsf{H}_{\mathbf{x},\mathbf{p}}\, \mathrm{e}^{\frac{\mathrm{i}}{2}\left(\overleftarrow{\partial}_{\mathbf{x}}\cdot\overrightarrow{\partial}_{\mathbf{p}} - \overleftarrow{\partial}_{\mathbf{p}}\cdot\overrightarrow{\partial}_{\mathbf{x}}\right)}\, \hat{\varrho}_{\mathbf{x},\mathbf{p}} - \hat{\varrho}_{\mathbf{x},\mathbf{p}}\, \mathrm{e}^{\frac{\mathrm{i}}{2}\left(\overleftarrow{\partial}_{\mathbf{x}}\cdot\overrightarrow{\partial}_{\mathbf{p}} - \overleftarrow{\partial}_{\mathbf{p}}\cdot\overrightarrow{\partial}_{\mathbf{x}}\right)}\, \mathsf{H}_{\mathbf{x},\mathbf{p}}\,. \tag{2.18}$$

An equation equivalent to this result was first derived by Moyal with two minor differences [102]. We here use matrices in flavor space as opposed to scalar functions and our matrix $\hat{\varrho}$ is derived from a second-quantized operator in contrast to a purely quantum-mechanical setting. We also note that if we were to keep Planck's constant $\hbar$, it would multiply the left hand side of equation (2.18) as well as the exponents on the right-hand side.

Under the assumption that the variation of H and $\hat{\varrho}$ is slow in coordinate and momentum space eq. (2.18) can be expanded to first order. The result is a modified version of the frequently used Liouville equation

$$\partial_t \hat{\varrho} + \tfrac{1}{2}\left\{\partial_{\mathbf{p}}\mathsf{H}\,, \partial_{\mathbf{x}}\hat{\varrho}\right\} - \tfrac{1}{2}\left\{\partial_{\mathbf{x}}\mathsf{H}\,, \partial_{\mathbf{p}}\hat{\varrho}\right\} = -\mathrm{i}\left[\mathsf{H}\,, \hat{\varrho}\right]. \tag{2.19}$$

Our notation implies that scalar products of the gradients in the anticommutators are taken.

The first anticommutator describes the advection of neutrinos, where $\partial_{\mathbf{p}}\mathsf{H}$ is interpreted as a matrix of velocities. This term is often simplified to $\mathbf{v}\cdot\partial_{\mathbf{x}}\hat{\varrho}$, where $\mathbf{v}$ is a unit vector without matrix character. A closer look at the momentum derivative of the Hamiltonian clarifies this approximation. In the relativistic limit one can write

$$\mathsf{H}_{ij} = \delta_{ij}\sqrt{\mathbf{p}^2 + m_i^2} \approx \delta_{ij}\left(|\mathbf{p}| - \frac{m_i^2}{2\,|\mathbf{p}|}\right). \tag{2.20}$$

The first term is proportional to the identity matrix, so that for this part the anticommutator vanishes. When calculating the momentum derivative explicitly, one obtains $\frac{\mathbf{p}}{|\mathbf{p}|}\cdot\partial_{\mathbf{x}}\hat{\varrho}$. The mass term in eq. (2.20) is non-diagonal in the flavour basis and is considered to be responsible for the kinematical decoherence of the propagation eigenstates [36]. This means that the accumulated

---

demonstrated by a simplified version of eq. (2.16),

$$\begin{aligned}\int \mathrm{d}x_1 \frac{\mathrm{d}\Delta}{2\pi} e^{-\mathrm{i}\Delta(x_1-x)} f\left(p+\Delta\right) g\left(x_1\right) &= \int \mathrm{d}x_1 \frac{\mathrm{d}\Delta}{2\pi} e^{-\mathrm{i}\Delta(x_1-x)} \sum_{n=0}^{\infty} \frac{1}{n!}\left(\Delta\partial_p\right)^n f(p) g\left(x_1\right) \\ &= \sum_n \frac{1}{n!} \int \mathrm{d}x_1 \frac{\mathrm{d}\Delta}{2\pi} e^{-\mathrm{i}\Delta(x_1-x)} \left(\mathrm{i}\overleftarrow{\partial}_{x_1-x}\overrightarrow{\partial}_p\right)^n f(p) g\left(x_1\right) \\ &= \sum_n \frac{\mathrm{i}^n}{n!} f^{(n)}(p) \int \mathrm{d}x_1 \delta^{(n)}\left(x_1 - x\right) g\left(x_1\right).\end{aligned}$$

After an integration by parts it is obvious that a δ-function of a derivative leads to the same result as a sum of derivatives of a δ-function in this specific context.

phase between flavour states becomes harder to measure with increasing distance. Comparing the scales of this decoherence term (with $\partial_{\mathbf{x}}\hat{\varrho} \sim 1/l_{\mathrm{osc}}\hat{\varrho}$ cf. eq. (1.8)) and the oscillation term on the right hand side of eq. (2.19) shows that the former is suppressed by $\frac{m_i^2}{\mathbf{p}^2}$. In this thesis only the leading mass term, responsible for neutrino oscillations, is taken into account and so the advection term becomes $\mathbf{v}\cdot\partial_{\mathbf{x}}\hat{\varrho}$, when identifying $\mathbf{v} \equiv \frac{\mathbf{p}}{|\mathbf{p}|}$. The vector $\mathbf{v}$ can be interpreted as a velocity, which matches our intuition for $\partial_{\mathbf{p}}\mathsf{H}$.

The second anticommutator describes the influence of a spatially varying potential on the momentum of the neutrinos. Possible effects of an external potential are redshift and deflection. This thesis concentrates on neutrino refraction that is sourced by interaction terms without considering the dynamical evolution when propagating in a changing medium. Accordingly the second anticommutator is neglected in following calculations.

In ref. [35] the analogue to eq. (2.19) is derived for two-point correlators. In contrast to the matrix of densities these objects have an explicit energy dependence, which sources an additional anticommutator term of the form $\{\partial_t\mathsf{H},\, \partial_E\hat{\varrho}\}$. Obviously it is only relevant for a time-dependent Hamiltonian and accounts for changes in the spectrum when the external potential varies.

There are no further assumptions necessary to deduce the evolution equation for the matrix of densities $\varrho = \langle\hat{\varrho}\rangle$ from eq. (2.18). The mean field approximation was already used to justify that H is not a Fock space operator and so only $\hat{\varrho}$ acts non-trivially on the Fock state of the system.

2.3.1 Oscillation in vacuum

As an example the derivation of the vacuum oscillation probability (1.9) from the Liouville equation (2.19) is illustrated. The system is assumed to be one-dimensional and stationary, so that the time derivative is zero and the advection term does not need a scalar product. Neutrinos are ultra-relativistic and for simplicity have only two flavours. With these approximations eq. (2.20) is applicable and for the derivative $\partial_{\mathbf{p}}\mathsf{H} \approx \mathbb{1}_2$ holds, where $\mathbb{1}_2$ represents the 2×2 identity matrix. In the mass basis the Hamiltonian is diagonal and so the commutator with ϱ is zero on the diagonal. The other entries are complex conjugated and satisfy the differential equation

$$\partial_x \varrho_{12} = -\mathrm{i}\frac{2\pi}{l_{\mathrm{osc}}}\varrho_{12}. \tag{2.21}$$

The occupation numbers of the mass eigenstates remain constant during the evolution and the differential equation for the mass correlation function is solved by

$$\varrho_{12}(x) = A_{12}\exp\left\{-\mathrm{i}\frac{2\pi}{l_{\mathrm{osc}}}x\right\}. \tag{2.22}$$

The variable A_{12} is an entry of the amplitude matrix, which must be fixed from boundary conditions. In order to obtain the matrix of densities in flavour space it needs to be rotated with the mixing matrix in eq. (1.5), i.e. $\varrho_{\alpha\beta} = U^*_{\alpha i}\varrho_{ij}U_{j\beta}$.

Assuming that the source emits electron neutrinos exclusively the boundary condition is $\varrho_{\alpha\beta}(0) = \delta_{\mathrm{ee}}$, which rotated to the mass basis is identical to the amplitude matrix

$$A_{ij} = U_{i\alpha}\varrho_{\alpha\beta}(0)\,U^*_{\beta j} = \begin{pmatrix} \cos^2\theta_{\mathrm{v}} & \frac{1}{2}\sin 2\theta_{\mathrm{v}} \\ -\frac{1}{2}\sin 2\theta_{\mathrm{v}} & \sin^2\theta_{\mathrm{v}} \end{pmatrix}. \tag{2.23}$$

With this input the solution for $\varrho_{ij}(x)$ can be rotated to the flavour basis and the $\varrho_{\mu\mu}(x)$ entry coincides with the oscillation probability in eq. (1.9).

Let us see what changes when the deviations of the matrix of velocities from the identity matrix are explicitly included in this setting. Then the term $\partial_{\mathbf{p}}\mathsf{H}$ has the structure

$$\mathsf{V} \equiv \partial_{\mathbf{p}} \begin{pmatrix} \sqrt{\mathbf{p}^2 + m_1^2} & 0 \\ 0 & \sqrt{\mathbf{p}^2 + m_2^2} \end{pmatrix} = \mathbf{v}\mathbb{1}_2 + \frac{\delta\mathbf{v}}{2}\sigma_3. \tag{2.24}$$

The first term $\mathbf{v}$ contains the contribution proportional to the identity matrix and the second term the difference $\delta\mathbf{v}$ with Pauli matrix σ_3. In the considered one-dimensional, stationary system the evolution equation becomes

$$\partial_x\varrho + \frac{\delta v}{2v}\{\sigma_3,\, \partial_x\varrho\} = -\frac{\mathrm{i}}{v}[\mathsf{H},\, \varrho]\,. \tag{2.25}$$

In comparison with eq. (2.21) the anticommutator is new, but it does not correspond to a damping term [37]. This can be derived from the fact, that the differential operator is identical to the one governing the evolution. Furthermore $\{\sigma_3,\, \partial_x\varrho\}$ is diagonal and so in the case of vacuum oscillations only nonzero for constant parts of ϱ, i.e. it does not change the evolution. The only modification comes from the factor $1/v$ on the right hand side and decreases the oscillation length slightly.

One should keep in mind that the proposed damping from the anticommutator was attributed to the separation of wave packets [36]. In a stationary scenario with plane waves the study of wave packet separation is certainly futile and so the calculated example cannot account for this effect.

2.4 Matter refraction

When the coupling of neutrinos with the surrounding matter or other neutrinos is relevant for the oscillation behaviour, the Hamiltonian in eq. (2.19) must be supplemented with the appropriate interaction terms. The most well-known and established consequence of matter refraction is the resonant conversion from the interaction of electron neutrinos with electrons, which leads to the MSW-effect [39, 40]. This section is intended to illuminate how the Standard Model coupling is transformed to the refractive terms as they can be found in the literature on neutrino oscillations.

The refraction of a neutrino via matter effects is sourced by scattering processes that change neither the kinematic components of the scattering partners nor their respective properties like the flavour. On the kinematical level this effect is implemented later by restricting the calculation to forward scattering. The other parts of the simplification are used from the start. For example it is not necessary to take neutrino creation and annihilation into account because these effects change the neutrino gas as well as the environment. In a realistic environment like a supernova this would be an unreasonable approximation, but it is sufficient for neutrino refraction.

Since neutrinos have neither electrical charge nor colour, the only coupling is to W and Z-bosons. It is assumed that the energy transfer is small, so that these particles can be integrated out and Fermi's theory for weak interactions is applicable. Then the interaction terms from the Standard Model for neutral and charged currents can be written as

$$\hat{H}_{\mathrm{CC}}^{\mathrm{int}} = \frac{G_{\mathrm{F}}}{\sqrt{2}} \sum_{l} \int \mathrm{d}^3x \, \hat{\bar{\psi}}_{\nu_l} \gamma^\mu \left(1 - \gamma^5\right) \hat{\psi}_l \hat{\bar{\psi}}_l \gamma_\mu \left(1 - \gamma^5\right) \hat{\psi}_{\nu_l} \tag{2.26}$$

$$\hat{H}_{\mathrm{NC}}^{\mathrm{int}} = \frac{G_{\mathrm{F}}}{\sqrt{2}} \sum_{f,\,l} \int \mathrm{d}^3x \, \hat{\bar{\psi}}_{\nu_l} \gamma^\mu \left(1 - \gamma^5\right) \hat{\psi}_{\nu_l} \tag{2.27}$$
$$\hat{\bar{\psi}}_f \gamma_\mu \left(I^3 \left(1 - \gamma^5\right) - 2 q_{\mathrm{em}} \sin^2 \theta_{\mathrm{W}}\right) \hat{\psi}_f .$$

In the first equation a lepton l and an (anti-)neutrino of the same flavour scatter via exchange of a W-boson. G_{F} is the Fermi coupling constant, which depends on the coupling constant of the weak interaction and the mass of the W-boson. In the second equation I^3 denotes the weak isospin and q_{em} the electromagnetic charge of the fermion; the latter appears in combination with the weak mixing angle θ_{W} which rotates the gauge fields W^3 and B to form the photon and Z-boson field. Due to this structure every left-handed or charged elementary particle couples to the Z-boson.

In the following it is explained how the scattering processes sourced by eqs. (2.26) and (2.27) can be brought to a form, which can be implemented in the transition matrix H in eq. (2.12). The important difference between them is the spinor term, which mainly contributes the kinematical part of the coupling and can be simplified notably for forward scattering. Before the derivation one should note that $\hat{H}_{\mathrm{CC}}^{\mathrm{int}}$ already has a form comparable to eq. (2.12) and after a Fierz transformation also $\hat{H}_{\mathrm{NC}}^{\mathrm{int}}$ has the structure $\hat{\bar{\psi}}_\nu \hat{\mathcal{O}} \hat{\psi}_\nu$.

As an example the scattering $\nu_{\mathrm{e}} + \mathrm{e}^- \to \nu_{\mathrm{e}} + \mathrm{e}^-$ under exchange of a W-boson is calculated. Effectively the neutral channel does not influence neutrino oscillation as it is independent of flavour and hence its contribution to H is proportional to the identity matrix in the flavour basis. Most scattering processes via exchange of a Z-boson are irrelevant for neutrino oscillation as long as the scattering partner is not in a mixed flavour state. Therefore the only particle species in the Standard Model for which $\hat{H}_{\mathrm{NC}}^{\mathrm{int}}$ is important in the context of neutrino oscillation are neutrinos themselves.

These considerations imply the Hamiltonian for ν_ee-scattering

$$\hat{H}^{\mathrm{int}}_{\nu_\mathrm{e}\mathrm{e}} = \frac{G_\mathrm{F}}{\sqrt{2}} \int \mathrm{d}^3x \, \hat{\bar{\psi}}_{\nu_\mathrm{e}} \gamma_\mu \left(1-\gamma^5\right) \hat{\psi}_\mathrm{e} \hat{\bar{\psi}}_\mathrm{e} \gamma^\mu \left(1-\gamma^5\right) \hat{\psi}_{\nu_\mathrm{e}}. \tag{2.28}$$

Inserting now the plane wave expansion for the Dirac fields[3] results in several terms, but only a single one describes the scattering diagram we are interested in. The operators on the neutrino Fock space and corresponding momentum integrals are removed from the formula to obtain the refraction term in the transition matrix H in eq. (2.12). Its only nonzero element in the flavour basis is

$$\mathsf{H}_{11}\left(\mathbf{p},\, \mathbf{p}'\right) = \frac{G_\mathrm{F}}{8\sqrt{2E_\mathbf{p}E_{\mathbf{p}'}}} \sum_{h_\mathrm{e},\, h'_\mathrm{e}} \int \mathrm{d}^3x \, \frac{\mathrm{d}^3p_\mathrm{e}}{(2\pi)^3} \frac{\mathrm{d}^3p'_\mathrm{e}}{(2\pi)^3} \frac{1}{\sqrt{E_{\mathbf{p}_\mathrm{e}}E_{\mathbf{p}'_\mathrm{e}}}} \mathrm{e}^{-\mathrm{i}(\mathbf{p}+\mathbf{p}_\mathrm{e}-\mathbf{p}'-\mathbf{p}'_\mathrm{e})\cdot\mathbf{x}} \tag{2.29}$$

$$\cdot\, \bar{u}_{\mathbf{p}'} \gamma^\mu \left(1-\gamma^5\right) u^{h_\mathrm{e}}_{\mathbf{p}_\mathrm{e}} \bar{u}^{h'_\mathrm{e}}_{\mathbf{p}'_\mathrm{e}} \gamma_\mu \left(1-\gamma^5\right) u_\mathbf{p} \left\langle \hat{a}^\dagger_{\mathbf{p}'_\mathrm{e},\, h'_\mathrm{e}} \hat{a}_{\mathbf{p}_\mathrm{e},\, h_\mathrm{e}} \right\rangle.$$

Here the average of electron helicities is computed. The integral over space and one electron momentum can be performed and together with the exponential enforce momentum conservation during the process.

At this point the limitation to neutrino refraction is implemented. On the one hand this means that the helicity of the electron does not change $h'_\mathrm{e} = h_\mathrm{e}$. On the other hand the respective initial and final momenta of the scattering partners are identical, i.e. $\mathbf{p}' = \mathbf{p}$ and $\mathbf{p}'_\mathrm{e} = \mathbf{p}_\mathrm{e}$. Both assumptions are mathematically integrated in eq. (2.29) by introducing the factor $\delta_{h'_\mathrm{e}h_\mathrm{e}} \left(2\pi\right)^3 \delta^{(3)}\left(\mathbf{p}'_\mathrm{e} - \mathbf{p}_\mathrm{e}\right)$. After performing the summation over h'_e and the integration over $\mathbf{p}'_\mathrm{e}$ eq. (2.29) becomes

$$\mathsf{H}_{11}\left(\mathbf{p},\, \mathbf{p}'\right) = \frac{G_\mathrm{F}}{8E_\mathbf{p}\sqrt{2}} \left(2\pi\right)^3 \delta^{(3)}\left(\mathbf{p}' - \mathbf{p}\right) \sum_{h_\mathrm{e}} \int \frac{\mathrm{d}^3p_\mathrm{e}}{(2\pi)^3} \frac{1}{E_{\mathbf{p}_\mathrm{e}}} \tag{2.30}$$

$$\times\, \bar{u}_\mathbf{p} \gamma^\mu \left(1-\gamma^5\right) u^{h_\mathrm{e}}_{\mathbf{p}_\mathrm{e}} \bar{u}^{h_\mathrm{e}}_{\mathbf{p}_\mathrm{e}} \gamma_\mu \left(1-\gamma^5\right) u_\mathbf{p} \left\langle \hat{a}^\dagger_{\mathbf{p}_\mathrm{e},\, h_\mathrm{e}} \hat{a}_{\mathbf{p}_\mathrm{e},\, h_\mathrm{e}} \right\rangle.$$

The last term is identical to the occupation number of an electron mode with specific helicity. For notational compactness we define

$$N_\mathrm{e}\left(\mathbf{p}_\mathrm{e},\, h_\mathrm{e}\right) \equiv \left\langle \hat{a}^\dagger_{\mathbf{p}_\mathrm{e},\, h_\mathrm{e}} \hat{a}_{\mathbf{p}_\mathrm{e},\, h_\mathrm{e}} \right\rangle. \tag{2.31}$$

In the following it is assumed that the medium is not polarised, which means that N_e is independent of helicity as the respective occupation numbers for $h_\mathrm{e} = \pm 1$ are identical.

The only part of the transition matrix that needs to be modified is the spinor product. It is simplified by plugging the formula for Dirac spinors in the helicity representation [38]

$$u^h_\mathbf{p} = \begin{pmatrix} \sqrt{E_\mathbf{p} + m}\, \chi^h_\mathbf{p} \\ h\sqrt{E_\mathbf{p} - m}\, \chi^h_\mathbf{p} \end{pmatrix}, \tag{2.32}$$

[3] Since the electrons are massive, the creation and annihilation operator have a helicity index and the sum over all helicity states must be added in eq. (2.4).

where $\chi^h_{\mathbf{p}}$ is an eigenstate of the helicity operator $\hat{\mathbf{p}} \cdot \boldsymbol{\sigma}$ corresponding to the eigenvalue $h = \pm 1$ (right/left-handed). During the calculation the identity $\chi^{h\,\dagger}_{\mathbf{p}} \sigma^\mu \chi^h_{\mathbf{p}} = (1,\, h\,\hat{\mathbf{p}})^\mu$ is useful and in the end one obtains

$$\bar{u}_{\mathbf{p}} \gamma^\mu \left(1 - \gamma^5\right) u^{h_\mathrm{e}}_{\mathbf{p}_\mathrm{e}} \bar{u}^{h_\mathrm{e}}_{\mathbf{p}_\mathrm{e}} \gamma_\mu \left(1 - \gamma^5\right) u_{\mathbf{p}} = 8 E_{\mathbf{p}} \left(E_{\mathbf{p}_\mathrm{e}} - h_\mathrm{e} p_\mathrm{e}\right) \left(1 + h_\mathrm{e} \frac{\mathbf{p} \cdot \mathbf{p}_\mathrm{e}}{p\, p_\mathrm{e}}\right) \tag{2.33}$$

with $p_f = |\mathbf{p}_f|$. When the sum over all helicity states is taken and $E_{\mathbf{p}} = p$, this equation becomes

$$\sum_{h_\mathrm{e}} E_{\mathbf{p}} \left(E_{\mathbf{p}_\mathrm{e}} - h_\mathrm{e} p_\mathrm{e}\right) \left(1 + h_\mathrm{e} \frac{\mathbf{p} \cdot \mathbf{p}_\mathrm{e}}{p\, p_\mathrm{e}}\right) = E_{\mathbf{p}} E_{\mathbf{p}_\mathrm{e}} - \mathbf{p} \cdot \mathbf{p}_\mathrm{e} = E_{\mathbf{p}} E_{\mathbf{p}_\mathrm{e}} v_{\mathbf{p},\,\mu} v^\mu_{\mathbf{p}_\mathrm{e}}. \tag{2.34}$$

The introduced variables $v^\mu_{\mathbf{p}_\mathrm{e}} \equiv (1,\, \mathbf{p}_\mathrm{e}/E_{\mathbf{p}_\mathrm{e}})$ correspond to four velocities. This vector-vector coupling is a consequence of the assumption that the electrons are not polarised. Otherwise an additional term with the product of two axial vectors would appear.

The final result for the transition matrix element is obtained by combining eqs. (2.30), (2.31) and (2.34)

$$\mathsf{H}^{\nu_\mathrm{e}\mathrm{e}}_{11}(\mathbf{p},\, \mathbf{p}') = \sqrt{2} G_\mathrm{F} (2\pi)^3 \delta^{(3)}(\mathbf{p} - \mathbf{p}')\, v_{\mathbf{p},\,\mu} \int \mathrm{d}^3 p_\mathrm{e}\, v^\mu_{\mathbf{p}_\mathrm{e}} N_\mathrm{e}(\mathbf{p}_\mathrm{e}) \,. \tag{2.35}$$

The integral is equivalent to the charged four-vector current of electrons. A similar vector current is obtained for electron neutrinos when eq. (2.35) is plugged into eq. (2.12), one integration performed, and $\hat{\varrho}_{11}(\mathbf{p})$ identified as the number operator for electron neutrinos $\hat{N}_{\nu_\mathrm{e}}(\mathbf{p})$. Then the Hamiltonian from this specific interaction is

$$\hat{H}_{\nu_\mathrm{e}\mathrm{e}} = \sqrt{2} G_\mathrm{F} \int \mathrm{d}^3 p\, v_{\mathbf{p},\,\mu} \hat{N}_{\nu_\mathrm{e}}(\mathbf{p}) \int \mathrm{d}^3 p_\mathrm{e}\, v^\mu_{\mathbf{p}_\mathrm{e}} N_\mathrm{e}(\mathbf{p}_\mathrm{e}) \,. \tag{2.36}$$

For positrons the calculation is almost identical, only a few signs change due to a different spinor for antiparticles eq. (2.32), e.g. $\chi^h_{\mathbf{p}} \to \chi^{-h}_{\mathbf{p}}$ as a positron with left chirality is right-handed. Although the interaction channel is different because now the two particles annihilate, in the end the result is the same up to an overall sign change. Thus when the neutrino interaction with one lepton family is summed up, due to the different signs only the net current appears in the transition matrix.

Also for neutrino-neutrino scattering the computation is very similar, although the interaction Hamiltonian for the neutral current must be applied, since neutrinos cannot exchange electromagnetic charge. In ref. [42] it was shown that a high neutrino density can also source an off-diagonal refractive index via the neutral current interaction, so that this process is important for flavour evolution. Differences in the calculation appear in eqs. (2.31) and (2.33). In the former equation the counterpart of the electron number must

be used, which is the matrix of densities $\varrho_{\alpha\beta}$ determining the flavour structure of the transition matrix. A minor difference is the disappearance of the minus sign in eq. (2.33) due to changed spinor contraction; otherwise the application of neutrino properties to electron quantities in eq. (2.33) produces the correct result, which is

$$\mathsf{H}^{\nu\nu}_{\alpha\beta}\left(\mathbf{p},\,\mathbf{p}'\right) = \sqrt{2}G_{\mathrm{F}}\left(2\pi\right)^{3}\delta^{(3)}\left(\mathbf{p}-\mathbf{p}'\right)v_{\mathbf{p},\,\mu}\int\frac{\mathrm{d}^{3}p_{\nu}}{\left(2\pi\right)^{3}}\,v^{\mu}_{\mathbf{p}_{\nu}}\varrho_{\alpha\beta}\left(\mathbf{p}_{\nu},\,\mathbf{p}_{\nu}\right). \quad (2.37)$$

For antineutrinos the same changes as for positrons apply, i.e. the only difference in eq. (2.37) is the overall sign, so that just the difference of ϱ and $\bar{\varrho}$ matters.

CHAPTER 3

Dispersion relation of flavour correlations

In the current and the following chapter the consequences of a high neutrino density on the stability of flavour waves are investigated for a linearised system. The stability of the flavour correlation function, i.e. the off-diagonal element in the matrix of densities, is accessible via its dispersion relation. When the oscillation frequency of a flavour wave attains a non-real value, the imaginary term causes the amplitude to undergo an exponential growth or decay.

A linearised stability analysis for the flavour correlation function is performed and the dispersion relation for that off-diagonal entry in the matrix of densities is calculated. After the general derivation the focus is turned to the investigation of fast modes alone, in particular the condition for instabilities is studied and how they can be classified. In the end the interplay of fast and slow modes is analysed. The mathematical difference between fast and slow modes can be found in the equation of motion, where for fast ones the vacuum oscillation frequency is set to zero and for slow modes it is explicitly included. Unless mentioned only two-flavour systems are studied here.

3.1 Polarisation Matrix

When neutrinos are ultra-relativistic and all momentum-changing, external potentials negligible, eq. (2.19) simplifies to Liouville's equation, cf. eq. (1.6)

$$\mathrm{i}\,(\partial_t + \mathbf{v}\cdot\partial_{\mathbf{x}})\,\varrho_{\mathbf{x},\mathbf{p}} = [\mathsf{H}_{\mathbf{p}},\ \varrho_{\mathbf{x},\mathbf{p}}]\,. \tag{3.1}$$

As in the previous chapter the time dependence is implicit for notational brevity. Here and in the following $\mathbf{v}$ is a unit vector, which points in the direction of the momentum $\mathbf{p}$. It can be interpreted as a velocity consistent with the relativistic limit. The corresponding velocity four-vectors satisfy $v^\mu = (1,\, \mathbf{p}/\,|\mathbf{p}|)$.

When not only forward scattering is taken into account, a collision term appears in the equation. This term incorporates the entanglement of neutrinos with their environment, potentially damping flavour correlations. This thesis focuses on propagation effects and so the influence of collisions on neutrino oscillation is not regarded.

3.1.1 Hamiltonian

The Hamiltonian in eq. (3.1) includes the vacuum term $\mathsf{H}_{\mathbf{p}}^{\mathrm{vac}} = \sqrt{\mathbf{p}^2 + \mathsf{M}^2}$ as well as the interaction with matter $\mathsf{H}_{\mathbf{p}}^{\mathrm{mat}}$ and the neutrino background $\mathsf{H}_{\mathbf{p}}^{\nu\nu}$, cf. eqs. (2.35) and (2.37) respectively. In this chapter the flavour basis is used and so the mass matrix M is not diagonal. The commutator on the right hand side of eq. (3.1) makes the equation insensitive to all terms proportional to the identity matrix. Consequently, when the ultra-relativistic limit is applied, the mass-independent momentum term drops out in the vacuum part, so that the approximation $\mathsf{H}_{\mathrm{vac}} = \frac{\mathsf{M}^2}{2E}$ is sufficient. Moreover contributions from the neutral current are proportional to the identity matrix at tree level and thus do not source neutrino refraction. However, this argument does not apply to radiative corrections, when the scattering terms become flavour dependent [103, 104]. Because in the upcoming analysis only the leading order in the coupling constant is considered, these terms are neglected.

With these assumptions the general form of the Hamiltonian in eq. (3.1) is

$$\mathsf{H}_{\mathbf{p}} = \frac{\mathsf{M}^2}{2E} + \sqrt{2} G_{\mathrm{F}} v_\mu \left(\mathsf{J}^\mu_{\mathrm{mat}} + \mathsf{J}^\mu_{\nu\nu} \right) . \tag{3.2}$$

The symbols $\mathsf{J}_{\mathrm{mat}}$ and $\mathsf{J}_{\nu\nu}$ describe a matrix of four-vector currents, which originate in the interaction of neutrinos with charged leptons and other neutrinos respectively. Their form was derived in sec. 2.4 for particular scattering processes. The formula for the matter current can be deduced from eq. (2.35). As explained there only the net current, i.e. the difference between leptons and antileptons, enters. In the flavour basis this implies the current matrix

$$\mathsf{J}^\rho_{\mathrm{mat}} = \int \frac{\mathrm{d}^3 p}{(2\pi)^3} \begin{pmatrix} v^\rho_{\mathbf{p},\,\mathrm{e}} \left(N_{\mathrm{e}} - \bar{N}_{\mathrm{e}} \right) & 0 & 0 \\ 0 & v^\rho_{\mathbf{p},\,\mu} \left(N_\mu - \bar{N}_\mu \right) & 0 \\ 0 & 0 & v^\rho_{\mathbf{p},\,\tau} \left(N_\tau - \bar{N}_\tau \right) \end{pmatrix} . \tag{3.3}$$

The occupation numbers N_l are functions of the momentum $\mathbf{p}$, which was not written down. Here the four-velocities are flavour dependent due to the different masses of the charged leptons. The current from neutrino-neutrino interaction has an identical structure with nonzero off-diagonal entries. The appropriate occupation numbers are subsumed in the matrices of densities for neutrinos and antineutrinos and from eq. (2.37) it follows that

$$\mathsf{J}^\mu_{\nu\nu} = \int \frac{\mathrm{d}^3 p}{(2\pi)^3} \, v^\mu_{\mathbf{p}} \left(\varrho_{\mathbf{x},\,\mathbf{p}} - \bar{\varrho}_{\mathbf{x},\,\mathbf{p}} \right) . \tag{3.4}$$

3.1.2 Linearisation

Our main interest is not the evolution of the complete matrix of densities ϱ, but only of its off-diagonal elements. Initially these are small because neutrinos are produced in flavour eigenstates and in a medium with large matter effect remain suppressed since flavour eigenstates are almost propagation eigenstates. Then the equation of motion can be linearised in these quantities and allows one to calculate the dispersion relation to search for unstable modes.

Due to the off-diagonal entry being close to zero a linearisation of the equation of motion is feasible. Before doing so it is useful to make the substitution

$$\varrho_{\mathbf{x},\mathbf{p}} = \frac{1}{2}\left(N_{\nu_\mathrm{e},\mathbf{p}} + N_{\nu_\mu,\mathbf{p}}\right) + \frac{1}{2}\left(N_{\nu_\mathrm{e},\mathbf{p}} - N_{\nu_\mu,\mathbf{p}}\right)\begin{pmatrix} s_{\mathbf{x},\mathbf{p}} & S_{\mathbf{x},\mathbf{p}} \\ S^*_{\mathbf{x},\mathbf{p}} & -s_{\mathbf{x},\mathbf{p}} \end{pmatrix}. \tag{3.5}$$

The functions $N_{\nu_l,\mathbf{p}}$ represent the occupation numbers for ν_l with momentum $\mathbf{p}$. Because ϱ comprises occupation numbers the equation $s^2_{\mathbf{x},\mathbf{p}} + |S_{\mathbf{x},\mathbf{p}}|^2 = 1$ holds. Linearising eq. (3.1) with respect to $S_{\mathbf{x},\mathbf{p}}$ one obtains

$$\begin{aligned} \mathrm{i}v^\mu\partial_\mu S_{\mathbf{x},\mathbf{p}} = &-\omega^\mathrm{s}_\mathrm{vac} + \left(\omega^\mathrm{c}_\mathrm{vac} + \sqrt{2}G_\mathrm{F}v_\mu \mathsf{J}^\mu_\mathrm{mat}\right) S_{\mathbf{x},\mathbf{p}} \\ &- \int \frac{\mathrm{d}^3p'}{(2\pi)^3}\, v_\mu v'^\mu \left(g_{\mathbf{p}'}S_{\mathbf{x},\mathbf{p}'} - \bar{g}_{\mathbf{p}'}\bar{S}_{\mathbf{x},\mathbf{p}'}\right), \end{aligned} \tag{3.6}$$

with the oscillation frequencies $\omega^\mathrm{s}_\mathrm{vac} = \frac{m_1^2-m_2^2}{2E}\sin\vartheta_\mathrm{v}$ and $\omega^\mathrm{c}_\mathrm{vac} = \frac{m_1^2-m_2^2}{2E}\cos\vartheta_\mathrm{v}$. Futhermore the neutrino and antineutrino spectrum were introduced

$$g_\mathbf{p} = \sqrt{2}G_\mathrm{F}\left(f_{\nu_\mathrm{e},\mathbf{p}} - f_{\nu_\mu,\mathbf{p}}\right), \tag{3.7a}$$

$$\bar{g}_\mathbf{p} = \sqrt{2}G_\mathrm{F}\left(f_{\bar{\nu}_\mathrm{e},\mathbf{p}} - f_{\bar{\nu}_\mu,\mathbf{p}}\right). \tag{3.7b}$$

The equation of motion for the antineutrino correlation function $\bar{S}$ is identical to eq. (3.6) except for a sign changes of the terms $\omega^{\mathrm{c,s}}_\mathrm{vac}$.

The constant term in eq. (3.6) originates in the non-diagonality of the mass matrix. It is the only known source for the flavour mixing and without it the flavour correlation function would not undergo a dynamical evolution, but remain zero. In this context it was discussed whether a stability analysis of $S_{\mathbf{x},\mathbf{p}}$ is possible altogether because $S_{\mathbf{x},\mathbf{p}} = 0$ is not a fixed point [69]. Furthermore the flavour mixing in the neutrino sector is not small and cannot be treated as a perturbation. The problem is solved with a large matter density, which suppresses the flavour mixing. Then $S_{\mathbf{x},\mathbf{p}}$ is close to zero for all modes and deviations from that initiate the dynamical evolution. Keeping this in mind the constant term $\omega^\mathrm{s}_\mathrm{vac}$ in eq. (3.6) is omitted in the upcoming calculations.

A more compact expression for eq. (3.6) and its antineutrino counterpart can be achieved by applying the "flavour isospin convention". It assigns negative energies to antiparticles and unifies the equations of motion, which only differ in the sign of the vacuum oscillation frequency. Altough this convention is physically intuitive, it is not necessarily straightforward to implement the

convention mathematically. For this reason the modification of the neutrino-neutrino interaction term is illustrated. In the first step the coordinates of the integration variable $\mathbf{p}$ are changed from Cartesian to spherical with $p = |\mathbf{p}|$ and $\mathbf{v} = \mathbf{p}/p$

$$\int \frac{\mathrm{d}^3 p}{(2\pi)^3}\, v^\mu_{\mathbf{p}} \left(g_{\mathbf{p}} S_{\mathbf{x},\,\mathbf{p}} - \bar{g}_{\mathbf{p}} \bar{S}_{\mathbf{x},\,\mathbf{p}}\right) \tag{3.8}$$
$$= \int_0^\infty \frac{\mathrm{d}p}{2\pi^2}\, p^2 \int_\Sigma \frac{\mathrm{d}\mathbf{v}}{4\pi}\, v^\mu \left(g_{p,\,\mathbf{v}} S_{\mathbf{x},\,p,\,\mathbf{v}} - \bar{g}_{p,\,\mathbf{v}} \bar{S}_{\mathbf{x},\,-p,\,\mathbf{v}}\right).$$

The variable Σ represents the surface of a unit sphere in three-dimensional space. Next the variable $E = \pm p$ is introduced, where the identification with a plus sign holds for particles and with a minus sign for antiparticles. Furthermore two new functions are defined

$$S_{\mathbf{x},\,E,\,\mathbf{v}} = \begin{cases} S_{\mathbf{x},\,p,\,\mathbf{v}} & \text{for } E > 0 \\ \bar{S}_{\mathbf{x},\,p,\,\mathbf{v}} & \text{for } E < 0 \end{cases}, \qquad G_{E,\,\mathbf{v}} = \begin{cases} g_{p,\,\mathbf{v}} & \text{for } E > 0 \\ -\bar{g}_{p,\,\mathbf{v}} & \text{for } E < 0 \end{cases}. \tag{3.9}$$

The difference between the newly defined $S_{\mathbf{x},\,E,\,\mathbf{v}}$ and $S_{\mathbf{x},\,p,\,\mathbf{v}}$ is that the second argument E of the former can attain negative values, whereas it is strictly positive in the other one. In an intermediate step the integral can be split up to clarify the difference between particles and antiparticles

$$\int_0^\infty \frac{\mathrm{d}p}{2\pi^2}\, p^2 \int_\Sigma \frac{\mathrm{d}\mathbf{v}}{4\pi}\, v^\mu \left(g_{p,\,\mathbf{v}} S_{\mathbf{x},\,p,\,\mathbf{v}} - \bar{g}_{p,\,\mathbf{v}} \bar{S}_{\mathbf{x},\,-p,\,\mathbf{v}}\right) \tag{3.10}$$
$$= \int_\Sigma \frac{\mathrm{d}\mathbf{v}}{4\pi}\, v^\mu \left(\int_0^\infty \frac{\mathrm{d}E}{2\pi^2}\, E^2 G_{E,\,\mathbf{v}} S_{\mathbf{x},\,E,\,\mathbf{v}} + \int_{-\infty}^0 \frac{\mathrm{d}E}{2\pi^2}\, E^2 G_{E,\,\mathbf{v}} S_{\mathbf{x},\,E,\,\mathbf{v}}\right).$$

Obviously the two terms can be subsumed in one integral and one obtains with the new variable $\Gamma = \{E,\, \mathbf{v}\}$ and the integral measure $\mathrm{d}\Gamma = \int_{-\infty}^{\infty} \frac{\mathrm{d}E}{2\pi^2}\, E^2 \int \frac{\mathrm{d}\mathbf{v}}{4\pi}$

$$\int \frac{\mathrm{d}^3 p}{(2\pi)^3}\, v^\mu_{\mathbf{p}} \left(g_{\mathbf{p}} S_{\mathbf{x},\,\mathbf{p}} - \bar{g}_{\mathbf{p}} \bar{S}_{\mathbf{x},\,\mathbf{p}}\right) = \int \mathrm{d}\Gamma\, v^\mu G_\Gamma S_{\mathbf{x},\,\Gamma}. \tag{3.11}$$

The other terms in eq. (3.6) do not change, when the substitution $S_{\mathbf{x},\,\mathbf{p}} \to S_{\mathbf{x},\,\Gamma}$ is applied.

3.1.3 Normal mode analysis

Equation (3.6) is linear in $S_{\mathbf{x},\,\Gamma}$ and so a plane wave ansatz is natural

$$S_{\mathbf{x},\,\Gamma} = Q_{K,\,\Gamma}\, \mathrm{e}^{-\mathrm{i}\left(K^0 t - \mathbf{K}\cdot\mathbf{x}\right)}. \tag{3.12}$$

The new variable $Q_{K,\,\Gamma}$ with four-momentum K^μ is the eigenfunction of the differential operator. The eigenfunction is investigated in the next chapter. After eq. (3.12) is plugged into eq. (3.6) one notices that the matter term Λ^μ

behaves like a constant momentum[1], which can be removed easily. The substitution $k^\mu = K^\mu - \Lambda^\mu$ transforms the system to a corotating frame. Therefore the matter current does not fundamentally affect the dispersion relation of a flavour wave. After that the evolution equation of the eigenfunction $Q_{k,\Gamma}$ has the form

$$(v^\mu k_\mu - \omega_{\text{vac}})\, Q_{k,\Gamma} = -v^\mu \int \mathrm{d}\Gamma' v'_\mu G_{\Gamma'} Q_{k,\Gamma'}. \tag{3.13}$$

It is instructive to consider first a system with no neutrino interaction. The dispersion relation is then $k^0(\mathbf{k}) = \omega_{\text{vac}} + \mathbf{v}\cdot\mathbf{k}$ and as one expects every $\mathbf{k}$-mode evolves independently of the others. The systems does not exhibit any collective properties.

Equation (3.13) is an eigenvalue equation for an infinite dimensional vector space. In order to find all eigenvalues a functional determinant must be solved. This intricate procedure can be circumvented by focussing on the dispersion relation of collective modes. The non-collective modes can be projected out by assuming $v^\mu k_\mu - \omega_{\text{vac}} \neq 0$ and then eq. (3.13) can be transformed to

$$Q_{k,\Gamma} = \frac{v_\mu A^\mu_k}{v^\mu k_\mu - \omega_{\text{vac}}} \quad \text{with} \quad A^\mu_k = -\int \mathrm{d}\Gamma' v'^\mu G_{\Gamma'} Q_{k,\Gamma'}. \tag{3.14}$$

This is only possible because the right hand side of eq. (3.13) does not depend on the Γ-dependent part of $Q_{k,\Gamma}$ as it is integrated out. Thus the general form of the eigenfunctions can be deduced and the unknown k-dependent part encoded in the variable A^μ_k. There is a one-to-one correspondence between $Q_{k,\Gamma}$ and A^μ_k, so that for a specific G_Γ one representation of the eigenfunction can be calculated from the other.

The partly derived form of the eigenfunctions can be used to rewrite eq. (3.13) in terms of A^μ_k

$$v^\mu \left[\eta_{\mu\nu} + \int \mathrm{d}\Gamma\, G_\Gamma \frac{v_\mu v_\nu}{v_\rho k^\rho - \omega_{\text{vac}}}\right] A^\nu_k = 0 \tag{3.15}$$

with the Minkowski metric $\eta_{\mu\nu} = \mathrm{diag}\,(+1, -1, -1, -1)$. For the matrix, which is called polarisation matrix, a new variable is introduced

$$\Pi_{\mu\nu} \equiv \eta_{\mu\nu} + \int \mathrm{d}\Gamma\, G_\Gamma \frac{v_\mu v_\nu}{v_\rho k^\rho - \omega_{\text{vac}}}. \tag{3.16}$$

Equation (3.15) must be satisfied for all values of v, which is just a parameter. This implies the linear system

$$\Pi_{\mu\nu} A^\mu_k = 0, \tag{3.17}$$

which only has non-trivial solutions for A_k, if the determinant of the polarisation matrix vanishes

$$\mathrm{Det}\,\Pi_{\mu\nu} = 0. \tag{3.18}$$

[1]Here and in the following the oscillation frequency and wave vector of the flavour wave are identified with the energy and momentum.

With eqs. (3.16) and (3.18) all tools were found to determine the energy of a flavour wave k^0 for a chosen momentum $\mathbf{k}$ and particle distribution G_Γ.

In its full form the polarisation matrix comprises slow and fast collective modes, which can have slow and/or fast instabilities. The difference between them is their behaviour in the fast flavour limit, where $\omega_{\text{vac}} = 0$. Then slow modes become purely kinematical and thus do not describe any collective phenomenon. At the same time slow instabilities vanish. Their respective fast counterparts do not change significantly. The interplay of these two collective effects are dealt with in sec. 3.3.

Depending on the question which is adressed, it is sufficient to consider only fast or slow modes. In a supernova for example fast flavour conversion occurs closer to the centre, where slow conversion is not relevant because the matter density suppresses the flavour mixing. Fast modes are picked out by applying the fast flavour limit to eq. (3.16). Then the integral can be reduced because only the distribution function G_Γ depends on the energy. After integrating it out we define

$$\begin{aligned} G_{\mathbf{v}} &\equiv \int_{-\infty}^{\infty} \frac{\mathrm{d}E}{2\pi^2}\, E^2 G_{E,\,\mathbf{v}} \\ &= \int_{0}^{\infty} \frac{\mathrm{d}E}{2\pi^2}\, E^2 \left(f_{\nu_\mathrm{e},\,E,\,\mathbf{v}} - f_{\bar{\nu}_\mathrm{e},\,E,\,\mathbf{v}} - f_{\nu_\mu,\,E,\,\mathbf{v}} + f_{\bar{\nu}_\mu,\,E,\,\mathbf{v}} \right). \end{aligned} \tag{3.19}$$

The restriction to collective flavour modes that persist in the fast flavour limit illustrates that these fast modes are insensitive to the energy spectrum and only depend on the angular distribution $G_{\mathbf{v}}$. This observation shows a difference between fast and slow modes because the stability of the latter mainly depends on the energy spectrum.

In practice it is useful to modify eq. (3.16) slightly. The reason for that is the intricacy to solve eq. (3.18) for k^0. Even if the integration can be performed analytically, the outcome can be a transcendental equation, which requires a numerical analysis after all. The risk to miss some solutions can be avoided with the parametric ansatz $|\mathbf{k}| = nk^0$ with $-1 < n < 1$. Then the polarisation matrix can be transformed to

$$\Pi_{\mu\nu} = k^0 \eta_{\mu\nu} + \int \frac{\mathrm{d}\mathbf{v}}{4\pi}\, G_{\mathbf{v}} \frac{v_\mu v_\nu}{1 - n\cos\theta_{\mathbf{vk}}}\,, \tag{3.20}$$

where $\theta_{\mathbf{vk}}$ the angle between the vectors $\mathbf{v}$ and $\mathbf{k}$. The determinant of Π in this form is a polynomial of degree four in k^0 and so the solutions $k^0(n)$ comprise the complete real part of the dispersion relation $k^0(|\mathbf{k}|)$.[2] The parametric plot of $\{nk^0(n),\, k^0(n)\}$ helps to get an impression of the dispersion relation and its stability. If the plot indicates the possibility of unstable behaviour, the complex branches can be calculated numerically, so that a full picture of the dispersion relation is obtained.

[2] Due to the arbitrariness of the coordinate system different directions of $\mathbf{k}$ correspond to different flavour isospin distributions $G_{\mathbf{v}}$. In the following the wave vector is usually chosen to point in the z-direction and $G_{\mathbf{v}}$ is changed.

3.2 Types of instabilities

For specific choices of $G_{\mathbf{v}}$ it can happen that for particular wave vectors $\mathbf{k}$ the corresponding frequency k^0 is not real, but has an imaginary contribution. This results in an exponentially growing or decaying amplitude of the wave. Specific modes of the flavour correlation function can become unstable until non-linear effects become relevant. It will be shown, under which conditions these run-away modes exist and how they can be classified.

3.2.1 Axial symmetry

It is helpful at the beginning to reduce the complexity of the polarisation matrix, in order to develop an intuition for its solutions. Therefore here and in the following chapter only configurations of $G_{\mathbf{v}}$ are considered that axially symmetric around the $\mathbf{k}$-vector. In such cases the flavour isospin distribution depends only on the parameter $u = \cos\theta$, with polar angle θ, after the azimuth angle has been integrated out. The polarisation matrix decomposes into a 2×2 block matrix and two diagonal entries so the determinant reduces to

$$\operatorname{Det}\Pi^{\mu\nu} = \left(-1 + \tfrac{1}{2}\langle 1-u^2\rangle_{k^0,\,k}\right)^2 \operatorname{Det}\begin{pmatrix} k^0 + \langle 1\rangle_{k^0,\,k} & \langle u\rangle_{k^0,\,k} \\ \langle u\rangle_{k^0,\,k} & -k^0 + \langle u^2\rangle_{k^0,\,k} \end{pmatrix} = 0, \tag{3.21}$$

where we used $k = |\mathbf{k}|$ and the abbreviation

$$\langle u^i\rangle_{a,\,b} = \frac{1}{2}\int_{-1}^{+1} \mathrm{d}u\, \frac{u^i\, G_u}{a - bu}\,. \tag{3.22}$$

The solution of the first term in eq. (3.21) describes two degenerate axial symmetry breaking modes of the system and is not of interest for the upcoming analysis. The determinant of the 2×2 matrix gives a formula for the dispersion relation of the symmetric modes. Althought the equation looks rather simple, it is usually transcendental as long as the variables k^0 and k are used. However, when the parametric ansatz from eq. (3.20) is applied, the real part of the solution is $\{nk^0,\, k^0\}$ with

$$k^0\,(n) = -\frac{1}{2}\left[\langle 1-u^2\rangle_{1,\,n} \pm \sqrt{\langle (1-u^2)^2\rangle_{1,\,n}\langle (1+u^2)^2\rangle_{1,\,n}}\right]. \tag{3.23}$$

One should not forget that the parametric ansatz $|\mathbf{k}| = nk^0$ breaks down as soon as $k^0\,(n)$ has an imaginary contribution. The resulting complex branches do not coincide with those of the dispersion relation $k^0\,(k)$. Nevertheless it is still possible to conclude that an imaginary term in eq. (3.23) implies a complex solution in the dispersion relation. Note that the reverse argumentation, complex dispersion relation requires complex parametric solution $k^0\,(n)$, does not always work because complex and real parts can be decoupled from each other.

Keeping this in mind it is clear from eq. (3.23) that as soon as the radicand becomes negative, i.e. one of $\langle(1 \pm u^2)^2\rangle$ is smaller than zero, there is a complex branch in the parametric representation as well as the dispersion relation. This observation allows the deduction of the necessary condition on G_u. Since $-1 \leq u \leq 1$ and $-1 < n < 1$ the factor $\frac{1 \pm u^2}{1 - nu}$ in the integral is positive definite and ergo the flavour isospin distribution needs to have a sign change.

3.2.2 Discrete polar angle distributions

In the early phase of research about fast flavour conversion it was common to choose axially symmetric isospin distributions with discrete polar angles, so that $G_{\mathbf{v}}$ describes a fixed number of double cones. Although it was noticed later that it leads to unrealistic results due to oversimplification, it is still instructive to address this case since the different kinds of unstable behaviour are clearly discerned.

The general form of the flavour isospin distribution is

$$G_u = 2G_1 \delta(u - u_1) + 2G_2 \delta(u - u_2), \tag{3.24}$$

where $G_{1,2}$ are numbers specifying the particle content of the respective cone. The factor of two was implemented to cancel the remaining $1/2$ from the spherical surface $1/4\pi$ after integrating over φ, cf. eq. (3.8). The solution can be derived from eq. (3.16) without the help of the parametric ansatz

$$k^0(k) = \frac{1}{2}\left[\Delta_1(k) \pm \sqrt{\Delta_2^2(k) + 4G_1G_2(1 - u_1u_2)^2}\right], \tag{3.25}$$

where

$$\Delta_1(k) = k(u_1 + u_2) - G_1\left(1 - u_1^2\right) - G_2\left(1 - u_2^2\right) \tag{3.26a}$$
$$\Delta_2(k) = k(u_1 - u_2) - G_1\left(1 - u_1^2\right) + G_2\left(1 - u_2^2\right) \tag{3.26b}$$

were introduced. Equation (3.25) describes hyperbolas and it is clear that the term under the square root can only be negative if G_1 and G_2 have opposite signs. One can also see that for a large momentum k the radicand is always positive.

In fig. 3.1 the four kinds of dispersion relation as they were found in ref. [61] are shown. According to the classification in ref. [63] we have:

1. **Complete stability**: The hyperbolas of the dispersion relation do not leave a gap in either k^0 or k, there are no complex branches.

2. **Stability with damping**: With the same particle content, but opposing directions, a region in k^0 opens up, where k is complex. It was analysed in ref. [63] that this case does not lead to a conversion of neutrino flavour because every perturbation is damped away.

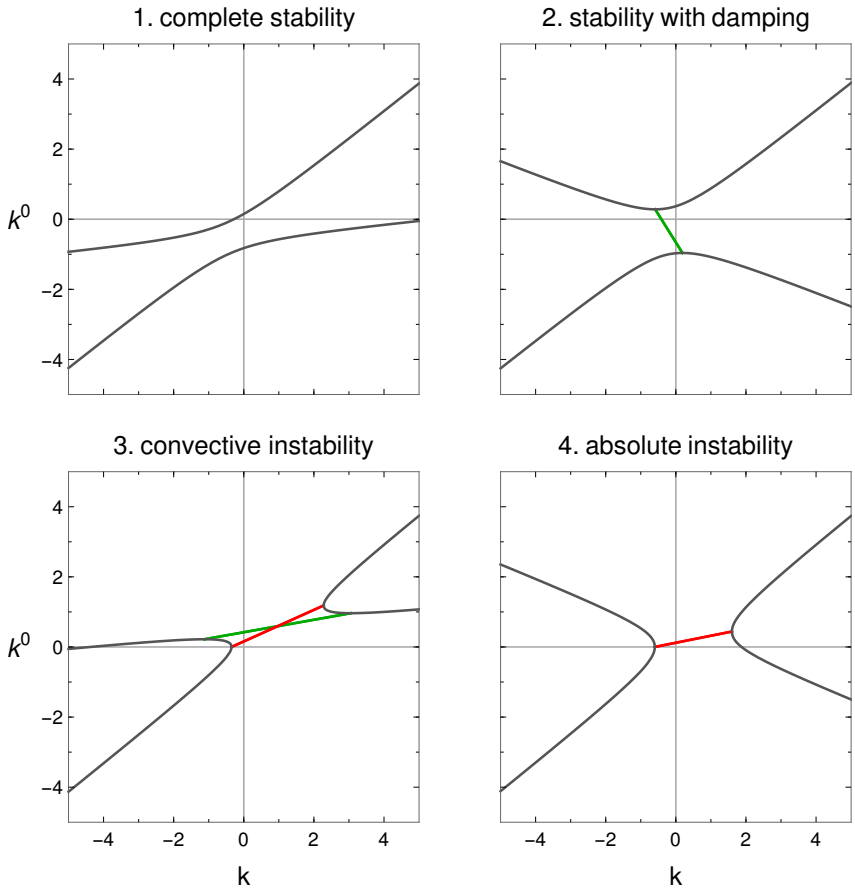

Figure 3.1: These graphs depict the four shapes for the dispersion relation in case of two beams. The red and green lines signify complex k^0 and k-branches respectively.

3. **Convective instability**: In this configuration there are regions with only complex values for oscillation frequency and wave number and so for each one exists a complex connection between the hyperbolas. It occurs when the G_i have opposite, but u_i same signs. The special feature of the convective instability is that locally perturbations in the unstable region grow at the beginning, but vanish afterwards. This is only possible because the propagation velocity is larger than the growth rate.

4. **Absolute instability**: For colliding beams with different particle content there are imaginary energies around $k = 0$. The amplitude of a mode in the unstable region grows exponentially in time until nonlinear effects become important.

A possible question arising from the lower plots of fig. 3.1 is whether causality can be violated. There the dispersion relation is comparable to that of a tachyon since the group velocity $\partial_k k^0$ can be greater than the speed of light. However, it was argued in refs. [69, 105] that the group velocity does not quantify the propagation speed of information. The modes with imaginary frequen-

cies are crucial in this context. One might argue that their contributions do not necessarily enter an arbitrary field excitation. This is true, but in such a case the information is already accessible in the whole spacetime and quantifying its propagation speed is futile. If information is localised in spacetime, i.e. the corresponding wave packet has a spatial cutoff, it requires all modes to have a nonzero amplitude, also the ones with imaginary frequency. In such a system the group velocity does not quantify the propagating speed of information as it is only sensitive to the vicinity of a point in the (k^0, k)-plane and does not include the full dispersion relation.

3.2.3 Continuous polar angle distributions

It was noticed in ref. [71] that as soon as a still axially symmetric, but non-discrete distribution is chosen the dispersion relation can change significantly compared to fig. 3.1. The reason for the change is the divergence caused by the denominator $k^0 - \mathbf{v}\cdot\mathbf{k}$. When the polar part of the distribution is changed from discrete to continuous, the space with divergencies in the (k^0, k)-plane is not a number of lines anymore, but an area. These lines, where the denominator becomes zero, correspond to the asymptotes of the hyperbolas in fig. 3.1 and it makes sense that the dispersion relation cannot attain real values there. For a continuous distribution the lines become a region, in which a unit vector $\mathbf{v}$ satisfies $k^0 - \mathbf{v}\cdot\mathbf{k} = 0$. The solution space is the area between $k^0 = \pm k$, which is called the "forbidden region" from now on.

Figures 3.2 to 3.4 show examples for dispersion relations from continuous flavour isospin distributions. For the first G_u is constant, but has a sign change for the other two as shown in the plots. The forbidden region is shaded in light yellow. In the isotropic case the shape of the collective mode is hyperbolic, comparable to a particle. Deviations from isotropy distort the shape and when a crossing occurs the upper and lower branch merge and one finds a form as in fig. 3.3. Furthermore small, complex k^0 branches appear represented by red lines. If the crossing is further deepened, the dispersion relation is transformed to the shape in fig. 3.4. From the plots it is clear, that for continuous distributions the association of instabilities with gaps between disconnected lines – like they exist for a hyperbola pair – does not work. In order to identify the instabilities of this system, its critical points must be investigated.

A critical point has the feature that complex branches attach to it. There are three different types of them [71], but only two are relevant for our purposes. The first type is directly connected to sign changes in the angular distribution. For each crossing they appear in the excluded region and are the starting points for a complex conjugated pair of k^0- and k-lines each. In the next chapter it will be explained further how and under which conditions they arise. The second type of critical points corresponds to turning points in k^0 or k and in contrast to the previous type their number is not fixed by the number of crossings. At such a turning point the group velocity, i.e. $\frac{\mathrm{d}}{\mathrm{d}k}k^0(k)$, is either

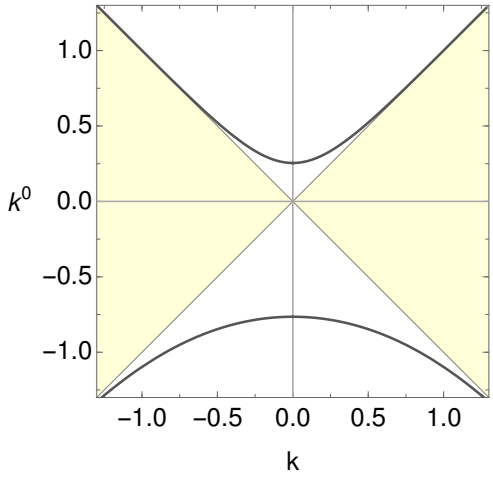

Figure 3.2: The graphic displays the symmetric collective mode for an isotropic flavour isospin distribution $G_u = 1$. The forbidden region, which appears for all continuous G_u, is shaded in light yellow.

zero or infinite. It is easy to see that the turning points of the hyperbolas in fig. 3.1 have either a horizontal or vertical tangent and accordingly a green/red line connects them.

These observations were used in ref. [71] to categorise the dispersion relations of flavour isospin distributions with a single crossing depending on the number of different critical points. The number of critical points in the forbidden region is fixed, but the turning points in k^0 and k can mutually merge and disappear. How this merging process occurs becomes clear, when a closer look at the green lines of figs. 3.3 and 3.4 is taken. In fig. 3.3 there are four separate k-branches with imaginary contribution. Two of them are clearly visible, while the others are two close to the complex k^0-branches to distinguish them. When the crossing is deepened, i.e. $G(-1)$ becomes smaller, the turning points approach each other and merge eventually. In fig. 3.4 this merging process has recently occurred, which has several consequences. First of all the number of green lines is decreased to two and the remaining ones feature sharp turns for real and imaginary k, where the disconnected parts have joined. Furthermore the type of the instability has changed from convective to absolute. The reason for that is the appearance of a branch cut in the $(\mathrm{Re}\,(k^0), \mathrm{Im}\,(k^0))$-plane (not shown in fig. 3.4). The branching points have become poles in that complex plane with a branch cut connecting them. These poles cannot be circumvented by a deformation of the k^0-curve and abruptly make the instability absolute [71].

One should keep in mind that this classification is customised for distributions with a single crossing. If there are multiple crossings, the shape of the real part of the dispersion relation can differ from the ones in this section. If for example $G\,(u)$ is a quadratic polynomial with two crossings between $u = \pm 1$, the real part of $k^0\,(k)$ can have the form of a distorted "8".

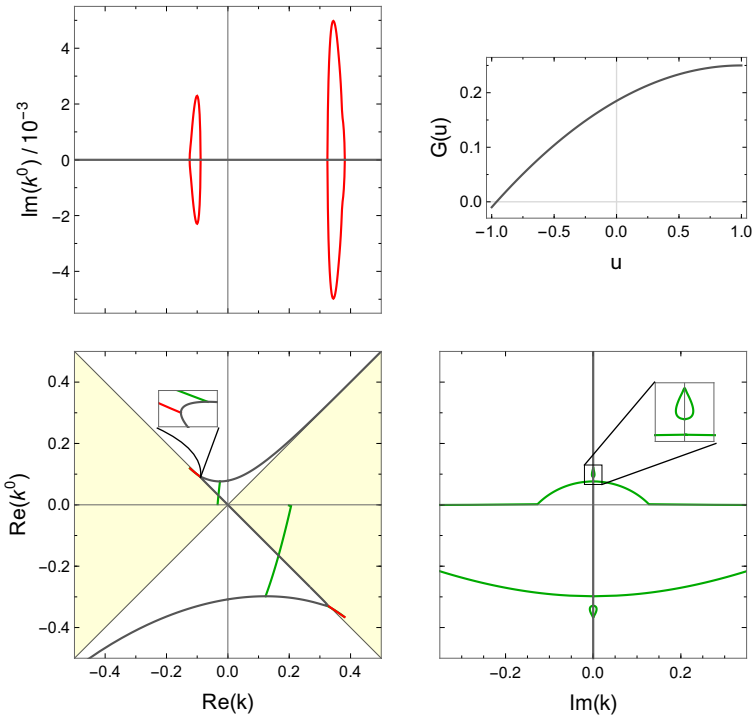

Figure 3.3: Real and imaginary parts of the dispersion relation for a flavour isospin distribution with a maximum at $G(1) = \frac{1}{4}$ and a tiny crossing $G(-1) = -10^{-2}$.

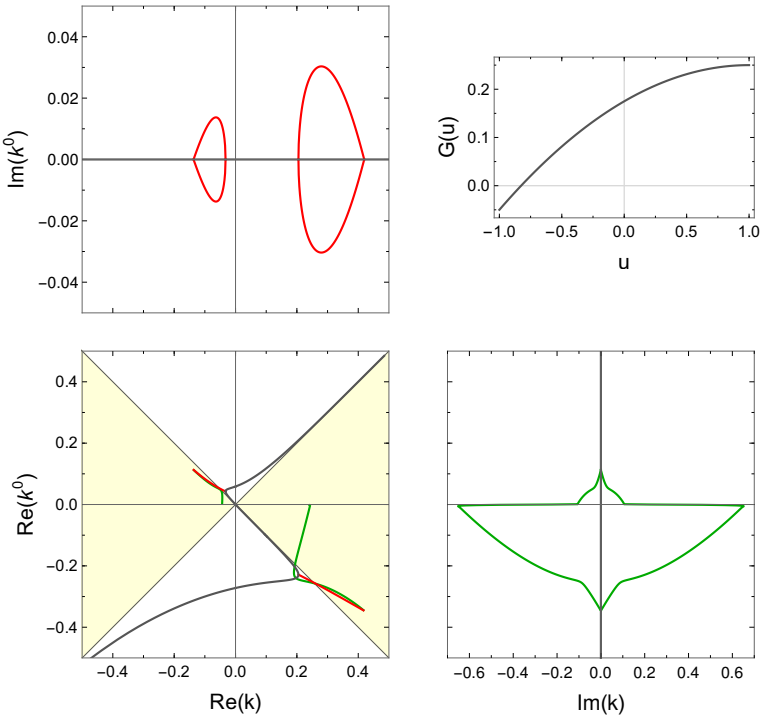

Figure 3.4: Dispersion relation for a deeper crossing $G(-1) = -5 \times 10^{-2}$.

3.3 Slow and fast modes

Until now flavour conversions were considered only in the limiting case $\omega_{\text{vac}} = 0$ in eq. (3.16). In this section it is investigated how a nonzero ω_{vac} influences slow and fast modes. To do so a system with two colliding, mono-energetic beams in one dimension is investigated [69]. Note that by the reduction from two to one dimension the conical shape as in subsection 3.2.2 is lost.

3.3.1 Colliding beams

The propagation direction of the beams is chosen to be parallel to the z-axis, so that $u = \pm 1$ holds. The beam energy is fixed at E_0 and alongside the vacuum oscillation frequency is determined $\omega_{\text{vac}} = \frac{\Delta m^2}{2E_0} \equiv \omega$. Note that due to the flavour isospin convention the signs of these quantities are different for neutrinos and antineutrinos. Consequently there are four different combinations of the parameters leading to four distinguished modes as evident from tab. 3.1.

mode no.	u	particle
1	$+1$	ν
2	$+1$	$\bar{\nu}$
3	-1	ν
4	-1	$\bar{\nu}$

Table 3.1: Direction and particle content of the four modes

In this system the correlation function $S_{E,\mathbf{v}}$ is discrete, so that eq. (3.6) splits up into four coupled differential equations. The modes are named according to the scheme of tab. 3.1

$$\mathrm{i}\,(\partial_t + \partial_z)\,S_1 = (+\omega + \Lambda_0 - \Lambda_z)\,S_1 - g_3 S_3 + g_4 S_4, \tag{3.27a}$$
$$\mathrm{i}\,(\partial_t + \partial_z)\,S_2 = (-\omega + \Lambda_0 - \Lambda_z)\,S_2 - g_3 S_3 + g_4 S_4, \tag{3.27b}$$
$$\mathrm{i}\,(\partial_t - \partial_z)\,S_3 = (+\omega + \Lambda_0 + \Lambda_z)\,S_3 - g_1 S_1 + g_2 S_2, \tag{3.27c}$$
$$\mathrm{i}\,(\partial_t - \partial_z)\,S_4 = (-\omega + \Lambda_0 + \Lambda_z)\,S_4 - g_1 S_1 + g_2 S_2. \tag{3.27d}$$

Note that the antiparticle contribution couples with a different sign to the mode, cf. eq. (3.6). The definition of g_i is along the lines of eq. (3.7a) normalised via $\sum_i g_i = 4$ and supplemented by a factor of two. It originates in the kinematical term $v^\mu v'_\mu$, which vanishes for parallel and is maximal for antiparallel propagation. There are additional equations to the above four describing the evolution along the other two spatial directions. They represent symmetry breaking modes and as before are not taken into consideration.

To derive the function $k^0(k)$ with a normal mode analysis the plane wave ansatz from eq. (3.12) is applied and a transfer to the corotating frame performed in order to remove the matter effect, Λ_μ. Then eqs. (3.27) can be

written as a matrix equation

$$\begin{pmatrix} (\omega - k^0 + k) & 0 & -g_3 & g_4 \\ 0 & (-\omega - k^0 + k) & -g_3 & g_4 \\ -g_1 & g_2 & (\omega - k^0 - k) & 0 \\ -g_1 & g_2 & 0 & (-\omega - k^0 - k) \end{pmatrix} \begin{pmatrix} Q_1 \\ Q_2 \\ Q_3 \\ Q_4 \end{pmatrix} = 0. \tag{3.28}$$

This is an eigenvalue equation for k^0, so that for non-trivial Q_i the determinant must be zero. The defining equation for $k^0(k)$ is thus a quartic polynomial

$$\begin{aligned} &\left(\left(k^0\right)^2 - k^2\right)\left[\left(k^0\right)^2 - k^2 - (g_1 - g_2)(g_3 - g_4)\right] \\ &\qquad = 2\left[(g_1 g_3 - g_2 g_4)\, k^0 - (g_1 g_4 - g_2 g_3)\, k\right]\omega \\ &\qquad\quad + \left[2\left(\left(k^0\right)^2 + k^2\right) + (g_1 + g_2)(g_3 + g_4)\right]\omega^2 - \omega^4. \end{aligned} \tag{3.29}$$

As its analytical solutions are neither intuitive nor illuminating in general, examples are used to point out the important features and distinctions to the fast flavour limit of previous calculations.

Equation (3.29) gives rise to slow and fast collective modes. As mentioned before, the distinguishing element is the vacuum oscillation frequency. When ω is set to zero, only fast modes remain like in the two-cone scenario, which was calculated in the fast flavour limit. This setting is similar to the colliding beams and one expects comparable solutions. However, there is a mismatch in the number of $k^0(k)$-branches. In the fast flavour limit with two cones only two branches (the hyperbolas) were found, whereas eq. (3.29) gives rise to four. The root of this difference is the fast flavour limit, which makes some modes kinematical, and the polarisation matrix approach, which is only sensitive to dynamical modes and not kinematical ones. Kinematical means that there are no collective effects, a wave packet only propagates along the beam line and hence satisfies the equation $k^0 - \mathbf{v}\cdot\mathbf{k} - \omega_{\text{vac}} = 0$. On the other hand dynamical cannot be reduced to a drift, they modulate a field perturbation. An example for purely kinematical modes are the results of eq. (3.29) in the limit $k \to \infty$. This is identical to the zero coupling limit, where naturally no collective effect arises. Solving the equation up to first order results in $k^0 = \pm k$ with a degeneracy of two each.

Accordingly the character of a mode is determined by the $\omega \to 0$ limit. If it becomes kinematical, we call it "slow" and otherwise "fast." In a similar way "slow" and "fast" instabilities are identified. If they are slow, they vanish for $\omega \to 0$ as kinematical modes must be real. Accordingly fast modes remain dynamical in the same limit. Note that a fast mode can have fast and slow instabilities, but the latter disappear for $\omega \to 0$. On the other hand slow modes only have slow instabilities because otherwise a drifiting wave packet would either decay or grow exponentially for $\omega = 0$, which is in contradiction with simple propagation.

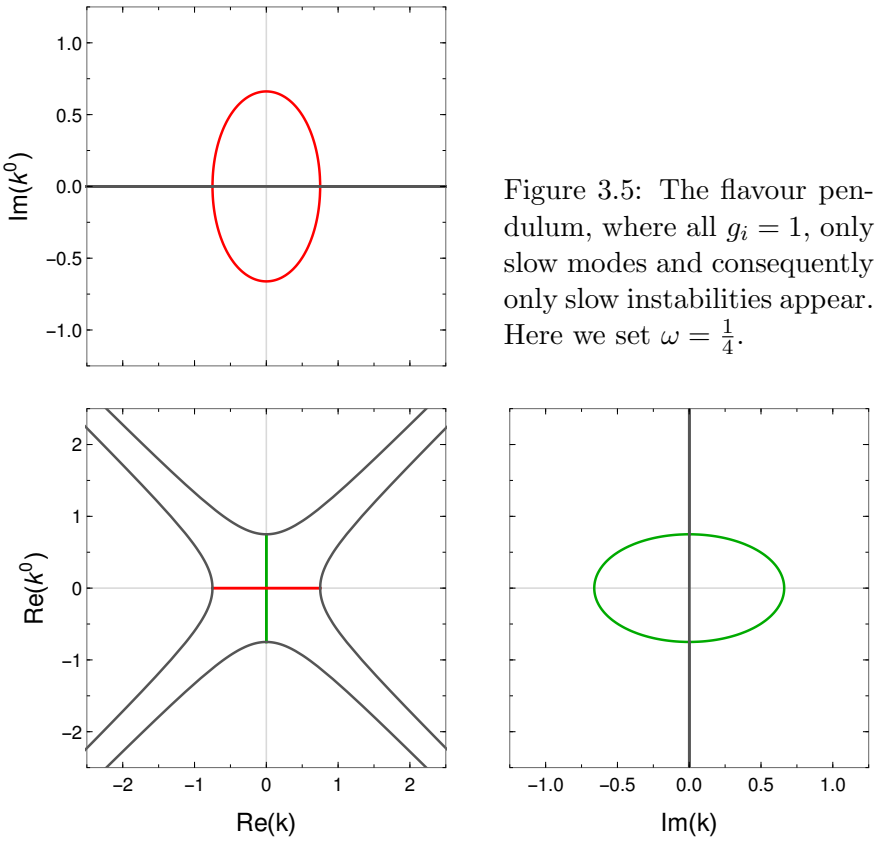

Figure 3.5: The flavour pendulum, where all $g_i = 1$, only slow modes and consequently only slow instabilities appear. Here we set $\omega = \frac{1}{4}$.

Before looking at the mixing of slow and fast modes it is instructive to consider first a setting with only slow modes. A convenient example due to its high symmetry is the flavour pendulum, where ν and $\bar{\nu}$ are present in equal amounts [49]. The corresponding numbers of the four modes are $g_1 = g_2 = g_3 = g_4 = 1$. Several terms become zero in eq. (3.29) and the emerging biquadratic equation has the solutions

$$\left(k^0\right)^2 = k^2 + \omega^2 \pm 2\omega\sqrt{1 + k^2}. \tag{3.30}$$

It is easy to see that the four solutions all become kinematical for $\omega \to 0$. Furthermore one can deduce that only the solutions with a minus sign have complex oscillation frequencies, since the square root in eq. (3.30) is strictly positive. From the high symmetry of the system follows that the other two hyperbolas are connected by a complex k-branch as shown in fig. 3.5.

This is not the only choice for g_i with exclusively kinematical modes for a vanishing vacuum oscillation frequency. In general the equation

$$(g_1 - g_2)(g_3 - g_4) = 0 \tag{3.31}$$

must be satisfied, which means that the term on the left hand side of eq. (3.29) is zero. However, not all configurations complying with eq. (3.31) converge

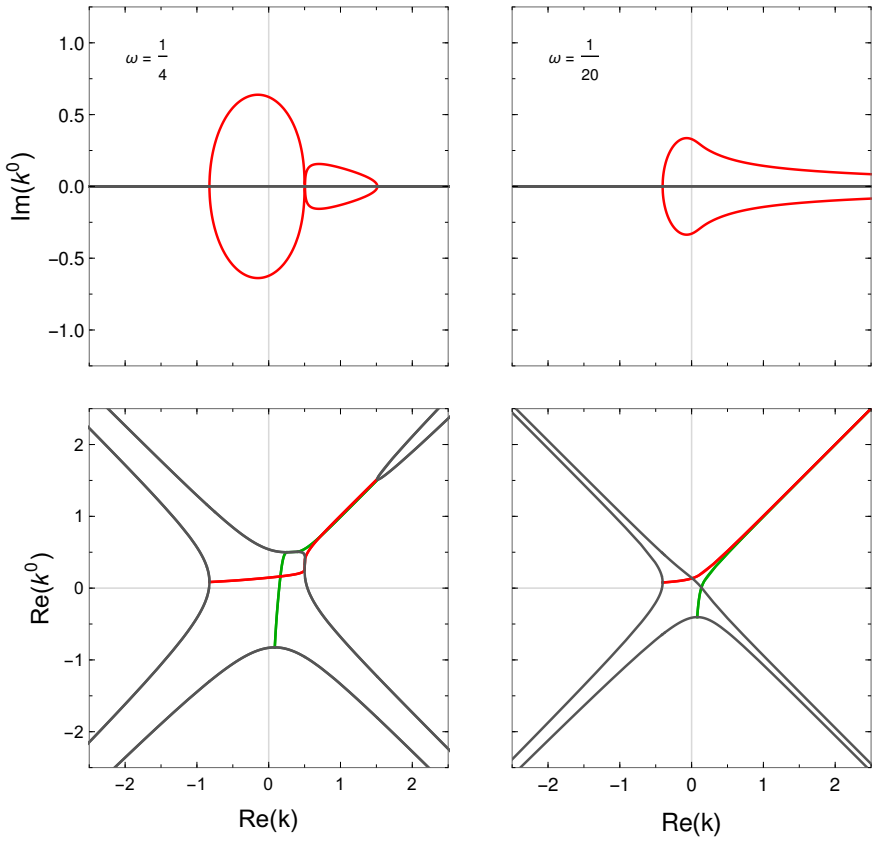

Figure 3.6: Real and imaginary parts of k^0 for $g_1 = g_2 = \frac{1}{2}$, $g_3 = 1$ and $g_4 = 2$. The vacuum oscillation frequency is set to $\omega = \frac{1}{4}$ for the left panel and $\omega = \frac{1}{20}$ for the right.

smoothly to kinematical behaviour. An example for that is shown in fig. 3.6. One can see that the length of the unstable branch increases for smaller ω and at the same time the imaginary contribution increases. For a tiny vacuum oscillation frequency there is a broad range of unstable modes, but their growth rate is small because $\mathrm{Im}\,(k^0)$ converges to zero in the fast flavour limit. For $\omega = 0$ the instability abruptly vanishes completely and the dispersion relation is purely kinematical. This behaviour can also be deduced directly from eq. (3.29). If one beam has a nonzero lepton number, the term linear in ω remains and causes the transition from dynamical to kinematical behaviour for $\omega = 0$.

Since in the colliding beams model a scenario with fast modes is similar to the lower right diagram of fig. 3.1, we refrain from discussing an explicit example. The main difference is the appearance of kinematical modes $k^0 = \pm k$, which are identical with the asymptotes of the tachyonic dispersion relation.

3.3.2 Mixing of slow and fast modes

With arbitrary values for g_i and nonzero ω slow and fast modes overlap and get mixed in general. The described picture with only fast modes changes slightly. Qualitatively the fast, absolute instability between the two dynamical branches remains unaffected as one would expect. In addition slow instabilities appear in two separate regions as long as ω is small. The first instability apears for small momenta where the slow modes obtain a shape similar to fig. 3.5. And the other occurs where the now nonzero vacuum oscillation frequency sources the mixing of slow and fast modes. The gap between them becomes smaller for higher k and so the unstable region moves to large momenta for decreasing ω.

The polynomial of eq. (3.29) can be solved approximately in the vicinity of the slow instabilities and for small vacuum oscillation frequencies. There are two different scales involved and so for the solution also two consecutive steps are needed. The first deals with the displacement of the symmetry point from the origin. There k^0, k and ω are all of the same order. Keeping only quadratic terms in eq. (3.29) one obtains

$$-\left(\left(k^0\right)^2 - k^2\right) a_0 = 2\left(a_1 k^0 + a_2 k\right)\omega + a_4\omega^2, \tag{3.32}$$

where the shorthand variables

$$a_0 = -\left(g_1 - g_2\right)\left(g_3 - g_4\right), \tag{3.33a}$$
$$a_1 = g_1 g_3 - g_2 g_4, \tag{3.33b}$$
$$a_2 = g_2 g_3 - g_1 g_4 \tag{3.33c}$$
$$a_3 = \left(g_1 + g_2\right)\left(g_3 + g_4\right) = \tfrac{1}{a_0}\left(a_2^2 - a_1^2\right) \tag{3.33d}$$

were introduced. The solution to the quadratic equation are two linear functions, which intersect in the point $\left(\frac{a_1}{a_0}\,\omega\middle|-\frac{a_2}{a_0}\,\omega\right)$. In the second step the variables $y = k^0 - \frac{a_1}{a_0}\omega$ and $x \equiv k + \frac{a_2}{a_0}\omega$ are defined and represent the deviation from the symmetry point. Using them in eq. (3.29) and keeping terms up to quadratic order of y, x and ω^2 gives a correction to the absolute value function. Note that the vacuum oscillation frequency is squared, so that terms proportional to ω^4 are included. Combining the solutions results in the pair of hyperbolas[3]

$$k^0 = -\frac{a_1}{a_0}\,\omega \pm \sqrt{\left(k + \frac{a_2}{a_0}\,\omega\right)^2 - 16\,\frac{g_1 g_2 g_3 g_4}{a_0^2}\,\omega^4}. \tag{3.34}$$

For a particular kind of distributions it is also not hard to calculate the range of momenta where the slow and fast modes form new instabilities. For

[3]This result differs from that in the original paper [69], where a perturbative iteration for small ω was used. However, in this region it is not applicable because the perturbation is of the same order as k^0 and k.

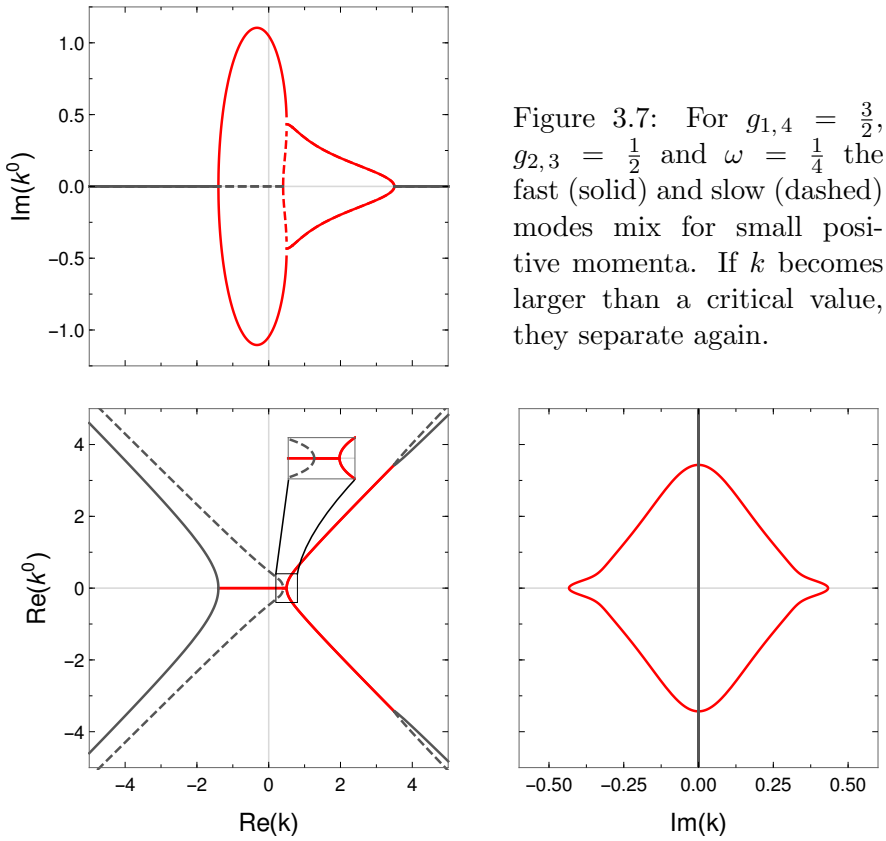

Figure 3.7: For $g_{1,4} = \frac{3}{2}$, $g_{2,3} = \frac{1}{2}$ and $\omega = \frac{1}{4}$ the fast (solid) and slow (dashed) modes mix for small positive momenta. If k becomes larger than a critical value, they separate again.

decreasing vacuum oscillation frequency these parts move away from the origin, so that the approximation k^0, $k \gg \omega$ is feasible. Including all terms up to second order eq. (3.29) becomes

$$\left(\left(k^0\right)^2 - k^2\right)\left[\left(k^0\right)^2 - k^2 - (g_1 - g_2)(g_3 - g_4)\right] = -2k\omega(g_1 g_3 - g_2 g_4) + 2\omega^2\left(\left(k^0\right)^2 + k^2\right). \tag{3.35}$$

The mentioned peculiarity ensures that the equation is biquadratic in k^0, i.e. the k^0-coefficient $g_1 g_3 - g_2 g_4$ vanishes. This happens for example when the beam composition is antisymmetric. Solving for $(k^0)^2$ and demanding it to develop an imaginary part results in a condition on k corresponding to the momentum interval $[k_-, k_+]$ with

$$k_\pm = \frac{1}{4\omega}\left(g_1 g_4 - g_2 g_3 \pm \sqrt{(g_1 g_4 - g_2 g_3)^2 - (g_1 - g_2)^2 (g_3 - g_4)^2}\right). \tag{3.36}$$

As an example the collision of a beam with neutrino and one with antineutrino excess is studied for arbitrary vacuum oscillation frequencies. In a system with $g_{1,4} = \frac{3}{2}$ and $g_{2,3} = \frac{1}{2}$ the condition to apply eq. (3.36) is fulfilled and hence the slow instabilities from mixing appear for $\frac{2-\sqrt{3}}{4\omega} < k < \frac{2+\sqrt{3}}{4\omega}$. Due to

the ω^{-1}-dependence the momentum values and the interval size increase with decreasing vacuum frequency. Figure 3.7 depicts the system for a rather large vacuum frequency, which leads to the specific structure of branch points in the upper plot. The slow absolute instability as already observed in fig. 3.5 and the convective instabilities are connected at small k. Inserting all the numbers an already good agreement of the approximations with the analytical solution is revealed.

CHAPTER 4

Non-collective modes and instabilities

Non-collective modes are excitations of the flavour field, where the equation $k^0 = \mathbf{v} \cdot \mathbf{k}$ has a solution. They are purely kinematical in the fast flavour limit, i.e. their contribution to a wave packet completely dissipates while the collective part remains. The transition from non-collective to collective behaviour can happen in two different ways. The first takes place in the limit of vanishing coupling strength, where no collective modes exist. As soon as the interaction is turned on some modes become collective. This is a smooth crossover and therefore appears at the edge of the forbidden region. However, the second type of transition is abrupt and occurs inside the forbidden region, where all collective modes must be complex and so this process is inherently related to instabilities.

In this chapter the connection between the kinematical, forbidden region and dynamical, collective modes is outlined. Here all calculations are performed for axially symmetric flavour isospin distribution and so one can distinguish between modes that preserve or break this symmetry. Without axial symmetry such a classification of flavour modes is not possible. Here it is important to distinguish between the symmetry of the system, i.e. the flavour isospin distribution, and the symmetry of the solutions, i.e. the flavour modes. We use the notation where quantities for symmetry preserving modes are denoted by the letter "S" and symmetry breaking ones by "B".

Based on our paper [72] the symmetry preserving eigenfunctions $Q^{\mathrm{S}}_{k,\mathbf{v}}$ are determined and a sufficient criterion for the occurrence of unstable collective modes is derived. These results are supplemented by the analogous calculation for symmetry breaking eigenfunctions $Q^{\mathrm{B}}_{k,\mathbf{v}}$, which have not been discussed in ref. [72]. Furthermore it is shown that the existence of crossings in the distribution is sufficient to source instabilities in the symmetry breaking sector. For symmetry preserving modes this is only the necessary condition.

4.1 Eigenfunctions of non-collective modes

Equation (3.13) does not only determine the oscillation frequency of collective flavour field excitations, but can also be used to find the eigenfunctions. For collective modes they follow from eq. (3.17). For their non-collective counterpart a different method is used to find the solution. As long as k^0 is smaller than or equal to $|\mathbf{k}|$ there is always a unit vector $\mathbf{v}$, so that the equation $k^0 = \mathbf{v} \cdot \mathbf{k}$ is satisfied. Therefore the area between $k^0 = \pm k$ is densely filled with eigenvalues and there is no need to calculate them. For the same reason the previously exploited trick of dividing by $k^0 - uk$ does not work any more. The only exception is a discrete distribution as it is used for the two-beam case in sub. 3.2.2.

Before taking a closer look at the integral structure of eq. (3.13), a substitution of parameters is undertaken to simplify the notation. After a division by k the new variables $w \equiv \omega/k$ and $\mu \equiv 1/k$ are defined. The former is now a dimesionless eigenvalue and the forbidden region is located between $w = \pm 1$. The latter is a coupling constant and substitutes the momentum as abscissa in the upcoming plots. In the fast flavour limit the energy can be integrated out and so eq. (3.13) yields for axially symmetric distributions $G_{\mathbf{v}} = G_u$

$$\begin{aligned}(w-u)\,Q_{w,\,\mathbf{v}} = -\,\mu \int \frac{\mathrm{d}\mathbf{v}'}{4\pi}\, G_{u'} Q_{w,\,\mathbf{v}'} \\ \times \left(1 - uu' - \mathrm{c}_{\varphi-\varphi'}\sqrt{(1-u^2)\,(1-u'^2)}\right).\end{aligned} \tag{4.1}$$

The velocity vector $\mathbf{v}$ was parameterised by the polar coordinate $u = \cos\theta$ with polar angle θ and the azimuthal angle φ. The shorthand notation $\mathrm{c}_\varphi \equiv \cos\varphi$ is used.

After a closer look at the right-hand side of eq. (4.1) it becomes apparent that the eigenfunction there does not depend on $\mathbf{v}$, but only $\mathbf{v}'$, which is integrated out. Only the second line of eq. (4.1) includes components of the velocity vector $\mathbf{v}$. Applying a trigonometric identity for $\mathrm{c}_{\varphi-\varphi'}$ the general form of the equation is

$$(w-u)\,Q_{w,\,\mathbf{v}} = a - bu + \sqrt{1-u^2}\,(c\,\mathrm{s}_\varphi + d\,\mathrm{c}_\varphi)\,. \tag{4.2}$$

The parameters a, b, c, d depend on the eigenvalue w and the distribution G_u. Now it is possible to split up the eigenfunction into a symmetric (S) and a symmetry breaking (B) contribution $Q_{w,\,\mathbf{v}} = Q^{\mathrm{S}}_{w,\,u} + Q^{\mathrm{B}}_{w,\,\mathbf{v}}$. Noting that $(w-u)\,\delta\,(w-u) = 0$ the natural ansatzes for them are

$$Q^{\mathrm{S}}_{w,\,u} = \mathcal{S}^{(1)}_w \left(\frac{1}{w-u} + \sigma_w \delta\,(w-u)\right) + \mathcal{S}^{(2)}_w \quad \text{and} \tag{4.3a}$$

$$Q^{\mathrm{B}}_{w,\,\mathbf{v}} = \left(\mathcal{B}^{(1)}_w \mathrm{c}_\varphi + \mathcal{B}^{(2)}_w \mathrm{s}_\varphi\right) \frac{\sqrt{1-u^2}}{w-u} + \left(\mathcal{B}^{(3)}_w \mathrm{c}_\varphi + \mathcal{B}^{(4)}_w \mathrm{s}_\varphi\right) \delta\,(w-u)\,. \tag{4.3b}$$

The δ-distribution is essential and guarantees that also in an uncoupled system $\mu = 0$ the eigenfunctions are non-zero. The ansatz above only works, when the principal value of the integral over $1/(w-u)$ is taken in eq. (4.1). In the new parameters the forbidden region, which is densely filled with modes, lies between $w = \pm 1$, so that the integrand always has a pole.

For Q^{B} the prefactor of the δ-function is an arbitrary, periodic function of φ in principle. However, only terms with $\sin\varphi$ and $\cos\varphi$ contribute to the eigenvalue w in eq. (4.1); the amplitudes of higher multipoles, e.g. for $\cos 2\varphi$, can be set to zero.

4.1.1 Symmetric eigenfunction

When the ansatz is inserted on both sides of eq. (4.1) the symmetric part is

$$\begin{aligned} 2\mathcal{S}_w^{(1)} + 2\mathcal{S}_w^{(2)}(w-u) = &-\mu\mathcal{S}_w^{(1)}\left[\fint \mathrm{d}u' \,\frac{1-uu'}{w-u'} G_{u'} + \sigma_w G_w (1-uw)\right] \\ &- \mu\mathcal{S}_w^{(2)} \int \mathrm{d}u' \,(1-uu')\, G_{u'}. \end{aligned} \tag{4.4}$$

The principal value integral can be modified to

$$\fint \mathrm{d}u' \,\frac{1-uu'}{w-u'} G_{u'} = (1-uw)\fint \mathrm{d}u' \frac{G_{u'}}{w-u'} + u\int \mathrm{d}u'\, G_{u'}. \tag{4.5}$$

For brevity the new symbols

$$F_{w,\,i} = \fint \mathrm{d}u \frac{u^i G_u}{w-u} \quad \text{and} \quad \mathcal{G}_i = \int \mathrm{d}u\, u^i G_u \tag{4.6}$$

are introduced. Plugging these definitions into eq. (4.4) results in

$$\begin{aligned} 2\mathcal{S}_w^{(1)} + 2\mathcal{S}_w^{(2)}(w-u) + \mu\mathcal{S}_w^{(1)}\big[(1-uw)(F_{w,\,0} + \alpha_w G_w) + u\mathcal{G}_0\big] \\ + \mu\mathcal{S}_w^{(2)}(\mathcal{G}_0 - u\mathcal{G}_1) = 0. \end{aligned} \tag{4.7}$$

This can be split into two separate equations – one for constant and the other for u-dependent contributions. Both equations must hold individually, otherwise it is not guaranteed that eq. (4.7) is satisfied for all u. Equation (4.7) can be written in matrix form

$$\begin{pmatrix} \mu(F_{w,\,0} + \alpha_w G_w) + 2 & \mu\mathcal{G}_0 + 2w \\ \mu w (F_{w,\,0} + \alpha_w G_w) - \mu\mathcal{G}_0 & \mu\mathcal{G}_1 + 2 \end{pmatrix} \begin{pmatrix} \mathcal{S}_w^{(1)} \\ \mathcal{S}_w^{(2)} \end{pmatrix} = 0\,. \tag{4.8}$$

For non-trivial eigenfunctions the determinant of the matrix must vanish. This yields an equation for the remaining parameter σ_w and can be further used to derive the ratio of $\mathcal{S}_w^{(1)}$ and $\mathcal{S}_w^{(2)}$

$$\sigma_w G_w = -F_{w,\,0} - \frac{4 + \mu\mathcal{G}_0(\mu\mathcal{G}_0 + 2w) + 2\mu\mathcal{G}_1}{\mu(2 - 2w^2 - \mu w\mathcal{G}_0 + \mu\mathcal{G}_1)}, \tag{4.9a}$$

$$\zeta_w \equiv \frac{\mathcal{S}_w^{(2)}}{\mathcal{S}_w^{(1)}} = \frac{2w + \mu\mathcal{G}_0}{2 - 2w^2 - \mu(w\mathcal{G}_0 - \mathcal{G}_1)}\,. \tag{4.9b}$$

When the angular distribution has a crossing at w, so that $G_w = 0$, σ_w is not determined by eq. (4.9a). In this special case the eigenfunction is just $\delta(w-u)$ leading to the conclusion that eq. (4.3a) is not applicable and σ_w a free parameter.

4.1.2 Axially breaking eigenfunction

With a similar procedure the parameters of the symmetry breaking eigenfunction are determined. One of them is redundant as becomes clear when inserting the ansatz in eq. (4.1). Instead we introduce

$$\beta_w G_w \equiv \frac{\mathcal{B}_w^{(3)} \mathrm{c}_\varphi + \mathcal{B}_w^{(4)} \mathrm{s}_\varphi}{\mathcal{B}_w^{(1)} \mathrm{c}_\varphi + \mathcal{B}_w^{(2)} \mathrm{s}_\varphi} = \frac{1}{\sqrt{1-w^2}} \left(\frac{4}{\mu} - F_{w,0} + F_{w,2} \right) , \tag{4.10}$$

with an analogous notation to the symmetric eigenfunction. Note that also β_w remains undetermined if there is a crossing at w. The symmetry of the system makes a further reduction of parameters possible by choosing a coordinate system in which $\mathcal{B}_w^{(2)} = 0$. The new version of $Q^{\mathrm{B}}_{w,\mathbf{v}}$ is then

$$Q^{\mathrm{B}}_{w,\mathbf{v}} = \mathcal{B}_w \mathrm{c}_\varphi \left(\frac{\sqrt{1-u^2}}{w-u} + \beta_w \delta(w-u) \right) \tag{4.11}$$

with $\mathcal{B}_w = \mathcal{B}_w^{(1)}$.

4.1.3 Normalisation

In contrast to collective eigenfunctions, those for non-collective modes cannot be normalised. The only possibility is to discretise the flavour isospin distribution in steps of Δu and substitute the integrals with sums

$$\int_{-1}^{+1} \mathrm{d}u \, f(u) \to \Delta u \sum_{i=1}^{N} f_i, \tag{4.12}$$

where $N = 2/\Delta u$ and $f_i = f(u_i)$.

The δ-distribution is normalised by definition and integrating over its square diverges. The discretisation leads to

$$\int \mathrm{d}u \, |\delta(u)|^2 \to \frac{1}{\Delta u} \tag{4.13}$$

because the discrete counterpart of the δ-distribution is a Kronecker delta weighted by the spacing to fulfil the normalisation condition.

Next the function $1/(w-u)$ is considered. While the principal-part integration is finite due to its antisymmetry around $u = w$, its square still diverges. This can be avoided by choosing carefully the evaluation points u_i.

With a grid symmetric around the pole w, i.e. $u_i = w + \left(\frac{1}{2} \pm i\right) \Delta u$, and the sum $\sum_{i=-\infty}^{+\infty} \left(\frac{1}{2} - i\right)^{-2} = \pi^2$ the discretised integral amounts to

$$\int \mathrm{d}u \, (w-u)^2 \to \frac{\pi^2}{\Delta u}. \tag{4.14}$$

Combining eqs. (4.13) and (4.14) the normalisation of $Q_{w,\mathbf{v}}$ can be derived. For that it is important to note that the products of different summands of the eigenfunction are finite for $\Delta u \to 0$, when the integration is performed. $\mathcal{S}_w^{(2)}$ is not relevant for the normalisation and notation is simplified with the substitution $\mathcal{S}_w^{(1)} \to \mathcal{S}_w$. Hence one obtains for the symmetric part

$$\begin{aligned} \frac{1}{2} \int \mathrm{d}u \, \left|Q^{\mathrm{S}}_{w,u}\right|^2 &= \mathcal{S}_w^2 \int \mathrm{d}u \left[\frac{1}{(w-u)^2} + \sigma_w^2 \left|\delta\left(w-u\right)\right|^2\right] \\ &= \frac{\mathcal{S}_w^2}{2\Delta u} \left(\pi^2 + \sigma_w^2\right). \end{aligned} \tag{4.15}$$

From this equation follows

$$\mathcal{S}_w = s_w \sqrt{\frac{2\Delta u}{\pi^2 + \sigma_w^2}} \tag{4.16}$$

and with eq. (4.9b) the symmetric eigenfunction is fully determined. The variable s_w represents an arbitrary phase.

For the axially breaking eigenfunction the procedure is almost identical. The term proportional to $\frac{u^2}{w-u}$ vanishes in the continuum limit and so the integral is equal to

$$\begin{aligned} \frac{1}{4\pi} \int \mathrm{d}\mathbf{v} \, \left|Q^{\mathrm{B}}_{w,\mathbf{v}}\right|^2 &= \mathcal{B}_w^2 \int \mathrm{d}\varphi \, \mathrm{c}_\varphi^2 \int \mathrm{d}u \left[\frac{1-u^2}{(w-u)^2} + \beta_w^2 \left|\delta\left(w-u\right)\right|^2\right] \\ &= \frac{\mathcal{B}_w^2}{4\Delta u} \left(\pi^2 + \beta_w^2\right) \end{aligned} \tag{4.17}$$

and accordingly

$$\mathcal{B}_w = 2b_w \sqrt{\frac{\Delta u}{\pi^2 + \beta_w^2}}. \tag{4.18}$$

Analogous to eq. (4.16) b_w is a complex phase.

The general structure of the eigenfunctions can also be understood in a different way, which is illustrated exemplarily for the symmetric eigenfunction. With the definition of

$$\sin\varphi_w = \frac{\sqrt{2}\pi s_w}{\sqrt{\pi^2 + \sigma_w^2}} \tag{4.19}$$

they take the form

$$Q^{\mathrm{S}}_{w,u} = \mathcal{S}\left[\frac{\sin\varphi_w}{\pi\left(w-u\right)} + \cos\varphi_w \delta\left(w-u\right) + \zeta_w\right]. \tag{4.20}$$

The discretisation parameter Δu is absorbed in $\mathcal{S}$ and from the appearance of the trigonometric functions it becomes clear that φ_w is a mixing angle. One can see that for example in a non-interacting system, where $\sigma_w \to -\infty$ and consequently $\varphi = 0$. Then only the δ-function contributes as one would expect. Note that on the other hand even an infinite interaction strength does not result in a maximal mixing with $\varphi_w = \frac{\pi}{2}$.

4.2 Crossings of the angular distribution

Before looking at the mathematical consequences of a crossing let us discuss how the non-collective eigenvalues are distributed in the forbidden region. Figure 4.1 displays $\mathrm{Re}\,(w)$ and $\mathrm{Im}\,(w)$ in terms of the coupling μ assuming that G_u has a single crossing. For $\mu = 0$ all modes are non-collective and evenly distributed in the forbidden region $w \in [-1, +1]$. As soon as the coupling is turned on the lines at the edge of the forbidden region peel off and the others rearrange to fill the area. The main feature of the graphic are the branching points, where two non-collective modes meet and form a complex conjugated pair. This pair can leave the forbidden region and split into a pair of real collective modes. It is crucial for every stability analysis to assess whether these branching points always exist in the presence of a crossing.

In eq. (4.9a) the left hand side vanishes, when G_w has a crossing at $w = u_\mathrm{c}$. The same observation holds for its axially breaking counterpart (4.10). Now these equations only depend on the coupling constants $\mu_\mathrm{c}^\mathrm{S}$ and $\mu_\mathrm{c}^\mathrm{B}$

$$0 = F_{u_\mathrm{c},\,0} + \frac{1 + \mu_\mathrm{c}^\mathrm{S}\mathcal{G}_0\left(\mu_\mathrm{c}^\mathrm{S}\mathcal{G}_0 + u_\mathrm{c}\right) + \mu_\mathrm{c}^\mathrm{S}\mathcal{G}_1}{\mu_\mathrm{c}^\mathrm{S}\left(1 - u_\mathrm{c}^2 - \mu_\mathrm{c}^\mathrm{S}u_\mathrm{c}\mathcal{G}_0 + \mu_\mathrm{c}^\mathrm{S}\mathcal{G}_1\right)}, \tag{4.21a}$$

$$0 = \frac{4}{\mu_\mathrm{c}^\mathrm{B}} - F_{u_\mathrm{c},\,0} + F_{u_\mathrm{c},\,2}. \tag{4.21b}$$

The respective solution of these equations are

$$\mu_\mathrm{c}^\mathrm{S} = -\,2\left[F_{u_\mathrm{c},\,0}\left(1 - u_\mathrm{c}^2\right) + \mathcal{G}_0 u_\mathrm{c} + \mathcal{G}_1 \pm \sqrt{\mathcal{D}}\right]^{-1}, \tag{4.22a}$$

$$\mu_\mathrm{c}^\mathrm{B} = \frac{4}{F_{u_\mathrm{c},\,0} - F_{u_\mathrm{c},\,2}} \tag{4.22b}$$

where $\mathcal{D}$ is the discriminant corresponding to the quadratic equation (4.21a) in $\mu_\mathrm{c}^\mathrm{S}$ and has the form

$$\mathcal{D} \equiv \left[F_{u_\mathrm{c},\,0}\left(1 - u_\mathrm{c}^2\right) + \mathcal{G}_0 u_\mathrm{c} + \mathcal{G}_1\right]^2 - 4\left[\mathcal{G}_0^2 + F_{u_\mathrm{c},\,0}\left(\mathcal{G}_1 - \mathcal{G}_0 u_\mathrm{c}\right)\right]. \tag{4.23}$$

Thus it was proven that two non-collective modes merge into a complex collective branch when $w = u_\mathrm{c}$ and the coupling constant satisfies either eq. (4.22a) or (4.21b). This result is confirmed by fig. 4.1 where the blue dashed lines indicate the branching points and match the numerical solutions of the discretised system.

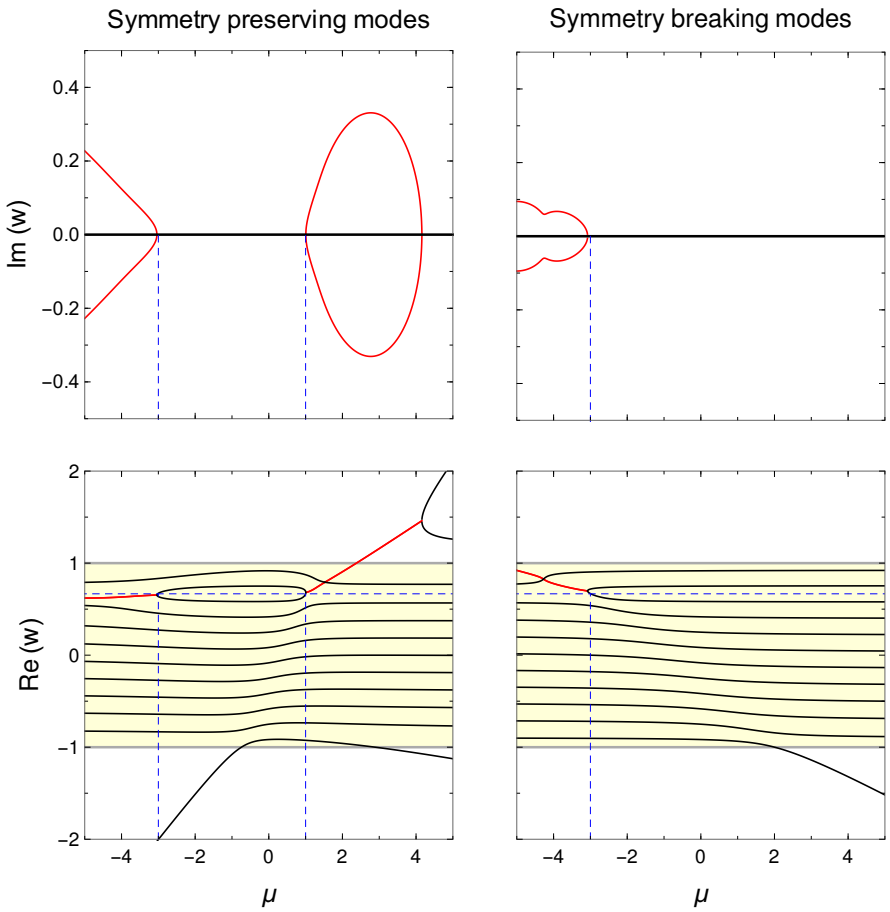

Figure 4.1: Eigenvalues w for the distribution $G_u = u - \frac{2}{3}$. The blue dashed lines indicate the crossing at u_c (horizontal) and the critical coupling constants $\mu_\mathrm{c}^{\mathrm{S,B}}$ (vertical) from the analytical calculation in eq. (4.22). As one can see the latter agree well with the merging points, already for a small number of bins $N = 12$. Because of the linearity of eq. (4.22b) there is only one critical coupling constant for each symmetry breaking modes as they are degenerate.

For the symmetry preserving modes to have an instability, $\mathrm{Im}\,(w)$ must be different from zero, so that eq. (4.22a) has two real solutions, which is equivalent to

$$\mathcal{D} > 0. \tag{4.24}$$

In sub. 4.2.2 it will be shown that not every crossing sources a complex branch, but that this inequality needs to be fulfilled as well.

For the solution for the axially breaking modes (4.22b) to be real, no such condition is needed as the equation is linear in the coupling constant. Thus there is always a real solution for $\mu_\mathrm{c}^\mathrm{B}$ if G_u has a crossing meaning that crossings are necessary and sufficient condition. This result goes beyond ref. [72] and shows that symmetry breaking modes are crucial for the question of stability.

4.2.1 Single crossing

A special case is the class of flavour isospin distributions that have a single crossing at $u = u_\mathrm{c}$, which always gives rise to an instability for symmetry preserving and breaking modes. In order to prove this point, G_u is factorised first

$$G_u = (u - u_\mathrm{c})\, P_u. \tag{4.25}$$

Here P_u is a strictly positive or negative function. Moreover it is assumed that P_u does not have any poles, which is also physically reasonable as the lepton number cannot diverge. Analogous to eq. (4.6) the moments of P_u are written as

$$\mathcal{P}_n = \int \mathrm{d}u\, u^n P_u\,. \tag{4.26}$$

First, we look at the consequences of eq. (4.25) for the symmetry preserving modes. When substituting $F_{u_\mathrm{c},0} = -\mathcal{P}_0$ and $\mathcal{G}_n = \mathcal{P}_{n+1} - u_c\mathcal{P}_n$ in eq. (4.22a), one obtains

$$\mu_\mathrm{c}^\mathrm{S} = \frac{2}{\mathcal{P}_0 - \mathcal{P}_2 \pm \sqrt{\left(\mathcal{P}_0 + \mathcal{P}_2\right)^2 - 4\mathcal{P}_1^2}}\,. \tag{4.27}$$

Note that there is no dependence on the eigenvalue, i.e. the crossing point u_c. The particular structure in eq. (4.22a) with pairwise appearance of $\mathcal{G}_{0,1}$ in combinations with $F_{u_\mathrm{c},0}$ is responsible for the cancellation.

With the definition $\langle\!\langle f(u) \rangle\!\rangle = \int \mathrm{d}u\, P_u f(u)$ we can rewrite eq. (4.27) as

$$\mu_\mathrm{c}^\mathrm{S} = \frac{2}{\langle\!\langle 1 - u^2 \rangle\!\rangle \pm \sqrt{\langle\!\langle \left(1+u\right)^2 \rangle\!\rangle \langle\!\langle \left(1-u\right)^2 \rangle\!\rangle}}\,. \tag{4.28}$$

Since P_u does not have a further crossing, the factors under the square root $\langle\!\langle \left(1 \pm u\right)^2 \rangle\!\rangle$ are either both positive or negative. Hence if eq. (4.25) applies, there always exist real $\mu_\mathrm{c}^\mathrm{S}$-values, where complex branches start and make the mode unstable.

The same steps can be performed for the symmetry breaking coupling constant in eq. (4.22b), which results in a simpler form

$$\mu_\mathrm{c}^\mathrm{B} = \frac{4}{\langle\!\langle 1 - u^2 \rangle\!\rangle}\,. \tag{4.29}$$

The only case in that this equation attains non-real values is when P_u has poles, which was excluded at the beginning.

In principle a multiple root at u_c is also possible, i.e. $G_u = (u - u_\mathrm{c})^n\, P_u$ where n is a positive integer. In this case the previous argumentation is only valid for odd n because G_u has a crossing then and moreover P_u is positive (or negative). For even n there is no sign change and also no instability.

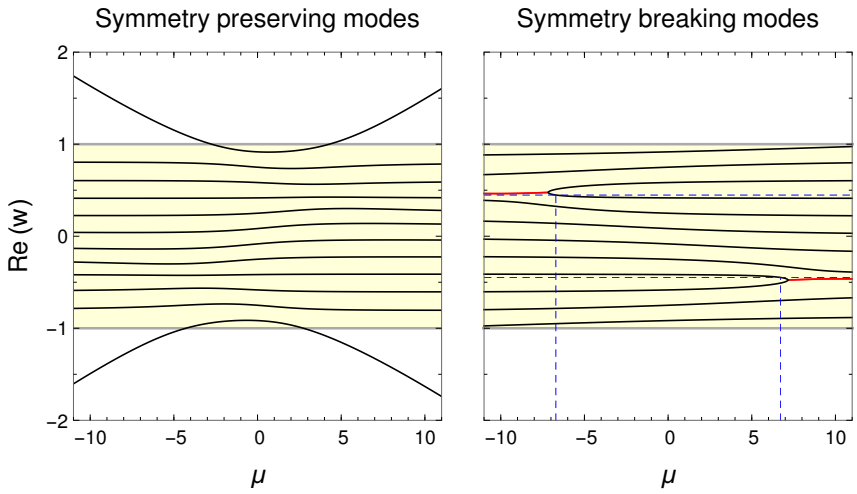

Figure 4.2: Eigenvalues for the distribution $G_u = u^2 - \frac{1}{5}$ for $N = 12$ bins. There is no unstable branch in the symmetry preserving solution, but one for each crossing in the symmetry breaking ones. The displacement of the numerical merging points and the analytical solution (blue lines) decreases for larger N.

4.2.2 Multiple crossings

In principle the number of crossings in the flavour isospin distribution is arbitrary. In analogy to eq. (4.25) a function with n crossings can be written in the form

$$G_u = P_u \prod_{i=1}^{n} (u - u_i)\,, \tag{4.30}$$

where again P_u does not change its sign or have any poles. The roots u_i are sorted according to their value.

For symmetry preserving modes it is not certain that there is an instability and if so, which root (or roots) is responsible for it. There is no simple formula as for the single crossing and so the sufficient condition (4.24) must be checked for every crossing. In order to illustrate that distributions with several crossings can be stable, an example is analysed with

$$G_u = (u - u_1)\,(u - u_2)\,, \tag{4.31}$$

where $u_{1,2} \in]-1, 1[$. With $u_c = u_1$ eq. (4.23) results in $\frac{16}{9}\,(4u_2^2 - 1)$ and thus is positive as long as $|u_2| > \frac{1}{2}$. Due to the symmetry under exchange of indices $1 \leftrightarrow 2$ the same condition with u_1 classifies the u_2-crossing. Figure 4.2 displays a dispersion relation with complete stability in the symmetric sector despite two crossings.

In the original paper [72] symmetry breaking modes were not taken into account and so it went unnoticed that these modes source an instability for every crossing. Equation (4.22b) indicates that for the exemplary distribution from

eq. (4.31) the unstable branches start at $\mu^{\mathrm{B}}_{\mathrm{c},\,i} = \frac{3}{u_i}$ with $i = 1,\, 2$. Figure 4.2 shows good agreement between the analytical and numerical calculation. A distribution with two crossings has two instabilities in the symmetry breaking sector and up to two additional ones in the symmetry preserving modes. Further calculations suggest that for $u_1 = u_2$ there are no instabilities although eqs. (4.22) have real solutions. Thus it is not sufficient that G_u has a root, but it also must change sign.

A similar analysis can be performed for a polynomial of third degree

$$G_u = (u - u_1)\,(u - u_2)\,(u - u_3)\ . \tag{4.32}$$

Additional calculations indicate that there is at least one tachyonic solution in the symmetry preserving sector, the exact number depends on the values of $u_{1,\,2,\,3}$. Based on these observations we conjectured that symmetry preserving modes for distributions with an odd number of roots, i.e. opposite signs at $u = \pm 1$, have at least one instability. For axial symmetry breaking modes the previous result holds, i.e. the number is instabilities is identical to the number of crossings.

4.3 Collective motion vs. dissipation

Although the properties of collective and non-collective modes are interesting for their own sake, the physically relevant question is how they modulate a wave packet, i.e. a superposition of modes. For the evolution of such a wave packet the dissipation from non-collective modes as well as the collective motion must be taken into account.

In order to investigate the influence of collectivity and dissipation, we analyse the evolution of flavour coherence in a stable system. This requires a definition of the overall flavour coherence. One possibility is to average over all modes [72]

$$S_{\mathrm{tot}}\,(t) = \frac{1}{2}\int_{-1}^{+1} \mathrm{d}u\, S_u\,(t)\,. \tag{4.33}$$

The coherence function for a particular mode $S_u\,(t)$ is derived from its assumed shape and the initial condition. The former is a wave packet in general, but for simplicity a plane wave like in the normal mode analysis is used, so the time evolution is a complex exponential $\mathrm{e}^{\mathrm{i}wt}$. At $t = 0$ each collective and non-collective eigenmode contributes to the coherence weighed by its amplitude T, so that at an arbitrary time only the proper phases are multiplied to each term and one obtains

$$S_u\,(t) = \int_{-1}^{+1} \mathrm{d}w\, T_w Q_{w,\,u}\, \mathrm{e}^{-\mathrm{i}wt} + \sum_{j=1,\,2} T_j Q_{w_j,\,u}\, \mathrm{e}^{-\mathrm{i}w_j t}. \tag{4.34}$$

The integral incorporates the non-collective modes labelled by their eigenfrequency whereas the sum covers the collective excitations.

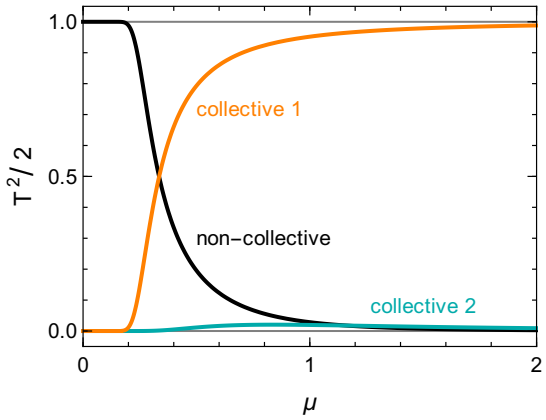

Figure 4.3: Contributions of the non-collective and collective modes to the total flavour coherence S_{tot}. The square and factor of one half on the vertical axis originates in combining eqs. (4.33), (4.34) and (4.36). The "collective 1 (2)" line corresponds to positive (negative) eigenvalues.

As a sanity check of the definition in eq. (4.33) the coherence of a non-interacting ensemble can be calculated. The non-collective eigenfunctions are δ-distributions $Q_{w,u} = \delta(w-u)$ with the normalisation factor $\mathcal{S} = 1$ from eq. (4.20) and collective modes do not exist. Assuming a normalised initial condition $T_w = 1$ for all w, the time evolution is given by

$$S_{\mathrm{tot}}(t) = \frac{1}{2}\int_{-1}^{+1} \mathrm{d}u \int_{-1}^{+1} \mathrm{d}w\, \delta(w-u)\, \mathrm{e}^{-\mathrm{i}wt} = \frac{\sin t}{t}. \tag{4.35}$$

Since there is no counteracting collective effect, kinematical decoherence dominates and consequently the initial flavour coherence dissipates with t^{-1}.

A more elaborate example is the isotropic system with $G_u = 1$. It has the special feature that due to the high symmetry the eigenfunctions are orthogonal. When the initial coherence $S_u(0) = 1$ is normalised, the amplitudes are calculable with the formula

$$T_w = \int \mathrm{d}u\, Q_{w,u}. \tag{4.36}$$

For collective modes the equation is analogous. All variables in eq. (4.20) can be calculated when the normalisation factor $\mathcal{S}$ is set to unity, so that eq. (4.36) implies

$$\begin{aligned} T_w^{-2} =& \pi^2\mu^2\left(1-2\mu w-w^2\right)^2 \\ &+\left[1+2\mu(2\mu+w)+\mu\left(1-2\mu w-w^2\right)\ln\left(\frac{1+w}{1-w}\right)\right]^2. \end{aligned} \tag{4.37}$$

The collective eigenmodes are determined by eq. (3.14), which in the fast flavour limit for an axially symmetric configuration can be brought in the

more simple form up to a normalisation factor

$$Q_{w,\,u} = \frac{1-\kappa u}{w-u}. \tag{4.38}$$

The variable κ and the normalisation factor can be calculated straightforwardly and one obtains for the amplitudes

$$\begin{aligned} T_{w_j}^2 = 2\left(1-w_j^2\right)\left(1-w\,\mathrm{acth}\,w_j\right)^2 \Big[1 - 2\left(w_j^2 + 2w_j\mu + 2\mu^2\right) \\ - 2\,\mathrm{acth}\,w_j\left(1-w_j^2\right)\left(w_j + 2\mu\left(w_j+\mu\right)\mathrm{acth}\,w_j\right)\Big]^{-1} \end{aligned} \tag{4.39}$$

with $\mathrm{acth}\,w_j$ the inverse hyperbolic cotangent. Here w_j represents a collective branch of the dispersion relation. It depends non-analytically on the coupling μ, as it is the solution of a transcendental equation.

Figure 4.3 displays the contributions of collective and non-collective amplitudes to the overall flavour coherence. For a small coupling constant the collective modes are negligible, but as soon as μ becomes of order one the picture changes to the opposite. Interestingly the collective mode with negative eigenvalue goes down for increasing μ, so that the other one with positive $w\,(\mu)$ comprises the flavour coherence. For a wave packet with different momenta follows that the weakly coupled fast modulations dissipate quickly and only the slow ones remain.

CHAPTER 5

Beyond axial symmetry

In the previous chapter we have seen that the existence of crossings in the flavour isospin distribution is sufficient for the appearance of instabilities in axially symmetric settings. This observation answered the question on the general stability of distributions with axial symmetry. The issue of instabilities from non-symmetric distributions has not been studied yet. Furthermore one might ask if the stability of flavour waves changes with their direction of propagation. Both issues are related with each other. The reason is that from the point of view of the wave vector $\mathbf{k}$ the flavour isospin distribution is non-symmetric in most cases, even if it is axially symmetric. As long as the symmetry axis and the wave vector do not coincide, $\mathbf{k}$ is blind to the symmetry.

In this chapter examples for the dispersion relation of systems without axial symmetry are presented. Embeddings these results in a comprehensive theory is part of the ongoing research.

5.1 Influence of momentum direction

When the direction of the momentum with respect to the flavour isospin distribution is arbitrary, previous results on the stability of collective flavour modes do not apply in general. In this section two examples are shown: a discrete and a continuous distribution. The continuous one is still axially symmetric to reduce the dimensionality, i.e. the amount of possible directions of the momentum vector.

5.1.1 Two-beam case

In order to get a first idea of possible changes to the stability of flavour correlation depending on the orientation of $\mathbf{k}$ it is useful to consider a minimal

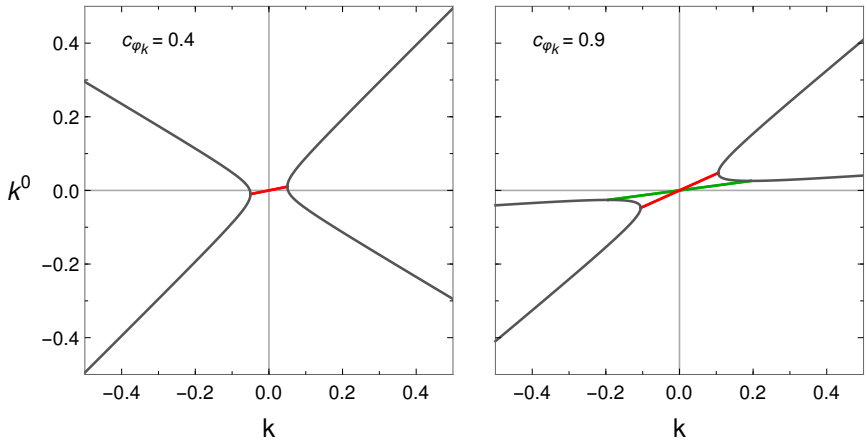

Figure 5.1: Dispersion relation for $G_{1,2} = \pm 0.5$ and different wave directions as indicated in the panels. The type of instability changes from absolute to convective, when the direction of the momentum vector is changed.

system with two beams. The general form of the corresponding flavour isospin distribution is

$$G_{\mathbf{v}} = 2\delta\left(\theta - \frac{\pi}{2}\right)\left[G_1\delta\left(\varphi - \varphi_{\mathrm{b}}\right) + G_2\delta\left(\varphi + \varphi_{\mathrm{b}}\right)\right], \tag{5.1}$$

where φ_{b} represent the beam angle. The coordinate system is chosen so that both beams are located in the equatorial plane. The wave vector is written in spherical coordinates $\mathbf{k} = k\left(\mathrm{s}_{\theta_k}\mathrm{c}_{\varphi_k},\, \mathrm{s}_{\theta_k}\mathrm{s}_{\varphi_k},\, \mathrm{c}_{\theta_k}\right)$ with the shorthand notation $\mathrm{c}_\alpha = \cos\alpha$ and $\mathrm{s}_\alpha = \sin\alpha$. In order to reduce the amount of possible configuration only the coplanar case is considered, where $\mathrm{c}_{\theta_k} = \frac{\pi}{2}$.

For the chosen distribution the dispersion relation is derivable analytically when applying eqs. (3.16) and (3.18)

$$k^0\left(k,\, \varphi_k\right) = k\mathrm{c}_{\varphi_{\mathrm{b}}}\mathrm{c}_{\varphi_k} \pm \frac{1}{2\pi}\sqrt{4\pi^2k^2\,\mathrm{s}^2_{\varphi_{\mathrm{b}}}\left(1 - \mathrm{c}_{2\varphi_k}\right) + G_1G_2\left(1 - c_{\varphi_{\mathrm{b}}}\right)^2}. \tag{5.2}$$

It is easy to see that the radicand is always positive as long as the product of G_1 and G_2 is positive. When these parameters have opposite signs, i.e. a crossing, complex branches appear in the dispersion relation. In this scenario the direction of $\mathbf{k}$ is changing only the length of the interval in $|\mathbf{k}|$ for which complex branches appear as shown in fig. 5.1. Nevertheless the system remains unstable regardless of the direction of $\mathbf{k}$. Furthermore in the depicted example the type of the instability changes according to the classification in sec. 3.2. In a special configuration the oscillation frequency k^0 is complex for all momenta. This occurs, when $\mathbf{k}$ is exactly between the beams, so that $1 - \mathrm{c}_{2\varphi_k} = 0$.

Summing up the results we conclude that in this simple setting the stability of modes can change, but not the stability of the whole system.

5.1.2 Multipole expansion

For a continuous distribution the eigenvalues are often not calculable analytically because the dispersion relation usually is a transcendental equation. There is no systematic way to solve the eigenvalue equation (4.1), which is[1]

$$(w-u)\,Q_{\mathbf{v}} = -\frac{\mu}{4\pi}\int_{-1}^{1}\mathrm{d}u'\int_{0}^{2\pi}\mathrm{d}\varphi'\;(1-\mathbf{v}\cdot\mathbf{v}')\,G_{\mathbf{v}'}Q_{\mathbf{v}'}. \tag{5.3}$$

The unit vector $\mathbf{v}$ (and $\mathbf{v}'$) is parameterised by the spherical coordinates $u = \cos\theta$ and φ.

In order to calculate the eigenvalues approximately the polar coordinate u is discretised as $\int_{-1}^{+1}\mathrm{d}u \to \Delta u\sum_{i=1}^{N}$ with $\Delta u = \frac{2}{N}$. For the discretisation of the azimuthal angle φ it is important to note that the functions $G_{\mathbf{v}}$ and $Q_{\mathbf{v}}$ are defined on a spherical surface and need to be periodic in φ, i.e. $Q\,(u,\,\varphi+2\pi) = Q\,(u,\,\varphi)$. This property can be used to rewrite both functions as Fourier series of the form

$$F_\varphi = \sum_{m=-\infty}^{\infty} f^{(m)}\mathrm{e}^{\mathrm{i}m\varphi} \quad \text{with} \quad f^{(m)} = \int_0^{2\pi}\frac{\mathrm{d}\varphi}{2\pi}F_\varphi\mathrm{e}^{-\mathrm{i}m\varphi}. \tag{5.4}$$

The coefficient $f^{(m)}$ is the mth multipole of the function F_φ. For all real functions like $G_{\mathbf{v}}$ the identity $f^{(m)^*} = f^{(-m)}$ holds, where the asterisk denotes complex conjugation.

When the multipole expansion is used, eq. (5.3) can be split up in an infinite number of equations, one for each multipole. On the right hand side of eq. (5.3) the entire φ-dependence is contained in $\mathbf{v}$, so that only the multipoles $q^{(m)}$ with $m = 0,\,\pm1$ have non-trivial equations. Therefore the system is characterised by

$$(w-u)\,q_u^{(0)} = -\frac{\mu}{2}\int\mathrm{d}u'\;(1-uu')\sum_{m=-\infty}^{\infty}g_{u'}^{(-m)}q_{u'}^{(m)}, \tag{5.5a}$$

$$(w-u)\,q_u^{(\pm1)} = \frac{\mu}{4}\sqrt{1-u^2}\int\mathrm{d}u'\,\sqrt{1-u'^2}\sum_{m=-\infty}^{\infty}g_{u'}^{(-m\pm1)}q_{u'}^{(m)}, \tag{5.5b}$$

$$(w-u)\,q_u^{(m)} = 0 \quad \text{for } |m|>1. \tag{5.5c}$$

It is nice to see that for an axially symmetric neutrino distribution, i.e. $g_u^{(m)} = 0$ for $m \neq 0$, the equations decouple from each other.

This set of equations can also be written as a matrix equation for the vector $q_{u'}^{(m)}$, where the particular structure becomes apparent. The right hand sides of eqs. (5.5) give rise to an infinite matrix, which is zero apart from a horizontal

[1] For notational simplicity in this chapter the dependence on the eigenvalue w is implied.

belt in the middle

$$(w-u)\begin{pmatrix} \vdots \\ q_u^{(+1)} \\ q_u^{(0)} \\ q_u^{(-1)} \\ \vdots \end{pmatrix} = \int_{-1}^{+1} \mathrm{d}u' \begin{pmatrix} \ddots & & \vdots & & \iddots \\ & 0 & 0 & 0 & \\ \dots & \mathcal{I}_{1,-1} & \mathcal{I}_{1,0} & \mathcal{I}_{1,1} & \dots \\ & \mathcal{I}_{0,-1} & \mathcal{I}_{0,0} & \mathcal{I}_{0,1} & \\ \dots & \mathcal{I}_{-1,-1} & \mathcal{I}_{-1,0} & \mathcal{I}_{-1,1} & \dots \\ & 0 & 0 & 0 & \\ \iddots & & \vdots & & \ddots \end{pmatrix} \begin{pmatrix} \vdots \\ q_{u'}^{(+1)} \\ q_{u'}^{(0)} \\ q_{u'}^{(-1)} \\ \vdots \end{pmatrix}. \tag{5.6}$$

The matrix element $\mathcal{I}_{k,l}$ represents the matching integrand from eqs. (5.5) including all prefactors, so that it depends on u and u'.

The multipole expansion (5.5) discretises the system with respect to φ and it becomes clear that the higher multipoles with $m > 1$ are not relevant. The solution to eq. (5.5c) is purely kinematical and does not contribute to the eigenvalue w. The reason for that is the same as in sec. 4.1, where the ansatz for the axially breaking eigenfunctions was justified. Therefore the discretisation of the system in the azimuthal direction does not lead to any approximation and in the end one obtains a $3N\times3N$-matrix for the eigenvalue equation.

We emphasise that the eigenvalues only depend on five multipoles of $G_{\mathbf{v}}$, more precisely those $g^{(m)}$ with $m = -2, -1, 0, 1, 2$. Even if the flavour isospin distributions is very complicated, this observation allows for the truncation of the multipole expansion without approximations.

5.1.3 Stability for different directions

Finally the dispersion relation for an exemplary flavour isospin distribution is discussed for different wave vector directions. The flavour isospin distribution is axially symmetric. One should keep in mind that the whole system is only symmetric, when the symmetry axis and the wave vector $\mathbf{k}$ are aligned. This configuration corresponds to $\alpha = 0$, where α parameterises the angle between the symmetry axis of $G_{\mathbf{v}}$ and $\mathbf{k}$. For $\alpha = 0$ the distribution has the form $G_u = u - \frac{2}{3}$, the same as in fig. 4.1.

Figure 5.2 depicts collective (and non-collective) modes for different angles α and different calculation methods. The first two columns are based on the previously described discretisation method with multipoles. For $N = 100$ the non-collective branches are not shown due to their high number. For the third column the polarisation-matrix approach was applied. There the real collective branches are exact, whereas unstable parts have been calculated numerically.

Let us first understand, what is shown in the first row, where $\alpha = 0$. Because of identical distributions the first panel with $N = 5$ is an overlay of the symmetry preserving and breaking modes from fig. 4.1, but with smaller N. The symmetry breaking modes are degenerate, so that the number of eigenvalues seems to be smaller than $3N = 15$ for $N = 5$. Furthermore the starting

points of instabilities that belong to the same crossing, here $u_c = \frac{2}{3}$, start at the same w-value. For small N there are still deviations, but for $N = 100$ and in the continuous case the equality of w-values becomes clear.

When α deviates from zero, several things change. The first difference can be best seen for $N = 5$. The eigenvalues of axial symmetry breaking modes are not degenerate anymore and in fact one cannot distinguish between symmetry breaking and preserving modes because they get mixed. For $\alpha = \frac{\pi}{5}$ the previously degenerate branches are still close to each other, but they drift apart further when α grows.

The second difference is the appearance of additional instabilities in the discretised solution, which are shown in the first and second column. These instabilities, also called spurious instabilities, are an artefact of the discretisation. In a linear stability analysis spurious modes appear because branch cuts in the dispersion relation cannot be resolved due to the discretisation, but result in a multitude of point singularities [106]. For low N the number of these singularities is small and it is hard to distinguish them from the physical instabilities, which also appear in the continuous calculation. With growing N the number of spurious modes increases, but their imaginary contribution decreases. This behaviour allows the definition of a threshold, which was done in the panel with $N = 100$. Modes with non-real eigenvalues, where $\mathrm{Im}(w) < 0.01$, are colored blue and the others red. The comparison with the exact calculation shows that for our example this threshold is well-chosen to distinguish between spurious and physical instabilities.

When deviating from $\alpha = 0$, one notices that the starting points of unstable branches do not share the same w-value. This difference becomes apparent when comparing the continuous case for $\alpha = 0$ and $\frac{\pi}{5}$. This feature is not surprising, which becomes clear when considering the mathematical changes in the distribution when $\alpha \neq 0$. In order to do so it is necessary to distinguish between a crossing and a crossing-value. Here a crossing is defined as a sign change in the flavour isospin distribution, i.e. a closed line on a spherical surface. A crossing-value can be treated as the coordinate of a specific crossing. In an axially symmetric setting it is easy to assign a value to a crossing, as the sign change takes place at a fixed polar coordinate, which was named u_c in ch. 4. The starting point of unstable branches always satisfy $w = u_c$. If the setting is non-symmetric, such an assignment of a single coordinate, i.e. a crossing-value, to a crossing is not possible. Therefore it is not surprising that the starting points of instabilities are not determined by one number. Ongoing research aims at the generalisation of crossing-values for non-symmetric distributions.

The final difference in the dispersion relation is the varying number of instabilities, when the direction of the wave vector is changed. In particular for $\alpha = \frac{\pi}{2}$ the system is completely stable. The disappearance of all unstable branches is a special feature and not all distributions exhibit it. Further computations indicate that for linear distributions of the form $G_u = u - a$ the transition from unstable to stable only occurs for $a > \frac{1}{2}$.

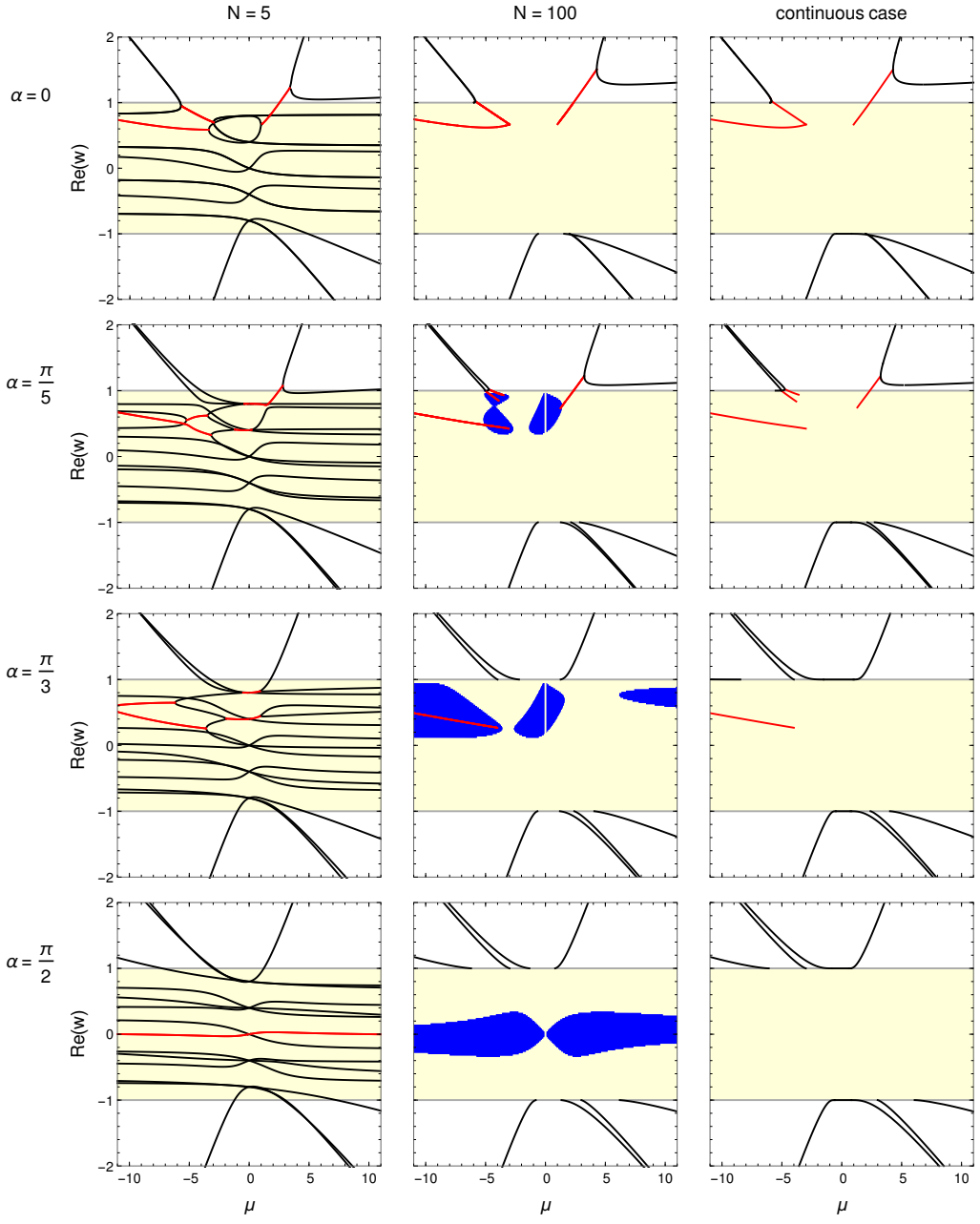

Figure 5.2: Real contribution to the eigenvalues for the distribution $G_u = u - \frac{2}{3}$ rotated by α. Black lines represent modes without imaginary contribution. Red and blue coloured modes have an imaginary part, which is smaller than 0.01 for blue ones. Non-collective modes are only shown in the left panel. In the middle panel they are not included for better visibility of the rest, whereas in the continuous calculation non-collective modes densely fill the region $-1 < w < 1$.

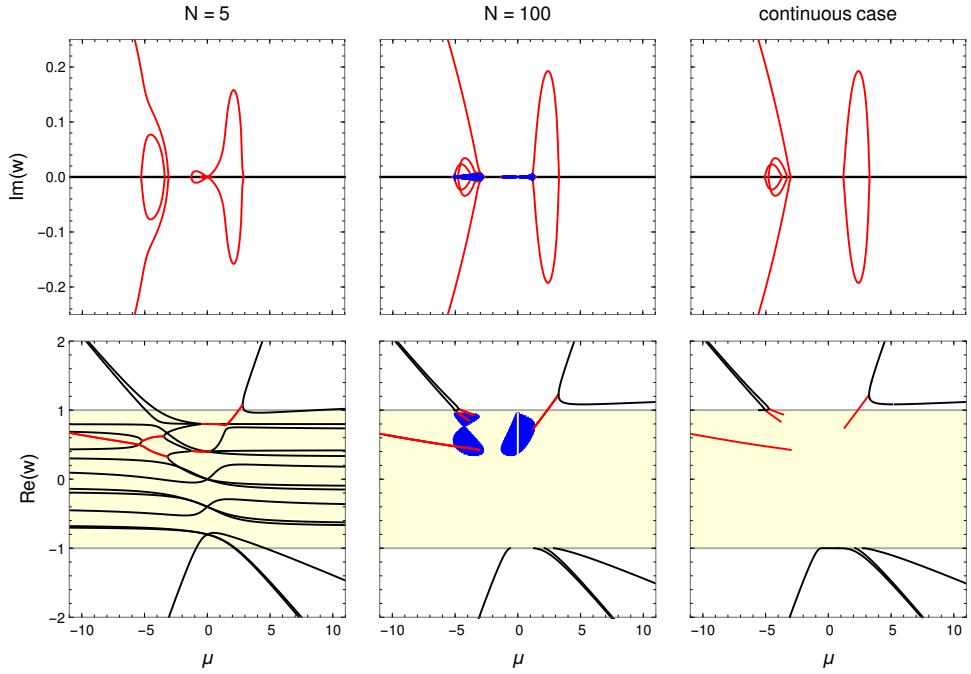

Figure 5.3: Imaginary and real parts of the eigenvalues for the distribution $G_u = u - \frac{2}{3}$ rotated by $\alpha = \frac{\pi}{5}$. In the middle panel the imaginary contribution of spurious instabilities becomes so small that they cannot be distinguished from $\mathrm{Im}(w) = 0$ or they form a blue blob.

When looking at the blue-coloured instabilities in fig. 5.2, their behaviour seems to be special around $\mu = 0$. At $\mu = 0$ all modes are real and kinematical as there is no interaction and hence no collectivity. However, already for small, non-zero μ the eigenvalues attain an imaginary contribution, which apparently indicates a discontinuity. This impression is created by the projection of eigenvalues on the real plane. When the imaginary parts are taken into account, the picture changes. Figure 5.3 displays the real and imaginary contributions of the eigenvalues for $\alpha = \frac{\pi}{5}$. The continuity around $\mu = 0$ is best visible in the upper panel for $N = 5$. At $\mu = 0$ the red lines cross $\mathrm{Im}(w) = 0$, so that the modes become immediately unstable for positive and negative coupling constants.

5.1.4 Stability criterion

Also for configurations without axial symmetry a criterion is desirable, which allows one to determine the stability of a specific flavour wave or the whole system straightforwardly. For this purpose a similar ansatz as in the previous chapter can be pursued. The multipoles from eqs. (5.12) have the form

$$q_u^{(0)} = A^{(0)} \left(\frac{1}{w-u} + \gamma^{(0)} \delta\left(w-u\right) \right) + B, \tag{5.7a}$$

$$q_u^{(\pm 1)} = A^{(\pm 1)} \left(\frac{\sqrt{1-u^2}}{w-u} + \gamma^{(\pm 1)} \delta\left(w-u\right) \right). \tag{5.7b}$$

Multipoles with $m > 1$ do not contribute to the collective behaviour and thus can be omitted.

Equations (5.7) can be inserted into eqs. (5.5) and written in a matrix form as it was done in the previous chapter. The parameters $A^{(0,\pm1)}$ and B form the vector. The determinant of the mentioned matrix needs to vanish and here the problem becomes apparent. The matrix depends on all three parameters $\gamma^{(0,\pm1)}$ and there is only one equation. In the symmetric case this equation can be written in terms of the functions f and g

$$f\left(\gamma^{(0)}\right) g\left(\gamma^{(+1)}\right) g\left(\gamma^{(-1)}\right) = 0. \tag{5.8}$$

Due to the mixing of symmetry preserving and breaking modes such a factorisation does not take place, so that another procedure must be found to determine each of the γ-parameters. This issue has not been resolved and so finding a stability criterion for non-symmetric distributions remains an open question.

The described difficulty with non-symmetric systems is not surprising as the notion of a crossing is less clear then. As explained before there is no procedure yet to assign crossing values to sign changes in the flavour isospin distribution. Only in the symmetric case it is clear how to find and use these values to fix the starting points of instabilities.

5.2 Azimuthal variation

After investigating the consequences of changing the direction of the wave vector we turn to completely non-symmetric flavour isospin distributions. In particular the question is addressed how the azimuthal variation of the distribution affects the stability of the system. For this purpose a φ-dependent distribution with support at a single polar angle is chosen, which implies

$$G_{\mathbf{v}} = \delta\left(u - u_{\mathrm{b}}\right)\left(g^{(0)} + 2g^{(1)}\cos\varphi + g^{(2)}\mathrm{e}^{2\mathrm{i}\varphi} + g^{(-2)}\mathrm{e}^{-2\mathrm{i}\varphi}\right). \tag{5.9}$$

The coordinate system was chosen in such a way that both dipoles are real $g^{(1)} = g^{(-1)}$ and so the angular function is a cosine.

When the polar angle is fixed, all u- and u'-dependent terms can be absorbed in eqs. (5.5a) and (5.5b). The eigenvalues can be calculated by deriving the characteristic equation from eq. (5.6). With the substitutions $w \to w + u$ and $\mu \to \mu/s_{\theta_b}^2$ the corresponding determinant simplifies to

$$\det\left[w\mathbb{1}_3 - \mu\begin{pmatrix} \frac{1}{2}g^{(0)} & \frac{1}{2}g^{(1)} & \frac{1}{2}g^{(2)} \\ -g^{(1)} & -g^{(0)} & -g^{(1)} \\ \frac{1}{2}g^{(-2)} & \frac{1}{2}g^{(1)} & \frac{1}{2}g^{(0)} \end{pmatrix}\right] = 0. \tag{5.10}$$

The structure of the second term determines whether the eigenvalues can be complex or not. If the matrix is Hermitian, w is always real. The dipole $g^{(1)}$ breaks Hermiticity and so sources every instability.

Equation (5.10) can be solved analytically, but it is hard to gain much insight from the formula. With a reduction of parameters the solution is more accessible. The higher multipole $g^{(\pm 2)}$ does not contribute to the instability, as it does not break hermiticity, and hence it is reasonable to set it to zero. This assumption results in the solution

$$w_1 = \frac{1}{2}\mu g^{(0)} \,, \quad w_{2,3} = -\frac{1}{4}\mu g^{(0)} \pm \mu\sqrt{\frac{9}{16}{g^{(0)}}^2 - {g^{(1)}}^2}. \tag{5.11}$$

The eigenvalues become complex for $g^{(1)} > \frac{3}{4}g^{(0)}$. Comparing this result with eq. (5.9) one finds that for an intermediate range $\frac{1}{2}g^{(0)} < g^{(1)} < \frac{3}{4}g^{(0)}$ there are no unstable modes despite the existence of a crossings.

5.3 Connection to polarisation matrix

When looking at eq. (5.6), one might conclude that the eigenvalues w belong to a 3×4-matrix, which is in contradiction with the 4×4-polarisation matrix in ch. 3. In order to clarify this point the connection is established between the multipole equations (5.5) and the polarisation matrix $\Pi_{\mu\nu}$ in eq. (3.16). The main reason is that in eq. (5.6) the polar coordinate u has not been taken into account, modifies the matrix structure.

The polarisation matrix approach only takes collective modes into account, for which $w - u \neq 0$. Therefore eqs. (5.5) can be divided by that factor, which implies

$$q_u^{(-1)} = \frac{\mu\sqrt{1-u^2}}{4\,(w-u)} \int \mathrm{d}u'\, \sqrt{1-u'^2} \left(g_{u'}^{(0)} q_{u'}^{(-1)} + g_{u'}^{(-1)} q_{u'}^{(0)} + g_{u'}^{(-2)} q_{u'}^{(+1)} \right) \tag{5.12a}$$

$$q_u^{(0)} = \frac{-\mu}{2\,(w-u)} \int \mathrm{d}u'\, (1-uu') \left(g_{u'}^{(+1)} q_{u'}^{(-1)} + g_{u'}^{(0)} q_{u'}^{(0)} + g_{u'}^{(-1)} q_{u'}^{(+1)} \right) \tag{5.12b}$$

$$q_u^{(+1)} = \frac{\mu\sqrt{1-u^2}}{4\,(w-u)} \int \mathrm{d}u'\, \sqrt{1-u'^2} \left(g_{u'}^{(2)} q_{u'}^{(-1)} + g_{u'}^{(+1)} q_{u'}^{(0)} + g_{u'}^{(0)} q_{u'}^{(+1)} \right). \tag{5.12c}$$

Here it was used that higher multipoles with $m > 1$ do not contribute to the eigenvalue w.

As the multipoles are completely integrated out on the right hand side of this system of equations, the general form of $q_u^{(0,\pm 1)}$ can be deduced

$$q_u^{(0)} = \frac{a + b^{(0)} u}{w - u} \tag{5.13a}$$

$$q_u^{(\pm 1)} = b^{(\pm 1)} \frac{\sqrt{1-u^2}}{w-u}. \tag{5.13b}$$

Plugging eqs. (5.13) into eqs. (5.12) results in three equations for the four parameters a, $b^{(0,\pm 1)}$. However, the monopole equation can be split into two equations for constant and u-dependent terms respectively.

For writing down the complete system of equations it is helpful to change notation. Firstly, u-dependent terms are substituted by trigonometric function of the polar angle θ, so that $u = \cos\theta \equiv \mathrm{c}_\theta$ and $\sqrt{1-u^2} = \sin\theta \equiv \mathrm{s}_\theta$. Secondly, the integrals over $\cos\theta$ are abbreviated as

$$I_f^{(i)} = \frac{1}{2}\int_{-1}^{+1} \mathrm{d}c_\theta \, \frac{g_\theta^{(i)} f_\theta}{w - c_\theta}. \tag{5.14}$$

The index can take the values $f = 1$, c, s, cc, cs or ss, for which $f_\theta = 1$, $\cos\theta$ and so forth. Then the parameters in eqs. (5.13) are determined by the following matrix equation

$$\begin{pmatrix} a \\ b^{(+1)} \\ b^{(-1)} \\ b^{(0)} \end{pmatrix} = \mu \begin{pmatrix} I_1^{(0)} & I_s^{(-1)} & I_s^{(+1)} & I_c^{(0)} \\ \frac{1}{2}I_s^{(+1)} & \frac{1}{2}I_{ss}^{(0)} & \frac{1}{2}I_{ss}^{(+2)} & \frac{1}{2}I_{cs}^{(+1)} \\ \frac{1}{2}I_s^{(-1)} & \frac{1}{2}I_{ss}^{(-2)} & \frac{1}{2}I_{ss}^{(0)} & \frac{1}{2}I_{cs}^{(-1)} \\ I_c^{(0)} & I_{cs}^{(-1)} & I_{cs}^{(+1)} & I_{cc}^{(0)} \end{pmatrix} \begin{pmatrix} a \\ b^{(+1)} \\ b^{(-1)} \\ b^{(0)} \end{pmatrix}. \tag{5.15}$$

By performing the substitution $b^{(\pm 1)} \to \frac{1}{\sqrt{2}} b^{(\pm 1)}$ the tensor on the right hand side becomes symmetric and with a rearrangement of terms eq. (5.15) can be written in the form $\tilde{\Pi}^{\mu\nu} a_\nu = 0$ for the vector $a_\nu = \left(a,\, b^{(+1)},\, b^{(-1)},\, b^{(0)}\right)$. The polarisation tensor $\tilde{\Pi}$ has the form

$$\tilde{\Pi}^{\mu\nu} = \begin{pmatrix} +1 & & & \\ & -1 & & \\ & & -1 & \\ & & & -1 \end{pmatrix} + \mu \begin{pmatrix} I_1^{(0)} & \frac{1}{\sqrt{2}}I_s^{(-1)} & \frac{1}{\sqrt{2}}I_s^{(+1)} & I_c^{(0)} \\ \frac{1}{\sqrt{2}}I_s^{(+1)} & \frac{1}{2}I_{ss}^{(0)} & \frac{1}{2}I_{ss}^{(+2)} & \frac{1}{\sqrt{2}}I_{cs}^{(+1)} \\ \frac{1}{\sqrt{2}}I_s^{(-1)} & \frac{1}{2}I_{ss}^{(-2)} & \frac{1}{2}I_{ss}^{(0)} & \frac{1}{\sqrt{2}}I_{cs}^{(-1)} \\ I_c^{(0)} & \frac{1}{\sqrt{2}}I_{cs}^{(-1)} & \frac{1}{\sqrt{2}}I_{cs}^{(+1)} & I_{cc}^{(0)} \end{pmatrix}. \tag{5.16}$$

If a_ν has non-trivial values, the determinant of $\tilde{\Pi}$ must vanish, which results in the defining equation for the collective eigenvalues w. Note that the polarisation tensors from eq. (3.16) in the fast flavour limit and eq. (5.16) are not identical. They are written in different coordinate bases and can be transformed into each other with a proper rotation in the $b^{(+1)}$-$b^{(-1)}$-plane.

5.4 Summary

This section dealt with several questions that arise when the assumption of axial symmetry is discarded. It was shown that for a chosen wave vector the existence of a crossing in the flavour isospin distribution is not sufficient to cause instabilities. Indeed, we have demonstrated that instabilities can disappear when changing the direction of propagation of the flavour wave. Also the calculation regarding the influence of azimuthal variations on the stability lead to this result as the crossing needs to reach a critical depth. Some questions still require an answer. For example it would be interesting to

know which underlying principles cause the stability variation. Furthermore it is not certain that in a non-symmetric setting a crossing in the flavour isospin distribution is necessary to cause instabilities.

CHAPTER 6

Conclusions and Outlook

Although the theoretical and experimental research on neutrino flavour conversion has been going on for decades there are still unresolved issues and possible new effects. On the one hand important progress has been made regarding the influence of matter on the neutrino flavour content, e.g. by solving the solar neutrino problem. On the other hand it remains unclear how refraction from neutrino-neutrino coupling affects the oscillation behaviour, which might be important for the physics of core-collapse supernovae among others. During such an explosion the majority of the energy is emitted as neutrinos, which leads to extremely high number densities, so that the requirement for neutrino-neutrino refraction is fulfilled. Furthermore neutrinos are considered to be a possible candidate to reenergise the stalled shock wave, which drives the explosion. In addition the neutrino flavour content is relevant for the synthesis of heavy nuclei, so that for a profound comprehension of these processes neutrino oscillations must be included. In this thesis several aspects of a particular effect from neutrino-neutrino interaction, the fast flavour conversion, were illustrated.

Before the investigation of fast neutrino flavour conversion the required equation of motion was derived. It was shown that the usually applied Liouville equation for the matrix of densities is an approximation of a more general expression. This complete version is called Moyal equation and is the consequence of forming the matrix of densities out of quantum fields. The Moyal equation features an infinite sum of spatial and momentum derivatives and the leading terms describe the advection and deflection of particles. When neutrinos are relativistic, the matrix of velocities in the advection term is close to the identity matrix and hence the simplification to the Liouville equation with unit velocity vector is reasonable. Nevertheless small deviations from the identity matrix remain. In case of a plane flavour wave these deviations give

rise to a small correction of the oscillation length, which can be neglected. Additionally, it was demonstrated how the neutrino interaction terms in the Standard Model provide the refraction terms, which are important for neutrino oscillation in matter.

It is also possible to derive a modified version of Moyal's equation which can model additional effects. For example the time component in the two-point correlators can be Wigner transformed as well, which leads to a term that is relevant for time-dependent Hamiltonians. Furthermore the whole derivation can be performed on the operator level without the mean field approximation, so that in the end also effects from entanglement can be studied.

The equation of motion derived in ch. 2 has been applied in the context of systems with high neutrino density, where neutrino-neutrino interaction play an important role for the flavour evolution. Then the equation of motion is non-linear and gives rise to new phenomena, which are called "collective" due to the arising compliance in the oscillation behaviour. Slow and fast neutrino flavour conversion denote two classes of collective effects and in both the conversion is linked to instabilities of the flavour correlation function. The underlying theoretical distinction between slow and fast conversion is the role of masses. For slow conversion their existence is mandatory, whereas fast conversions can also occur without them. The different attributes "slow" and "fast" originate in the different length scales at which the conversion appears. These differences have phenomenological consequences because for example the region in a supernova, where fast effects arise, is closer to the core than the layer where slow conversion would be expected.

As long as flavour coherence is small, the equation of motion can be linearised, which is necessary to apply a plane-wave ansatz and define the dispersion relation for these flavour waves. If the oscillation frequency of a mode has an imaginary contribution, the mode is unstable. Depending on the vacuum oscillation frequency and the angular neutrino distribution, different kinds of instabilities can appear in the dispersion relation. One classification is necessary when slow and fast modes are dealt with simultaneously. Then their behaviour in the fast flavour limit, i.e. $\omega_{\text{vac}} = 0$, is used to distinguish between "slow" and "fast" instabilities. The former are sourced by the vacuum oscillation frequency and accordingly vanish in that limit, whereas fast instabilities remain. When both types are present, the nonzero vacuum oscillation frequency can mix them and give rise to additional non-real branches in the dispersion relation. For this reason fast modes can have slow instabilities and so there is no one-to-one correspondence between the classification of instabilities and the naming of collective flavour modes. For fast instabilities there is a second attribute, which describes the growth behaviour. An absolute instability always grows locally. On the other hand convective instability grows while propagating, so that locally the amplitude of the mode decays after some time. Apart from the classification of unstable modes it was shown that instabilities appear when there is a crossing, i.e. a sign change, in the angular part of the flavour isospin distribution.

The origin of instabilities in the flavour correlation function was investigated further. Outside of the forbidden region unstable branches start, where two real, collective branches merge. The location of this process is called a critical or branching point. It was shown that an analogous process also occurs in the forbidden region. There two kinematical, non-collective modes merge and become a complex conjugated pair of collective modes. Therefore at the branching point a transition between collective and non-collective modes takes place, which requires that their respective eigenfunctions coincide there. The observation of this matching of functions enables one to calculate the exact eigenvalue and coupling constant of the critical point for a specific distribution. Demanding that the solution is real results in the wanted sufficient condition on the distribution to feature unstable modes. The sufficient condition depends crucially on the symmetry properties of the flavour modes. Those modes that break the axial symmetry are always unstable as soon as the flavour isospin distribution has at least one crossing. For symmetry preserving modes there is no such general criterion. If the distribution has a single crossing, also these modes are certain to be unstable, but for multiple crossings the sufficient condition needs to be checked for each crossing value u_c. Furthermore it was shown how an increasing interaction strength modulates the flavour coherence carried by the non-collective and collective modes. In agreement with physical intuition, an increasing neutrino-neutrino coupling shifts the dominance from non-collective to collective modes.

When axial symmetry is broken, the system becomes more complicated because symmetric and non-symmetric modes are not distinguishable, but mix with each other. Calculations for exemplary distributions indicate that a crossing is still required to have instabilities, but it is possible that for another direction of the wave vector all modes are stable. As a next step these qualitative results are to be put on a quantitative basis. A part of this can be the derivation of the starting points for instabilities, analogous to the axially symmetric case.

Theoretical investigations of fast neutrino flavour conversion have been advanced in the past few years and improved the insight into this collective phenomenon. In particular the connection between a crossing in the angular flavour isospin distribution and the occurrence of unstable modes is well-established by now. However, most of the calculations have been performed for axially symmetric and linearised systems. Both assumptions should just be provisional to gain some intuition for the phenomenon. Some research was accomplished on the late-time behaviour of unstable modes, but results on the stability of non-symmetric distributions are still lacking and it is necessary to analyse them to complete the theoretical understanding of fast flavour transformations.

The phenomenological investigation has only recently begun and concentrated on the question whether fast flavour conversions occur in core-collapse supernovae and neutron-star mergers by either looking for imaginary oscillation

frequencies or crossings of the flavour isospin distribution. The few analyses for neutron-star mergers confirmed the occurrence of angular crossings, while the results for supernovae are more numerous, but not conclusive. For example, regions with instabilities were found deep inside the proto-neutron star and it is unclear if fast conversions there have an effect on the dynamics of a supernova. In this area a lot more research needs to be done with the purpose of implementing fast flavour conversions consistently in the simulations. Then it might be possible to address the big questions, i.e. to which extent fast conversions have an impact on nucleosynthesis and supernova dynamics.

Bibliography

[1] F. Hoyle, *Concluding remarks*, *Proc. Roy. Soc. Lon. A* **301** (1967) 171.

[2] C. L. Cowan, F. Reines, F. B. Harrison, H. W. Kruse and A. D. McGuire, *Detection of the free neutrino: A confirmation*, *Science* **124** (1956) 103.

[3] G. Danby, J.-M. Gaillard, K. Goulianos, L. M. Lederman, N. Mistry, M. Schwartz and J. Steinberger, *Observation of high-energy neutrino reactions and the existence of two kinds of neutrinos*, *Phys. Rev. Lett.* **9** (1962) 36.

[4] DONUT collaboration, *Observation of tau neutrino interactions*, *Phys. Lett.* **504** (2001) 218 [hep-ex/0012035].

[5] ALEPH Collaboration, *A direct measurement of the invisible width of the Z from single photon counting*, *Phys. Lett. B* **313** (1993) 520.

[6] Super-Kamiokande Collaboration, *Evidence for oscillation of atmospheric neutrinos*, *Phys. Rev. Lett.* **81** (1998) 1562 [hep-ex/9807003].

[7] SNO Collaboration, *Measurement of the rate of $\nu_e + d \to p + p + e^-$ interactions produced by ^8B solar neutrinos at the Sudbury Neutrino Observatory*, *Phys. Rev. Lett.* **87** (2001) 071301 [nucl-ex/0106015].

[8] IceCube, Fermi-LAT, MAGIC, AGILE, ASAS-SN, HAWC, H.E.S.S., INTEGRAL, Kanata, Kiso, Kapteyn, Liverpool Telescope, Subaru, Swift/NuSTAR, VERITAS, and VLA/17B-403 teams, *Multimessenger observations of a flaring blazar coincident with high-energy neutrino IceCube-170922A*, *Science* **361** (2018) [1807.08816].

[9] O. W. Greenberg, *Spin and unitary-spin independence in a paraquark model of baryons and mesons*, *Phys. Rev. Lett.* **13** (1964) 598.

[10] M. Y. Han and Y. Nambu, *Three-triplet model with double* SU(3) *symmetry*, *Phys. Rev.* **139** (1965) B1006.

[11] S. L. Glashow, *The renormalizability of vector meson interactions*, *Nucl. Phys.* **10** (1959) 107.

[12] A. Salam and J. C. Ward, *Weak and electromagnetic interactions*, *Nuovo Cim.* **11** (1959) 568.

[13] S. Weinberg, *A model of leptons*, *Phys. Rev. Lett.* **19** (1967) 1264.

[14] F. Englert and R. Brout, *Broken symmetry and the mass of gauge vector mesons*, *Phys. Rev. Lett.* **13** (1964) 321.

[15] P. W. Higgs, *Broken symmetries and the masses of gauge bosons*, *Phys. Rev. Lett.* **13** (1964) 508.

[16] C. Broggini, C. Giunti and A. Studenikin, *Electromagnetic properties of neutrinos*, *Adv. High Energy Phys.* **2012** (2012) 459526 [1207.3980].

[17] A. Strumia and F. Vissani, *Precise quasielastic neutrino/nucleon cross-section*, *Phys. Lett. B* **564** (2003) 42 [astro-ph/0302055].

[18] P. A. M. Dirac and R. H. Fowler, *The quantum theory of the electron*, *Proc. Roy. Soc. Lon. A* **117** (1928) 610.

[19] E. Majorana, *Teoria simmetrica dell'elettrone e del positrone*, *Nuovo Cim.* **14** (1937) 171.

[20] KamLAND-Zen Collaboration, *Search for Majorana neutrinos near the inverted mass hierarchy region with KamLAND-Zen*, *Phys. Rev. Lett.* **117** (2016) 082503 [1605.02889].

[21] KATRIN Collaboration, *Improved upper limit on the neutrino mass from a direct kinematic method by KATRIN*, *Phys. Rev. Lett.* **123** (2019) 221802 [1909.06048].

[22] Planck Collaboration, *Planck 2018 results. VI. cosmological parameters*, 1807.06209.

[23] Particle Data Group, *Review of particle physics*, *Phys. Rev. D* **98** (2018) 030001.

[24] N. Cabibbo, *Unitary symmetry and leptonic decays*, *Phys. Rev. Lett.* **10** (1963) 531.

[25] M. Kobayashi and T. Maskawa, *CP-violation in the renormalizable theory of weak interaction*, *Prog. Theor. Phys.* **49** (1973) 652.

[26] B. Pontecorvo, *Mesonium and anti-mesonium*, *Sov. Phys. JETP* **6** (1957) 429.

[27] Z. Maki, M. Nakagawa and S. Sakata, *Remarks on the unified model of elementary particles*, *Prog. Theor. Phys.* **28** (1962) 870.

[28] S. Pakvasa, *Charged-lepton oscillations*, *Lett. Nuovo Cim.* **31** (1981) 497.

[29] A. D. Dolgov, A. Y. Morozov, L. B. Okun and M. G. Schepkin, *Do muons oscillate?*, *Nucl. Phys. B* **502** (1997) 3 [hep-ph/9703241].

[30] E. K. Akhmedov, *Do charged leptons oscillate?*, *JHEP* **2007** (2007) 116 [0706.1216].

[31] G. Sigl and G. G. Raffelt, *General kinetic description of relativistic mixed neutrinos*, *Nucl. Phys. B* **406** (1993) 423.

[32] M. Sirera and A. Perez, *Relativistic Wigner function approach to neutrino propagation in matter*, *Phys. Rev. D* **59** (1999) 125011 [hep-ph/9810347].

[33] S. Yamada, *Boltzmann equations for neutrinos with flavor mixings*, *Phys. Rev. D* **62** (2000) 093026 [astro-ph/0002502].

[34] C. Y. Cardall, *Liouville equations for neutrino distribution matrices*, *Phys. Rev. D* **78** (2008) 085017 [0712.1188].

[35] A. Kartavtsev, *Relating quantum mechanics and kinetics of neutrino oscillations*, *JHEP* **01** (2020) 138 [1404.5626].

[36] R. S. L. Hansen and A. Yu. Smirnov, *The Liouville equation for flavour evolution of neutrinos and neutrino wave packets*, *JCAP* **1612** (2016) 019 [1610.00910].

[37] T. Stirner, G. Sigl and G. G. Raffelt, *Liouville term for neutrinos: Flavor structure and wave interpretation*, *JCAP* **1805** (2018) 016 [1803.04693].

[38] C. Giunti and C. W. Kim, *Fundamentals of Neutrino Physics and Astrophysics*. 2007.

[39] L. Wolfenstein, *Neutrino oscillations in matter*, *Phys. Rev. D* **17** (1978) 2369.

[40] S. P. Mikheyev and A. Y. Smirnov, *Resonance amplification of oscillations in matter and spectroscopy of solar neutrinos*, *Sov. J. Nucl. Phys.* **42** (1985) 913.

[41] Super-Kamiokande Collaboration, *First indication of terrestrial matter effects on solar neutrino oscillation*, *Phys. Rev. Lett.* **112** (2014) 091805 [1312.5176].

[42] J. T. Pantaleone, *Neutrino oscillations at high densities*, *Phys. Lett. B* **287** (1992) 128.

[43] S. Samuel, *Neutrino oscillations in dense neutrino gases*, *Phys. Rev. D* **48** (1993) 1462.

[44] V. A. Kostelecký and S. Samuel, *Self-maintained coherent oscillations in dense neutrino gases*, *Phys. Rev. D* **52** (1995) 621 [hep-ph/9506262].

[45] H. Duan, G. M. Fuller and Y.-Z. Qian, *Simple picture for neutrino flavor transformation in supernovae*, *Phys. Rev. D* **76** (2007) 085013 [0706.4293].

[46] H. Duan, G. M. Fuller and Y.-Z. Qian, *Collective neutrino oscillations*, *Ann. Rev. Nucl. Part. Sci.* **60** (2010) 569 [1001.2799].

[47] S. Samuel, *Bimodal coherence in dense self-interacting neutrino gases*, *Phys. Rev. D* **53** (1996) 5382 [hep-ph/9604341].

[48] H. Duan, G. M. Fuller and Y.-Z. Qian, *Collective neutrino flavor transformation in supernovae*, *Phys. Rev. D* **74** (2006) 123004 [astro-ph/0511275].

[49] S. Hannestad, G. G. Raffelt, G. Sigl and Y. Y. Y. Wong, *Self-induced conversion in dense neutrino gases: Pendulum in flavor space*, *Phys. Rev. D* **74** (2006) 105010 [astro-ph/0608695].

[50] H. Duan, G. M. Fuller, J. Carlson and Y.-Z. Qian, *Simulation of coherent nonlinear neutrino flavor transformation in the supernova environment: Correlated neutrino trajectories*, *Phys. Rev. D* **74** (2006) 105014 [astro-ph/0606616].

[51] G. G. Raffelt and A. Y. Smirnov, *Self-induced spectral splits in supernova neutrino fluxes*, *Phys. Rev. D* **76** (2007) 081301 [0705.1830].

[52] G. G. Raffelt and A. Y. Smirnov, *Adiabaticity and spectral splits in collective neutrino transformations*, *Phys. Rev. D* **76** (2007) 125008 [0709.4641].

[53] G. G. Raffelt and G. Sigl, *Self-induced decoherence in dense neutrino gases*, *Phys. Rev. D* **75** (2007) 083002 [hep-ph/0701182].

[54] G. G. Raffelt and I. Tamborra, *Synchronization versus decoherence of neutrino oscillations at intermediate densities*, *Phys. Rev. D* **82** (2010) 125004 [1006.0002].

[55] R. F. Sawyer, *Speed-up of neutrino transformations in a supernova environment*, *Phys. Rev. D* **72** (2005) 045003 [hep-ph/0503013].

[56] R. F. Sawyer, *Multiangle instability in dense neutrino systems*, *Phys. Rev. D* **79** (2009) 105003 [0803.4319].

[57] A. Banerjee, A. Dighe and G. G. Raffelt, *Linearized flavor-stability analysis of dense neutrino streams*, *Phys. Rev. D* **84** (2011) 053013 [1107.2308].

[58] S. Chakraborty, R. S. Hansen, I. Izaguirre and G. G. Raffelt, *Self-induced flavor conversion of supernova neutrinos on small scales*, *JCAP* **1601** (2016) 028 [1507.07569].

[59] R. F. Sawyer, *Neutrino cloud instabilities just above the neutrino sphere of a supernova*, *Phys. Rev. Lett.* **116** (2016) 081101 [1509.03323].

[60] S. Chakraborty, R. S. Hansen, I. Izaguirre and G. G. Raffelt, *Self-induced neutrino flavor conversion without flavor mixing*, *JCAP* **1603** (2016) 042 [1602.00698].

[61] I. Izaguirre, G. G. Raffelt and I. Tamborra, *Fast pairwise conversion of supernova neutrinos: A dispersion-relation approach*, *Phys. Rev. Lett.* **118** (2017) 021101 [1610.01612].

[62] B. Dasgupta, A. Mirizzi and M. Sen, *Fast neutrino flavor conversions near the supernova core with realistic flavor-dependent angular distributions*, *JCAP* **1702** (2017) 019 [1609.00528].

[63] F. Capozzi, B. Dasgupta, E. Lisi, A. Marrone and A. Mirizzi, *Fast flavor conversions of supernova neutrinos: Classifying instabilities via dispersion relations*, *Phys. Rev. D* **96** (2017) 043016 [1706.03360].

[64] A. Dighe and M. Sen, *Nonstandard neutrino self-interactions in a supernova and fast flavor conversions*, *Phys. Rev. D* **97** (2018) 043011 [1709.06858].

[65] B. Dasgupta and M. Sen, *Fast neutrino flavor conversion as oscillations in a quartic potential*, *Phys. Rev. D* **97** (2018) 023017 [1709.08671].

[66] S. Abbar and H. Duan, *Fast neutrino flavor conversion: Roles of dense matter and spectrum crossing*, *Phys. Rev. D* **98** (2018) 043014 [1712.07013].

[67] B. Dasgupta, A. Mirizzi and M. Sen, *Simple method of diagnosing fast flavor conversions of supernova neutrinos*, *Phys. Rev. D* **98** (2018) 103001 [1807.03322].

[68] F. Capozzi, B. Dasgupta, A. Mirizzi, M. Sen and G. Sigl, *Collisional triggering of fast flavor conversions of supernova neutrinos*, *Phys. Rev. Lett.* **122** (2019) 091101 [1808.06618].

[69] S. Airen, F. Capozzi, S. Chakraborty, B. Dasgupta, G. G. Raffelt and T. Stirner, *Normal-mode analysis for collective neutrino oscillations*, *JCAP* **1812** (2018) 019 [1809.09137].

[70] S. Abbar and M. C. Volpe, *On fast neutrino flavor conversion modes in the nonlinear regime*, *Phys. Lett. B* **790** (2019) 545 [1811.04215].

[71] C. Yi, L. Ma, J. D. Martin and H. Duan, *Dispersion relation of the fast neutrino oscillation wave*, *Phys. Rev. D* **99** (2019) 063005 [1901.01546].

[72] F. Capozzi, G. G. Raffelt and T. Stirner, *Fast neutrino flavor conversion: Collective motion vs. decoherence*, *JCAP* **1909** (2019) 002 [1906.08794].

[73] M. Chakraborty and S. Chakraborty, *Three flavor neutrino conversions in supernovae: slow & fast instabilities*, *JCAP* **2001** (2020) 005 [1909.10420].

[74] S. Bhattacharyya and B. Dasgupta, *Fast neutrino flavor conversion at late time*, [2005.00459].

[75] S. Abbar and H. Duan, *Neutrino flavor instabilities in a time-dependent supernova model*, *Phys. Lett. B* **751** (2015) 43 [1509.01538].

[76] I. Tamborra, L. Hüdepohl, G. G. Raffelt and H.-T. Janka, *Flavor-dependent neutrino angular distribution in core-collapse supernovae*, *Astrophys. J.* **839** (2017) 132 [1702.00060].

[77] S. Abbar, H. Duan, K. Sumiyoshi, T. Takiwaki and M. C. Volpe, *On the occurrence of fast neutrino flavor conversions in multidimensional supernova models*, *Phys. Rev. D* **100** (2019) 043004 [1812.06883].

[78] M. Delfan Azari, S. Yamada, T. Morinaga, W. Iwakami, H. Okawa, H. Nagakura and K. Sumiyoshi, *Linear analysis of fast-pairwise collective neutrino oscillations in core-collapse supernovae based on the*

results of Boltzmann simulations, *Phys. Rev. D* **99** (2019) 103011 [1902.07467].

[79] S. Shalgar and I. Tamborra, *On the occurrence of crossings between the angular distributions of electron neutrinos and antineutrinos in the supernova core*, *Astrophys. J.* **883** (2019) 80 [1904.07236].

[80] J. D. Martin, C. Yi and H. Duan, *Dynamic fast flavor oscillation waves in dense neutrino gases*, *Phys. Lett. B* **800** (2020) 135088 [1909.05225].

[81] T. Morinaga, H. Nagakura, C. Kato and S. Yamada, *Fast neutrino-flavor conversion in the preshock region of core-collapse supernovae*, *Phys. Rev. Res.* **2** (2020) 012046 [1909.13131].

[82] H. Nagakura, T. Morinaga, C. Kato and S. Yamada, *Fast-pairwise collective neutrino oscillations associated with asymmetric neutrino emissions in core-collapse supernovae*, *Astrophys. J.* **886** (2019) 139 [1910.04288].

[83] L. Johns, H. Nagakura, G. M. Fuller and A. Burrows, *Neutrino oscillations in supernovae: Angular moments and fast instabilities*, *Phys. Rev. D* **101** (2020) 043009 [1910.05682].

[84] M. Delfan Azari, S. Yamada, T. Morinaga, H. Nagakura, S. Furusawa, A. Harada, H. Okawa, W. Iwakami and K. Sumiyoshi, *Fast collective neutrino oscillations inside the neutrino sphere in core-collapse supernovae*, *Phys. Rev. D* **101** (2020) 023018 [1910.06176].

[85] S. Abbar, H. Duan, K. Sumiyoshi, T. Takiwaki and M. C. Volpe, *Fast neutrino flavor conversion modes in multidimensional core-collapse supernova models: The role of the asymmetric neutrino distributions*, *Phys. Rev. D* **101** (2020) 043016 [1911.01983].

[86] R. Glas, H.-T. Janka, F. Capozzi, M. Sen, B. Dasgupta, A. Mirizzi and G. Sigl, *Fast neutrino flavor instability in the neutron-star convection layer of three-dimensional supernova models*, *Phys. Rev. D* **101** (2020) 063001 [1912.00274].

[87] M.-R. Wu and I. Tamborra, *Fast neutrino conversions: Ubiquitous in compact binary merger remnants*, *Phys. Rev. D* **95** (2017) 103007 [1701.06580].

[88] M.-R. Wu, I. Tamborra, O. Just and H.-T. Janka, *Imprints of neutrino-pair flavor conversions on nucleosynthesis in ejecta from neutron-star merger remnants*, *Phys. Rev. D* **96** (2017) 123015 [1711.00477].

[89] H.-T. Janka, K. Langanke, A. Marek, G. Martinez-Pinedo and B. Müller, *Theory of core-collapse supernovae*, *Phys. Rept.* **442** (2007) 38 [astro-ph/0612072].

[90] H. A. Bethe and J. R. Wilson, *Revival of a stalled supernova shock by neutrino heating*, *Astrophysical Journal* **295** (1985) 14.

[91] R. S. L. Hansen and A. Y. Smirnov, *Neutrino conversion in a neutrino flux: towards an effective theory of collective oscillations*, *JCAP* **1804** (2018) 057 [1801.09751].

[92] M. J. Cervia, A. V. Patwardhan, A. B. Balantekin, S. N. Coppersmith and C. W. Johnson, *Entanglement and collective flavor oscillations in a dense neutrino gas*, *Phys. Rev. D* **100** (2019) 083001 [1908.03511].

[93] A. Manohar, *Statistical mechanics of noninteracting particles*, *Phys. Lett. B* **186** (1987) 370.

[94] L. Stodolsky, *On the treatment of neutrino oscillations in a thermal environment*, *Phys. Rev. D* **36** (1987) 2273.

[95] M. J. Thomson, *The damping of quantum coherence by elastic and inelastic processes*, *Phys. Rev. A* **45** (1992) 2243.

[96] A. Vlasenko, G. M. Fuller and V. Cirigliano, *Neutrino quantum kinetics*, *Phys. Rev. D* **89** (2014) 105004 [1309.2628].

[97] E. P. Wigner, *On the quantum correction for thermodynamic equilibrium*, *Phys. Rev.* **40** (1932) 749.

[98] N. D. Cartwright, *A non-negative Wigner-type distribution*, *Physica A* **83** (1976) 210.

[99] K. Husimi, *Some formal properties of the density matrix*, *Proc. Phys. Math. Soc. Jap.* **22** (1940) 264.

[100] A. Friedland and C. Lunardini, *Neutrino flavor conversion in a neutrino background: Single particle versus multiparticle description*, *Phys. Rev. D* **68** (2003) 013007 [hep-ph/0304055].

[101] A. Friedland and C. Lunardini, *Do many particle neutrino interactions cause a novel coherent effect?*, *JHEP* **10** (2003) 043 [hep-ph/0307140].

[102] J. E. Moyal, *Quantum mechanics as a statistical theory*, *Proc. Cambridge Phil. Soc.* **45** (1949) 99.

[103] F. J. Botella, C.-S. Lim and W. J. Marciano, *Radiative corrections to neutrino indices of refraction*, *Phys. Rev. D* **35** (1987) 896.

[104] A. Mirizzi, S. Pozzorini, G. G. Raffelt and P. D. Serpico, *Flavour-dependent radiative correction to neutrino-neutrino refraction*, *JHEP* **2009** (2009) 020 [0907.3674].

[105] Y. Aharonov, A. Komar and L. Susskind, *Superluminal behavior, causality, and instability*, *Phys. Rev.* **182** (1969) 1400.

[106] T. Morinaga and S. Yamada, *Linear stability analysis of collective neutrino oscillations without spurious modes*, *Phys. Rev. D* **97** (2018) 023024 [1803.05913].

Acknowledgements

Many people have contributed in a direct or indirect way to this thesis, for which they have earned my gratitude.

First and foremost I thank my supervisor Georg Raffelt for his outstanding way of giving suggestion and orientation about research projects while at the same time creating an environment of academic freedom. Discussions with him were a reliable source for new perspectives and physical insight. Furthermore I am indebted to Francesco for the great collaboration on different projects and our free-time activities in India. I am much obliged to him and Sajad for their tremendous effort on improving my writing style. Without it I probably would have struggled some weeks more to express the content in a comprehensive way. Moreover I thank the current and former members of the astroparticle group for contributing to a working atmosphere that made me really feel at ease. Special thanks to David for the many unscientific, but often funny discussions we had at work, the teamwork at the Deutsche Schülerakademie and his patience in defending string theory against my prejudices; I am still not convinced, though.

Finally I thank my family for the stable environment I am fortunate to have. Particular thanks to my parents, Ute and Gunnar, for their continuous support and to my wife Sarah for her affectionate love, and her endurance in the last weeks.